



A study  
on roll  
inertial mass

roll con-  
trol for  
ships

A.J. Eijsbouts



# A study on moving mass roll control for ships

A feasibility approach

by

A.J. Eijsbouts

to obtain the degree of Master of Science at the Delft University of Technology, to be defended on Monday  
July 03, 2017 at 16:00.

Student number:	4037960	
Project duration:	November, 2016 – July, 2017	
Thesis committee:	Prof. dr. ir. R. Huijsmans,	TU Delft, supervisor
	Prof. dr. ir. R. van 't Veer	TU Delft
	Dr. Ir. J.W. van Wingerden,	TU Delft
	Ir. M. Stofregen,	Huisman equipment B.V.

*This thesis is confidential and cannot be made public until December 31, 2022.*

An electronic version of this thesis is available at <http://repository.tudelft.nl/>.



# Abstract

Due to a low restoring force as well as lack of damping, the roll motion of a vessel is usually the motion with the highest amplitude of all degrees of freedom. Therefore, in history many have tried to stabilize rolling ship starting with Watts [45] in 1883. He described the damping of the roll motion by having a group of men running to the "high" side of the vessel. Since then, a great deal have been written about the subject of roll damping for stationary vessels. The principle however has been the same ever since, a shift of mass to counter the roll motion. Water tanks, carts on a curved track and sliding masses, all tend work with this principle. In 1904 Schlick [35] introduced another device to damp roll motions was introduced, the gyroscope. By controlling the precession angle, the roll motion could be damped. Following from an increase in computational power more advanced control strategies could be applied, leading to a renewed interest in the subject as well as different methods to model the vessel for controller design.

In the current paper, the performance of a gyroscope is compared with the performance of a moving mass, modeled as a double pendulum, for dynamic performance of a showcase vessel, the Huisdrill P10000. Results of this analytic study are promising, a reduction of more than 80% for both systems was achieved at the natural frequency of the Huisdrill. The decay time after a roll amplitude of 5.7 deg was reduced from about 250 seconds to 60 seconds for the gyroscope controller model and 70 seconds for the double-pendulum controller model. A static heel control system is modeled based on the double-pendulum equations. This proves to be able to compensate for the heeling moment depending on the weight at the crane tip as well as the weight and distance available to compensate. Combining the static and dynamic approach is possible with the note that there should be sufficient space for the mass to deviate after compensating for static heel.

In irregular waves the 4 – *DoF* model shows good performance for the showcase of the Huisdrill P10000. The *RMS* value for the roll-roll motion was decreased by 65%. For other degrees of freedom, similar reductions were obtained. From this it can be included that for the given seastate, significant reductions can be achieved using the ballast train. In the time domain, it was shown that great reductions in most probable maximum of reduction of roll amplitude were achieved for time periods close to the natural frequency of the vessel. For no time period, reductions in performance were measured. It was found that the most probable maximum roll angle linearly increased with the wave height, as well as the most probable deviation did.

Interpreting the results of this study, it can be stated that both the gyroscopic control system as well as the double-pendulum system are able to introduce great reduction in dynamic roll motions. The main benefit of using the double-pendulum system is its ability to compensate for the heeling moment induced by the swiveling crane as well as compensating for the dynamic motions that a vessel will undergo offshore.

It is recommended to do a simulation of a non-linear time-domain model or to perform model tests for verification of the results found in this report. The gap between static and dynamic control should be filled by a master control which is to be designed and run in the time domain.



# Preface

This research is commissioned by Huisman equipment located in Schiedam and is part of my graduation thesis project in order to obtain the Masters degree in engineering (Msc) at the Delft University of Technology. In this paper it was aimed for to objectively compare different methods of roll damping control systems for vessels which are not in transit condition. The main interest was in compensating for harmonic excitations due to wave loads as well as to static heel which is induced by a swiveling crane. As an example case throughout the report the Huisdrill P10000 as designed by Huisman is used. I would like to specially thank Prof. dr. ir. R.H.M. Huijsmans for his support and enthusiasm, prof. dr. ir. R. van 't Veer for his critical mindset, dr. ir. J.W. van Wingerden for his valuable advice on controller design, and last but not least, ir. F. van Heerd & ir. M. Stofregen for helping me with my everyday problems. Next to the professional support, I also want to thank my parents for granting me the opportunity to learn and study the first 26 years of my life as well as my girlfriend Laura as she always engaged me during the ups and downs of my graduation project.

*A.J. Eijsbouts  
Delft, July 2017*



# Nomenclature

## Acronyms

ARX	Autoregressive eXogenous	
CoG	Center of Gravity	m
DoF	Degree of Freedom	
DP	Dynamic Positioning	
EOM	Equations Of Motions	
FD	Frequency Domain	
FRAO	Force Response Amplitude Operator	
GDP	Gross Domestic Product	\$
GM	Metacentric Height	m
GM(control)	Gain Margin	
GoM	Gulf of Mexico	
GUI	Graphical User Interface	
IPTO	Increase of Time Operable	
ITTC	International Towing Tank Conference	
JONSWAP	Joint North Sea WAve Project	
LAMP	Large Amplitude Motion Program	
LQR	Linear Quadratic Regulator	
MODU	Mobile Offshore Drilling Unit	
NMP	Non Minimum Phase	
PID	Proportional Integral Derivative	
PM	Phase Margin	
RAO	Response Amplitude Operator	
RMS	Root Mean Square	
RRO	Percentage Reduction of Probability of Roll Peak Occurrence	
RRR	Percentage reduction of Roll at Resonance	
RSR	Percentage Reduction of Statistics of Roll	
SMC	Sliding Mode Controller	
SWATH	Small Waterplane Area Twin Hull	
TD	Time Domain	

**Greek Symbols**

$\alpha$	Angle of pendulum with z-axis	rad
$\epsilon$	Phase lag	rad
$\omega$	Frequency	rad/s
$\phi$	Roll angle	rad
$\psi$	Precession angle, yaw angle	rad
$\rho$	Density	kg/m <sup>3</sup>
$\sigma$	Stress	N/m <sup>2</sup>
$\zeta$	Wave elevation	m

**Roman Symbols**

$B$	Damping constant	N · s/m
$C$	Spring constant	N/m
$D$	Diameter	m
$d$	Distance from COG	m
$g$	Gravity constant(9.81)	m/s <sup>2</sup>
$h$	Height	m
$J$	Mass moment of inertia	kgm <sup>2</sup>
$K$	Constant	
$L$	Length	m
$l$	Length	m
$M$	Moment	N · m
$m$	Mass	kg
$n$	Number of	
$Q$	Generalized force	
$q$	Generalized coordinate	
$t$	Time	s
$t$	Torque	N · m
$V$	Volume	m <sup>3</sup>
$v$	Velocity	m/s
$y$	Righting lever arm	m

**Subscripts**

$a$	Amplitude
$cl$	Closed loop
$d$	Damping

---

<i>dp</i>	double pendulum
<i>g</i>	Gyroscopic
<i>n</i>	Natural
<i>ol</i>	Open loop
<i>r</i>	Restoring
<i>s</i>	Degree of freedom or ship parameter



# Contents

<b>List of Figures</b>	<b>xv</b>
<b>List of Tables</b>	<b>xix</b>
<b>1 Introduction</b>	<b>1</b>
1.1 Problem statement . . . . .	1
1.2 Research goal . . . . .	1
1.3 Research question . . . . .	1
1.4 Research aims. . . . .	2
1.5 Research approach . . . . .	3
1.5.1 Literature study . . . . .	3
1.5.2 Analytic study . . . . .	3
1.5.3 Frequency domain model . . . . .	3
1.5.4 Time-domain verification . . . . .	3
1.5.5 Controller design . . . . .	4
1.5.6 Sensitivity and feasibility study . . . . .	4
1.5.7 Flowchart . . . . .	5
1.5.8 Assumptions. . . . .	6
<b>2 Literature Study</b>	<b>7</b>
2.1 Introduction . . . . .	7
2.2 History and purpose of roll control systems for ships . . . . .	7
2.3 General information about drilling vessels and offshore drilling . . . . .	7
2.3.1 Offshore drilling . . . . .	8
2.3.2 Different drilling vessels . . . . .	8
2.3.3 Maximum tolerable angle of roll . . . . .	8
2.4 Coordinate systems . . . . .	8
2.4.1 Sea keeping coordinate system. . . . .	9
2.4.2 Motion superposition . . . . .	10
2.5 Roll control systems. . . . .	10
2.5.1 Anti-roll tanks . . . . .	10
2.5.2 Gyrostabilizers. . . . .	12
2.5.3 Moving mass roll control. . . . .	13
2.5.4 Other control systems . . . . .	13
2.5.5 Conclusion. . . . .	14
2.6 Control strategy. . . . .	14
2.6.1 Feedback control. . . . .	15
2.6.2 Feedforward control . . . . .	16
2.6.3 Filtering . . . . .	17
2.6.4 Conclusion. . . . .	17
2.7 Computational methods . . . . .	17
2.7.1 Frequency domain models. . . . .	17
2.7.2 Time domain models . . . . .	17
2.7.3 Hybrid frequency-time domain modeling . . . . .	17
2.7.4 Conclusion. . . . .	18

<b>3</b>	<b>Analytic study: Dynamic roll compensation</b>	<b>19</b>
3.1	Introduction . . . . .	19
3.2	Ship modeling . . . . .	19
3.3	Modeling of moving mass control system . . . . .	20
3.3.1	Modeling method . . . . .	20
3.3.2	Model verification . . . . .	22
3.3.3	Conclusion. . . . .	22
3.4	Modeling of gyroscopic control system . . . . .	22
3.4.1	Modeling method . . . . .	23
3.4.2	Model verification . . . . .	23
3.4.3	Conclusion. . . . .	24
3.5	State-space description . . . . .	24
3.6	Estimation of parameters for Huisdrill P10000 case study. . . . .	25
3.6.1	Double pendulum model parameters . . . . .	25
3.6.2	Gyroscopic model parameters . . . . .	25
3.7	System properties. . . . .	27
3.7.1	Pole-zero plots. . . . .	27
3.7.2	Bode plot . . . . .	28
3.7.3	Controllability . . . . .	28
3.7.4	Verification . . . . .	29
3.8	Controller design . . . . .	29
3.8.1	Double Pendulum Controller . . . . .	30
3.8.2	Gyroscope control . . . . .	33
3.9	Conclusion . . . . .	35
<b>4</b>	<b>Analytic study: Static Heel</b>	<b>37</b>
4.1	Introduction . . . . .	37
4.2	Ship Modelling . . . . .	37
4.3	Heeling moment modeling . . . . .	38
4.4	Controller design . . . . .	38
4.5	Conclusion . . . . .	41
<b>5</b>	<b>Analytic study: Combined static &amp; dynamic behavior</b>	<b>43</b>
5.1	Introduction . . . . .	43
5.2	Mass size . . . . .	43
5.3	Control strategy. . . . .	44
5.4	Relation pendulum versus moving mass control system . . . . .	44
5.5	Conclusion . . . . .	44
<b>6</b>	<b>Performance of control system</b>	<b>45</b>
6.1	Introduction . . . . .	45
6.1.1	The Percentage Reduction of Roll at Resonance . . . . .	45
6.1.2	Percentage Reduction of Statistics of Roll . . . . .	46
6.1.3	RRO . . . . .	46
6.1.4	Increase in Percentage of Time Operable. . . . .	46
6.2	Conclusion . . . . .	47
<b>7</b>	<b>4-Dof model reviewed in frequency domain</b>	<b>49</b>
7.1	Introduction . . . . .	49
7.2	Reference frames . . . . .	49
7.3	Wave spectra . . . . .	50
7.3.1	Statistical description . . . . .	50
7.3.2	Standard Wave Spectra. . . . .	51

7.4	Ship modeling . . . . .	51
7.5	From wave spectrum to ship response spectrum . . . . .	53
7.6	Parameters . . . . .	54
7.7	Controller implementation . . . . .	55
7.8	Results . . . . .	55
7.9	Conclusion . . . . .	58
<b>8</b>	<b>Time domain study</b>	<b>59</b>
8.1	Introduction . . . . .	59
8.2	Frequency study limitations . . . . .	59
8.3	Model . . . . .	59
8.4	Time Record generation. . . . .	59
8.5	Results . . . . .	61
8.5.1	Motion response. . . . .	62
8.5.2	Extreme Wave Amplitude . . . . .	62
8.5.3	Different seastates . . . . .	63
8.6	Non-linear Time Domain simulation . . . . .	65
8.6.1	Non-linear equations of motion . . . . .	65
8.6.2	Non-linear wave loads . . . . .	65
8.6.3	Control. . . . .	65
8.7	Conclusion . . . . .	66
<b>9</b>	<b>Conclusion and recommendations</b>	<b>67</b>
9.1	Conclusion . . . . .	67
9.2	Recommendations . . . . .	67
9.2.1	Controller design . . . . .	67
9.2.2	Model improvement . . . . .	67
9.2.3	Model testing . . . . .	68
	<b>Bibliography</b>	<b>69</b>
<b>A</b>	<b>Research planning</b>	<b>73</b>
A.1	Overview . . . . .	73
A.2	Gantt chart . . . . .	74
<b>B</b>	<b>Minutes</b>	<b>75</b>
B.1	Internal meeting 15-11-2016 . . . . .	75
B.1.1	Project goals . . . . .	75
B.1.2	Starting points . . . . .	75
B.1.3	What does Huisman wants. . . . .	75
B.1.4	What does the TU wants . . . . .	75
B.1.5	Leads . . . . .	75
B.2	Internal meeting 06-12-2016 . . . . .	76
B.2.1	feedback on report. . . . .	76
B.2.2	To do's . . . . .	76
B.2.3	Ancillary matters. . . . .	76
B.3	Kick-off meeting 20-12-2016 . . . . .	77
B.3.1	Received documents. . . . .	77
B.3.2	Points discussed . . . . .	77
B.3.3	Points of attention . . . . .	77
B.3.4	To do's Prof. Huijismans . . . . .	77
B.3.5	Next meeting. . . . .	77
B.4	Meeting 08-05-2017. . . . .	78
B.4.1	Received documents. . . . .	78
B.4.2	Points discussed . . . . .	78
B.4.3	Points of attention . . . . .	78
B.4.4	To do's Prof. Huijismans . . . . .	78
B.4.5	Next meeting. . . . .	78

---

<b>C</b>	<b>Huisman Model test</b>	<b>79</b>
C.1	Introduction . . . . .	79
C.1.1	Results . . . . .	80
C.1.2	Conclusion. . . . .	81
<b>D</b>	<b>Gyroscopes</b>	<b>83</b>
<b>E</b>	<b>Hydrostatics</b>	<b>87</b>
E.1	Hydrostatics . . . . .	87
E.1.1	Definitions. . . . .	87
E.1.2	Horizontal equilibrium . . . . .	88
E.1.3	Vertical equilibrium . . . . .	88
E.1.4	Rotational equilibrium. . . . .	88
E.1.5	Restoring moment & Stability curve . . . . .	88
E.1.6	Crane action . . . . .	89
E.1.7	Eccentric loading . . . . .	89

# List of Figures

1.1	Simplified front view of drillship with ballast train . . . . .	2
1.2	Simplified model of ballast train . . . . .	3
1.3	Flowchart of project approach . . . . .	5
2.1	Two types of commonly used MODU's . . . . .	8
2.2	Definitions of ship motions, source: Journee et al. [11] . . . . .	9
2.3	Ship rolling right . . . . .	10
2.4	Ship at biggest roll amplitude . . . . .	10
2.5	Ship rolling left . . . . .	11
2.6	Ship at biggest roll amplitude . . . . .	11
2.7	Passive U-tube . . . . .	11
2.8	Active tank system, source:www.hoppe-marine.com . . . . .	12
2.9	2 Gyroscopes installed on the USS Henderson in 1917, source:US Navy Historical Center, Dept. of the Navy, Washington D.C . . . . .	12
2.10	Example of Halycon's twin gyro stabilizer, source: Perez and Steinmann [31] . . . . .	12
2.11	Simplified front view of drillship with ballast train . . . . .	13
2.12	Render of wind turbine shuttle . . . . .	14
2.13	Double pendulum model . . . . .	14
2.14	Common feedback control loop . . . . .	15
2.15	Common feed forward scheme . . . . .	16
2.16	Wave prediction control scheme, source: Moaleji and Greig [22] . . . . .	16
2.17	Inverse adaptive control scheme, source: Moaleji and Greig [22] . . . . .	16
3.1	Ship model . . . . .	19
3.2	Ship model with crane . . . . .	19
3.3	Model of ship and control system . . . . .	20
3.4	Coordinate system for Lagrangian derivation . . . . .	21
3.5	Model of ship and gyro control system Perez and Steinmann [31] . . . . .	23
3.6	State space with output feedback scheme . . . . .	24
3.7	Schematic of pendulum length and angle derivation . . . . .	26
3.8	Explanation pendulum effect . . . . .	27
3.9	Pole plot Huisdrill P10000 . . . . .	28
3.10	Pole plot Huisdrill P10000 with double pendulum . . . . .	28
3.11	Pole plot of Huisdrill P10000 with gyroscope . . . . .	28
3.12	Bode plot of Huisdrill P10000 roll motion without additional compensation systems . . . . .	28
3.13	Bode plot of Huisdrill P10000 roll motion with the double pendulum compensation systems . . . . .	28
3.14	Bode plot of Huisdrill P10000 roll motion with a gyroscopic compensating system . . . . .	28
3.15	State space with output feedback scheme . . . . .	30
3.16	Open loop Bode plot . . . . .	31
3.17	Controller Bode plot . . . . .	31
3.18	Bode plot of controlled and uncontrolled frequency response . . . . .	31
3.19	Initial value response to an angle of 0.1 rad . . . . .	31
3.20	Open loop Bode plot . . . . .	32
3.21	Controller Bode plot . . . . .	32
3.22	Schematic for deviation explanation . . . . .	32
3.23	Initial value response plot . . . . .	32
3.24	$\alpha$ and $\phi$ as a function of time . . . . .	33
3.25	Huisdrill P10000 with and without active control . . . . .	33
3.26	Huisdrill bode plot, no control system . . . . .	34

3.27	Bode plot of Huisdrill roll motion with the gyroscopic control system . . . . .	34
3.28	Bode plot of controlled and uncontrolled response . . . . .	34
3.29	Controller for gyroscopic control system . . . . .	34
3.30	Initial value response of three different systems . . . . .	34
3.31	Initial value angle response of roll and precession angle . . . . .	34
3.32	Bode plot of PD-controller . . . . .	35
3.33	Initial value angle response of roll and precession angle . . . . .	35
3.34	Initial value response of three different systems . . . . .	35
3.35	Bode plot of controlled vs uncontrolled system . . . . .	35
4.1	Model of ship and control system . . . . .	37
4.2	The forcing moment induced by the swiveling motion of the crane . . . . .	39
4.3	How the crane swiveling motion translates to a movement in sway direction . . . . .	39
4.4	Common feedback control loop . . . . .	39
4.5	TD simulation of the controlled and uncontrolled ship . . . . .	40
4.6	TD simulation of the controlled(PI-controller) and uncontrolled ship . . . . .	40
5.1	Control moment as a function of mass . . . . .	43
6.1	Probability distributions for short and long term Journee et al. [11] . . . . .	46
7.1	The hydrodynamic frame proposed by Journee et al. [11] . . . . .	49
7.2	Reference frame as proposed by Perez [28] . . . . .	49
7.3	How a wave spectrum is obtained Journee et al. [11] . . . . .	50
7.4	Irregular waves with directionality . . . . .	50
7.5	Pierson Moskowitz spectrum for different values of $T_1$ . . . . .	51
7.6	Pierson Moskowitz spectrum for different values of $H_s$ . . . . .	51
7.7	Pierson Moskowitz spectrum for west-African swell . . . . .	52
7.8	State space with output feedback scheme . . . . .	55
7.9	Transfer function from sway force to roll angle . . . . .	56
7.10	Transfer function from heave force to roll angle . . . . .	56
7.11	Transfer function from roll moment to roll angle . . . . .	56
7.12	Transfer function from yaw moment to roll angle . . . . .	56
7.13	RAO sway to roll . . . . .	57
7.14	RAO heave to roll . . . . .	57
7.15	RAO roll to roll . . . . .	57
7.16	RAO yaw to roll . . . . .	57
7.17	Moment RAO: roll moment/wave height . . . . .	58
7.18	Reduction of Statistics of Roll for $H_s = 1.5m, T_1 = 20s$ . . . . .	58
8.1	State space with output feedback scheme for Simulink . . . . .	60
8.2	Wave record creation Journee et al. [11] . . . . .	60
8.3	Wave spectrum divided in 40 bins $H_s = 1.5m, T_1 = 20s$ . . . . .	61
8.4	A realization of the wave spectrum in 8.3 . . . . .	61
8.5	Roll response to irregular waves 1 . . . . .	61
8.6	Roll response to irregular waves 2 . . . . .	61
8.7	Roll and pendulum angle response in irregular waves . . . . .	62
8.8	Pendulum deviation response to irregular waves . . . . .	62
8.9	Probability distributions for short and long term Journee et al. [11] . . . . .	62
8.10	Histogram of maximum roll angle . . . . .	63
8.11	Reduction in Most probable maximum of a given seastate as a function of $T_1$ . . . . .	63
8.12	Reduction in Most probable maximum of a given seastate as a function of $H_s$ . . . . .	63
8.13	Most probable maximum deviation of the pendulum as a function of $T_1$ . . . . .	64
8.14	Most probable maximum deviation of the pendulum as a function of $H_s$ . . . . .	64
8.15	Most probable maximum roll angle as a function of $T_1$ . . . . .	64
8.16	Most probable maximum roll angle as a function of $H_s$ . . . . .	64
8.17	Visualization of wave envelope that might induce non-linear behavior . . . . .	65

---

A.1	Gantt Chart Nov-Mar . . . . .	74
A.2	Gantt Chart Apr-Jul . . . . .	74
C.1	Modeltests as performed by Huisman 2008 . . . . .	79
C.2	Decay tests LC1 . . . . .	80
E.1	Heeling angle explained . . . . .	87
E.2	Definition of heeling moment, source: Journee et al. [11] . . . . .	88
E.3	Rotational equilibrium, source: Journee et al. [11] . . . . .	89
E.4	A typical GZ-curve . . . . .	89
E.5	Swiveling motion . . . . .	90
E.6	The shifting of a load on deck, source: Journee et al. [11] . . . . .	91



# List of Tables

3.1	Ship and general parameters . . . . .	25
3.2	Moving mass parameters . . . . .	26
3.3	Gyroscope parameters . . . . .	27
4.1	250 mt crane parameters . . . . .	38
7.1	Key characteristics wave output spectrum for $H_s = 1.5m, T_p = 20s$ . . . . .	57
A.1	Planning . . . . .	73
C.1	Regular waves(full scale values) . . . . .	79
C.2	Regular waves(full scale values) . . . . .	80
C.3	Irregular waves(full scale values)-JONSWAP spectrum; $\gamma = 3.3$ . . . . .	80
C.4	Performance regular waves . . . . .	81
C.5	Performance irregular waves . . . . .	81





# Introduction

For drilling offshore wells, some well-known types of drilling units can be used, for example: semi-submersibles, jack-ups, barges and drillships. All with different characteristics. Drillships are ship-shaped vessels that are used for drilling wells and for well maintenance. Due to their ship shape, drillships can attain high transit speeds compared to other types of drilling units. This comes at a price; due to their greater water-plane areas, ships shaped drilling units undergo appreciably greater motion in waves than do semi-submersibles; both in terms of magnitude and bandwidth. Korde [14]

As stated by Sarpkaya and Isaacson [34] wave-induced motions can induce considerable load on the drill-string. This has led to various studies in the field of motion control systems. For example: Korde [14] for heave compensation and Moaleji and Greig [22] summarize the different possibilities for roll control systems. Present study will mainly focus on designing a roll compensation system, for a drillship, the results however should be in general be applicable on any similar vessel of which the RAO are known. Conditions for applying the found theory to different vessels should be derived.

## 1.1. Problem statement

Drillships like the P10000 or the Huisdrill are in general having a low metacentric height,  $GM$ , which induces a low initial stability, as well as a high natural period, around about 20 seconds. Due to the low stability, a roll angle is easily obtained by for example pivoting the crane boom. This is unwanted since the roll angles of the vessel should remain small to prevent the drill string from being damaged and to prevent the crew from not being able to operate. Ships that are drilling near the coast of West-Africa, experience long swell waves are being excited in their natural frequency leading to great roll excursions which are again unwanted. An additional problem in this case is the lack of viscous damping due to the low rolling frequency. These conditions induce at least a reduction in workability, in the worst case, they can lead to unsafe situations. Therefore a system should be designed to compensate for these unwanted motions. In addition to the roll motion damping, the moving mass should be able to compensate for the heeling moment induced by the swiveling board crane.

## 1.2. Research goal

Create and verify a practically applicable model for designing the roll damping control system of ship shaped drilling vessels. Design a controller based on this model.

## 1.3. Research question

How can a control system be designed and optimized for static heel reduction as well as for dynamic roll damping? To answer this question some additional research questions have been formulated.

- What is the cause of the roll motions for a ship shaped drilling rig, is it allowed to assume linear wave force-motion responses?
- In what seastates is roll damping control most viable?

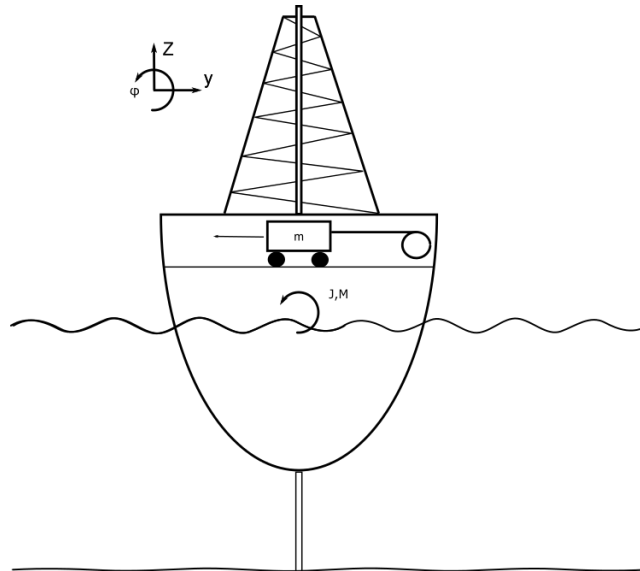


Figure 1.1: Simplified front view of drillship with ballast train

- Is a frequency domain model or hybrid-frequency model, as mentioned in Taghipour et al. [40], usable as a base for controller design? How will controller designed based on this model perform in irregular sea-states.
- What is the magnitude of improvement in controlled roll behavior compared to the non-controlled situation?
- Can the proposed roll control system be used for compensation of heeling moment by the swivelling crane?
- **Optional** Will a hybrid moving mass compensating system as proposed by Koike and Saeki [13] compensate roll motion properly?

#### 1.4. Research aims

- Obtaining an accurate overview of the state-of-the-art research in the field of the research. This includes, different compensation systems, control systems, filtering and computational methods.
- Comparing the performance of different roll-compensation systems on performance, efficiency and power consumption.
- Determine the viability of using the roll control system to compensate for a heeling moment.
- Creating a (hybrid) frequency domain model capable of describing vessel motions with a high level of accuracy.
- Verifying the above model by doing model tests or performing non-linear time-domain simulations.
- Integrate the motion control device in the (hybrid) frequency domain model.
- To verify the (hybrid) frequency domain model by model tests or by analytic study.
- Some effects will not be captured in a frequency domain model. Therefore a time-domain simulation with the designed controller should be performed to investigate the nature of those effects and to validate the simpler frequency domain model.
- Perform a sensitivity analysis on the control system. Investigate optimal weight of the balancing mass. Investigate the resulting moment of placing the control system outside the center of yaw rotation.
- Investigate the feasibility of a roll compensation system for different vessel displacement, GM, compensation mass, RAO's and sea states.

## 1.5. Research approach

The outline of the research will be summarized below. Together with the research question, research aims, problem statement and research goal, the approach should be clear.

### 1.5.1. Literature study

The base for any serious academic research is a literature study. Regarding the topic of roll compensation a lot has been written the last century. With the transition from ships powered by wind to ships that are powered by steam engines a whole new problem has risen; roll motions. Large keels and force on the sails dampened the roll motions tremendously. This has led several researchers like Schlick [35] and Chalmers [3] to investigate the topic in the early 20th century. Since then, U-tank stabilisers have gained in popularity. However with the uprise in the 1960's the control system engineering, a renewed interest in roll compensating systems arose. Perez and Fossen [30] This trend mainly focused on control system design, rather than developments in roll compensating systems.

The goal of the literature study will be to collect 'just enough' information on different subjects, and create an overview, in the field of roll compensation, such as various roll compensating systems, control methods, computational methods, the maximum acceptable roll angle and hydrodynamic behavior of ship shaped vessels.

### 1.5.2. Analytic study

Following the literature study, the next step is to analytically compare several roll compensating systems in terms of performance using simplified calculations. This is to get a starting point for the capabilities of the ballast train as well as to check if it is even a viable option compared to the other available solutions. A simplified double pendulum model with control of the top hinge is created as a baseline for further research. It should be investigated if this simple model is reachable. If so, a controller is designed to get some sense of the order of magnitude of roll reduction. The crane will be modeled, to investigate performance of heel compensation.

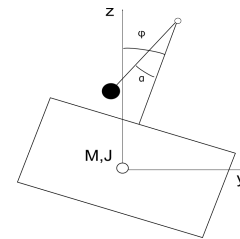


Figure 1.2: Simplified model of ballast train

### 1.5.3. Frequency domain model

The base of this study will be a frequency domain model as proposed by Newman [23]. Under some assumptions, which are stated later on, this is allowed. The behavior of this model will be compared with the model tests performed earlier by Huisman and with a time-domain simulation. Fluid memory properties can be added later, by system identification principles, as proposed by Taghipour et al. [40] to increase model accuracy. The main benefit of using a FD model is the decrease in computational efforts which will be beneficial for designing one or multiple controllers for a vessel, or different vessel characteristics (lifting, transit, storm, etc). Secondly, designing controllers in the frequency domain is a well understood practice. For testing the controller in irregular waves, the model can be converted to a state-space representation. When the hybrid frequency domain model responds in correspondence to the time-domain simulation a controller can be based on this.

Part of this study is to implement a complex curve-fitting algorithm as described in Levy [19] to mimic the RAO of a vessel in a linear algebraic fashion. The benefit of using this proposed method is that it can decrease computational time compared to non-linear time-domain simulations as well as that it can be used for any vessel for which the uncompensated RAO is known. Even experimental determination of RAO's can be used for controller design. This method can help in improving the controller performance by using real data or just as a base for controller design. Taking this procedure a step further, by applying real-time system identification, adaptive control can be implemented.

### 1.5.4. Time-domain verification

A time-domain model of the Huisdrill will be created for verification purposes. Where the frequency domain model should be more generally applicable, the time-domain model will be created for testing and verification purposes. Effects that time-domain models can capture in contrary to FD-models are for example: nonlinear wave forces, second order wave-drift forces, non-linear sliding mass behaviour, time lag. The test

case for this will be the Huisdrill. The focus will be on investigating and explaining the differences between the two models for controller design, as well as investigating for what cases it is allowable to model the ship in the frequency domain.

#### **1.5.5. Controller design**

A controller will be designed based on the frequency domain model. The controller however should be tested on stability and robustness like any other controller needs to be tested on. The controller design should be funded on literature research. A filter needs to be implemented, as stated by St Jago [39] to filter the noise produced by wave frequencies and sensor noise. A highly advanced filter however is not the scope of the research.

#### **1.5.6. Sensitivity and feasibility study**

With the chosen model, a sensitivity analysis is desirable. For Huisman it is important to know when a ballast train is feasible, and what the design parameters should be. The drillship can have a variable metacentric height. It will be investigated how the control system should adapt to these changes in system behaviour. The proposed method of complex curve-fitting should benefit this process. A practical guide on designing a roll compensating system using this system identification is desirable since it can help in designing systems for similar vessels. The ultimate goal for Huisman would be to create a Matlab code and GUI next to this guide.

**1.5.7. Flowchart**

In the chart below the approach is visualized using a flowchart. Each phase ends with a meeting at the Delft University of Technology. Each block should be finished before the process can continue. Sometimes, to go 2 steps forward, 1 step back should be taken, as is for example visualized in phase 0 and phase 1.

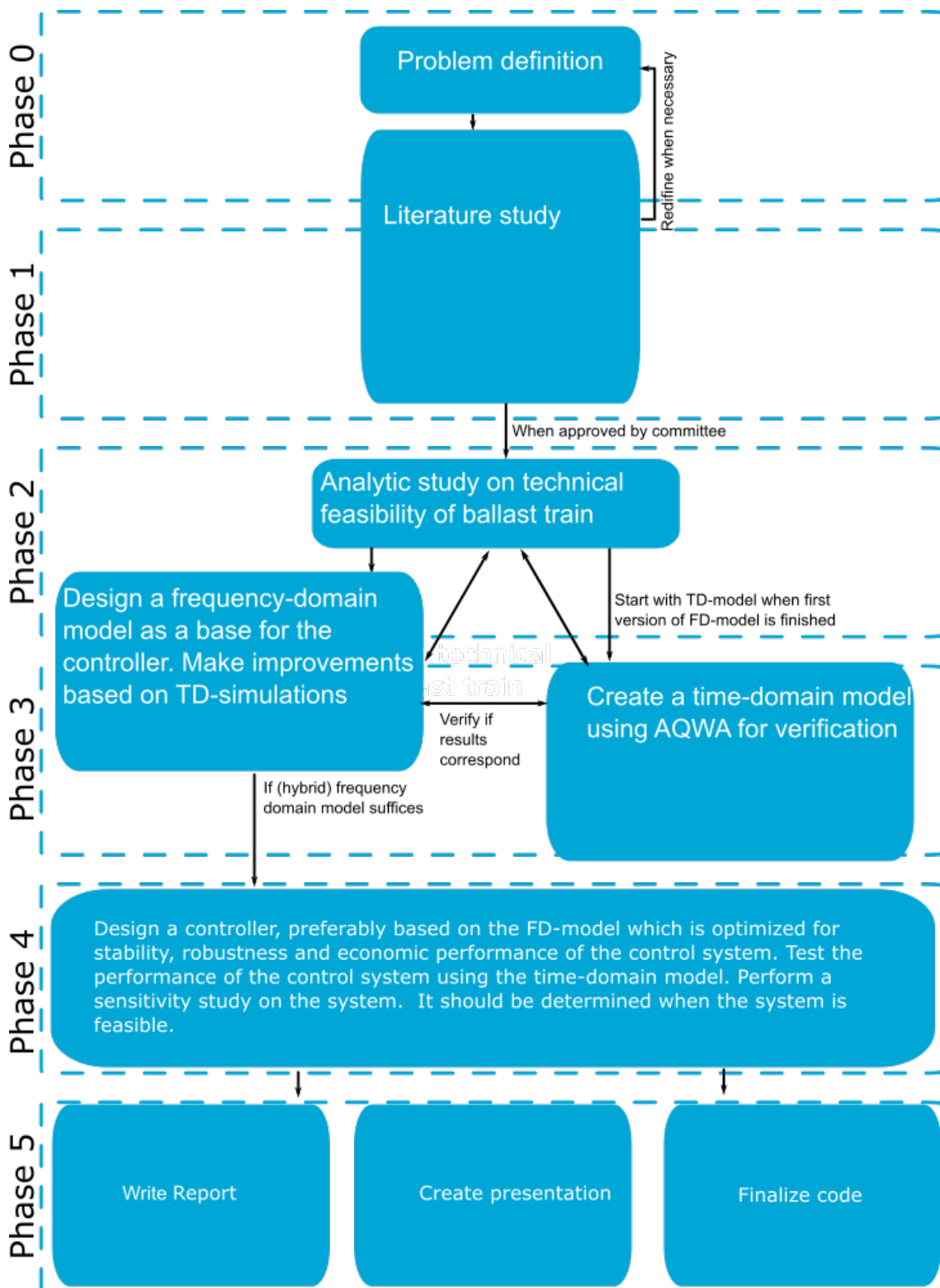


Figure 1.3: Flowchart of project approach

### **1.5.8. Assumptions**

- In literature the study of ship dynamics there has traditionally been a separation between maneuvering and seakeeping. Fossen [5] In this study only seakeeping abilities will be considered. So the forward velocity is always assumed as 0. The assumption is made to simplify the design of the control system.
- Influence of risers and drillstring on ship motion dynamics is neglected in first instance. The weight of this equipment is very small compared to the ship displacement.
- Linear wave theory can be used.
- Weight of crane and load are small compared to displacement of vessel
- The impact of crane swiveling on the heel angle of the vessel can be considered quasi-static.
- The influence of mooring lines is neglected.

# 2

## Literature Study

### 2.1. Introduction

The coming section will cover what has been published in the domain of ship roll control systems by accredited researchers. The purpose of this chapter is to convey the reader what knowledge and ideas have been established around the topic of roll control systems for vessels.

### 2.2. History and purpose of roll control systems for ships

Since the end of the era of sailing, various attempts have been made to compensate for roll motions. Roll motion of a ship typically has the largest amplitude of all the degrees of freedom. Moaleji and Greig [22] Excessive motions can interfere with the activities of the crew or passengers, reduce combat readiness, cause the loss of containers and, most importantly for this thesis; reduce the operational parameters of various ships, i.e. decrease the work ability. Treakle et al. [41] Therefore various attempts have been made to compensate for those roll motions. Most papers refer to the first successfully applied control system in a German torpedo boat in 1906, See-Bar in which a large gyroscopic roll stabilization system was installed to oppose the roll motions. Treakle et al. [41], Moaleji and Greig [22] etc. It was however, Schlick [35] who first proposed using gyroscopic ship roll stabilizers. Anti-roll tanks were introduced earlier in 1875 according to Treakle et al. [41] and Moaleji and Greig [22] Free surface tanks were the starting point, however U-tanks were introduced not much later. As the name implies, the tank has the form of a U, and is tune-able by changing the water height in the tank. Later Webster and Dogan [47] showed that using an actively-controlled anti-roll tanks significantly improved the roll-behavior compared to the passive anti-roll tanks. Koike and Saeki [13] presented the first serious attempt of roll-control by a sliding mass. This principle was first applied in the aircraft carrier Charles de Gaulle; it was mainly used for heel compensation during tight turning in that case. This highlights one of the other possibilities for a moving mass roll control system. A company in France, Sirehna is using moving mass to counteract rudder action. This brings us to another way which has been invented for ship roll control; rudder roll stabilization as stated by Van Perez [27]. In their paper, they also speak about fin control for roll damping in ships. In later sections the potential benefits of the different systems will be discussed. In recent works, the focus of research on roll control systems, was not so much on the, physical system, as well as on the control system. For example Koshkouei and Nowak [15] propose control by switched controllers and Saari and Djemai [33] propose a different linearized controller on different working points. This will be more thoroughly discussed in later sections.

### 2.3. General information about drilling vessels and offshore drilling

In the last three or four decades, the offshore industry has been booming. Further, bigger, deeper and more advanced. Offshore industry was mainly connected with oil and gas. Since a couple of years, development of offshore wind turbines took a flight. In the Netherlands, different parks have been build, and even more are announced. However this does not mean that fossil resources are not of importance anymore. According to Spencer [38], fossil fuels will remain to be the worlds main energy source (80% in 2035). This is due to the growing global GDP. For extraction of those precious resources offshore, drilling rigs are used As the name imposes, offshore drilling rigs are used for drilling offshore wells.

### 2.3.1. Offshore drilling

First reports of offshore drilling stem from the late 19th century. In California drilling took place from wooden piers of the coast of Santa Barbara. In the 1930's the first floating drilling rigs were used in the swamp's close to the Gulf of Mexico. In 1947 the first "real" offshore drilling took place PetroWiki [32] meaning that a tender assisted drilling unit, owned by Kerr-McGee, to drill out of sight. The first MODU was the Mr. Charlie, designed by ODECO and first used by Shell in the GoM. In later years, different MODU 's were designed such as jack-ups, barges, semi-submersibles, fixed platforms and drillships. Being popular at first due to their their transit speed and ease of mobilization, drillships got gradually replaced by jackup's and semi-submersibles. There is one exception on this, the DP drillship is still a popular solution, especially in situations where there are multiple wells to be drilled in a field, as well as in deep water. In 2003 there were about 6 times as many semi-submersible drilling rigs compared to drillships.



(a) Drillship



(b) Semi submersible drilling rig, source: www.gazprom.com

Figure 2.1: Two types of commonly used MODU's

### 2.3.2. Different drilling vessels

According to Journee et al. [11] there are two main types of drilling vessels. Drill ships and semi-submersible drilling rigs.

**Drill ships** are ship shaped drilling vessels, simply stated a ship with a drilling rig on top of it, see 2.1a. As stated before they are praised for their mobility, drillships will take 20 days to transit from the GoM to Offshore Angola, whereas other alternatives will take significantly longer to get there.

**Semi-submersibles**, shown in 2.1b, are vessels with two pontoons which are submerged. This leads to a small water plane area, which should lead to improved stability, which is beneficiary in many cases. Semi-submersibles can be tow-able or self-propelled. Transit times are usually three times as high as for a drill ship

### 2.3.3. Maximum tolerable angle of roll

Small angles of roll cannot be prevented. However, angles that are too large are not tolerable. Large angles can cause large stresses in drillstring with unwanted consequences such as fatigue. Other operations can be influenced as well by roll angles exceeding certain amounts.

## 2.4. Coordinate systems

Various coordinate systems are proposed to describe ship motions. Coordinate systems exists for describing vessel position with respect to the earth, to describe hull structure. For sea keeping and maneuvering there are different systems which can be used. Of interest for this paper are the earth bound coordinate system, which is used for describing wind and waves, as well as the steadily translating or stationary coordinate system, which can be used to describe vessel motions. A clear description of this is given in Journee et al. [11]. A short summary is given in the section to come.

### 2.4.1. Sea keeping coordinate system

The sea keeping coordinate system is based on 2 assumptions.

1. Mean forward speed is constant (or zero)
2. There is an oscillatory motion

The resulting six ship motions in the zero speed model can be described by three translational movements and three rotational. In which  $\epsilon$  represents the phase angle and symbols with the subscript a depict the amplitude of the motions. The phase shift is related to the (virtual) wave elevation at the origin at the CoG defined by 2.1 By definition  $\epsilon$  should always be positive.

#### Wave elevation at origin

$$\zeta = \zeta_a \cos(\omega_e t) \quad (2.1)$$

Below described the vessels motions in six DoF

#### Surge

$$x = x_a \cos(\omega_e t + \epsilon_x \zeta) \quad (2.2)$$

#### Sway

$$y = y_a \cos(\omega_e t + \epsilon_y \zeta) \quad (2.3)$$

#### Heave

$$z = z_a \cos(\omega_e t + \epsilon_z \zeta) \quad (2.4)$$

#### Roll

$$\phi = \phi_a \cos(\omega_e t + \epsilon_\phi \zeta) \quad (2.5)$$

#### Pitch

$$\theta = \theta_a \cos(\omega_e t + \epsilon_\theta \zeta) \quad (2.6)$$

#### Yaw

$$\psi = \psi_a \cos(\omega_e t + \epsilon_\psi \zeta) \quad (2.7)$$

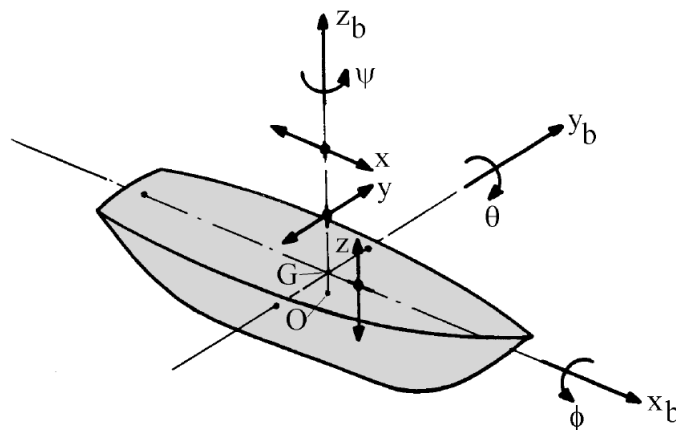


Figure 2.2: Definitions of ship motions, source: Journee et al. [11]

### 2.4.2. Motion superposition

The motions above are to describe the movements of a vessel in six degrees of freedom at the center of gravity. However for various purposes one could be interested in motions at different locations, for example the tip of an offshore crane. This can be done by using the super positioning principle. Motion at any position on the vessel can be described this way.

It will be demonstrated how this is derived for the coordinate  $z_p$ , the instantaneous height of the point  $P(x_b, y_b, z_b)$ . This height is determined by 3 components:  $z_b$ , the height of point P above the origin, minus the sine of the pitch angle times the x-coordinate of point P  $x_b$  and finally the sine of the roll angle times the y-coordinate of the point P,  $y_b$ . This can also be written by:

$$z_p = z - x_b \sin \theta + y_b \sin \phi \quad (2.8)$$

For small angles of roll and pitch, these motions can be linearized. By creating a Taylor series expansion of function around the origin and only taking the first order terms, a function can be linearized. Doing this for  $\sin(x)$  and  $\cos(x)$  yields respectively  $x$  and 1. Applying this linearization principle to 2.8, the following expression for the arbitrarily point P is derived:

$$z_p = z - x_b \theta + y_b \phi \quad (2.9)$$

It is left for the reader to derive the non-linearized motions in the point P. It should be noted that linearization is only allowed for small angles.  $\theta$ ,  $\phi$  and  $\psi$  are therefore given in radians. Below the resulting linearized matrix is given for P. It should be kept in mind that this matrix is linearized if for example large angles of heel are produced.

$$\begin{pmatrix} x_p \\ y_p \\ z_p \end{pmatrix} = \begin{pmatrix} 1 & -\psi & \theta \\ \psi & 1 & -\phi \\ -\theta & \phi & 1 \end{pmatrix} \cdot \begin{pmatrix} x_b \\ y_b \\ z_b \end{pmatrix}$$

## 2.5. Roll control systems

Different roll compensating systems have been proposed in the last century, all with different characteristics. In this section an in-depth review of the various methods will be provided. In general, a division can be made between active and passive anti-roll devices. In the early years passive system were most common, however during recent years recent developments on control systems have paved the way for different control systems to be effective. In this section the working principles of systems that will operate at zero forward speed are described, thus assuming zero-forward speed.

### 2.5.1. Anti-roll tanks

It is stated by Perez and Blanke [29] that the benefits of using ballast tanks for roll control were first noticed by a study on the HMS Inflexible in 1878 as Watts [45] describes. The main interest for this research was the damaged stability of the vessel, not the roll compensating ability. As a result of the study, the ship was permanently fitted with water chambers. Watts [45], Watts [46]. The system proposed was based on work Froude [6] in the field of bilge-keels. A big disadvantage of those keels Froude [6] proposed, is the dimensions the keels need to have for ships with great moments of inertia. This has led Watts to investigate the possibility of using anti-roll tanks. He demonstrated the working principle of this tank by a group of men running across the deck. Moaleji and Greig [22] used a clear explanation in their report, on which the figure below is based.

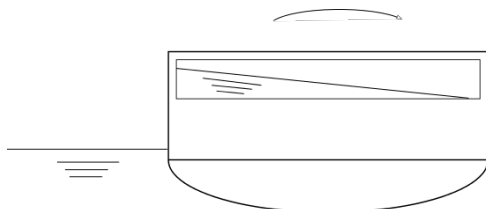


Figure 2.3: Ship rolling right

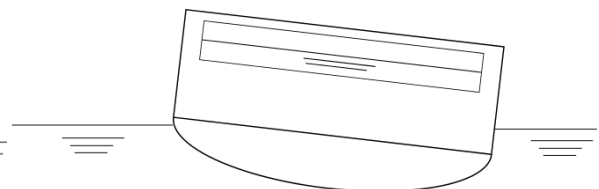


Figure 2.4: Ship at biggest roll amplitude

It can be seen from the figure that the center of gravity of the mass shifts to the high side of the ship as the ship rolls and due to the fact that the water in tank is lagging the roll motion. Watts & Froude found in

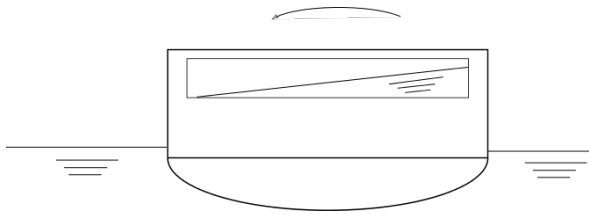


Figure 2.5: Ship rolling left

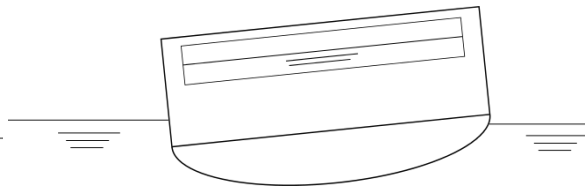


Figure 2.6: Ship at biggest roll amplitude

a full scale test that, that the roll damping peaked at when the tank was about half filled which Moaleji and Greig [22] implied that the anti-roll tank was having the same natural period as the vessel it was tested on. Reductions of more than 30% are proven for this specific case. Watts [45], Vugts [43] Researched the subject, by using a simplified model. They have found that a reduction of roll motion of up to 80% was possible for regular waves and up to 50% for irregular waves. The big advantage of using free surface according to Vugts [43] is the ability to change the water level, and thus the natural frequency of the free-surface anti-roll tank.

In later years some improvements have been proposed on the passive free surface anti roll tank, in the form of baffles. Lee and Vassalos [18] have showed by experiment the effects of different configurations of baffles. They have experimentally validated, that using baffled tanks can reduce roll amplitude at frequencies at the natural frequency significantly, while not creating unwanted ship dynamics at lower excitation frequencies.

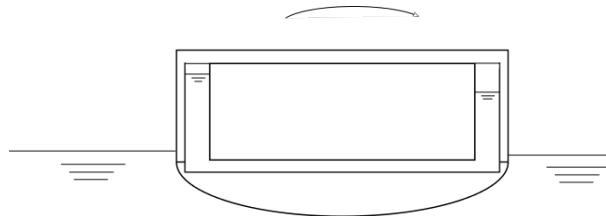


Figure 2.7: Passive U-tube

Horn [10] Is the first to speak about u-tanks for ship-stabilizing in literature. Free surface tank have proven their functionality, especially in the case were baffles are present. However some big disadvantages have become apparent. Firstly free surface anti-roll tanks can decrease stability due to sloshing. Secondly, the free surface anti-roll tanks will use precious space on a ship, due to the placement above the CoG. Moaleji and Greig [22]. This is partly solved by using u-tanks.

As is shown in 2.7, the name U-tank is well chosen. The tank is relying on the same-working principle as the free-surface tanks, by having the same natural roll period with a phase lag. Due to a shift in center of gravity of the fluid a restoring moment is applied on the vessel. In some designs, at the top of the u-tank is an air duct, which can be used to stop water motions completely or adapt the u-tube to changing sea-states, this is called a passive controlled tank.

U-tube tanks are in general divided in three categories Kula [17]:

1. Passive tanks
2. Passive controlled tanks
3. Active tanks

An active controlled u-tank can actively control the position of water by means of an actuator in the form of a water or air pump. The benefits of such a system is that it can be used in great variety of sea-states, however active tanks will consume power. In 2.8 an active tank is shown.

Next to free surface and u-tanks there is a third type of tank which is commonly used in the industry; the free-flooding tank. The free-flooding tank consists of an airduct with two wing tanks at the sides. Those tanks are directly connected with the sea water, and are controlled by the air duct. Some disadvantages are occurring in this systems such as corrosion due to salt water, reduced effectivity at forward speed as well as added ship resistance.

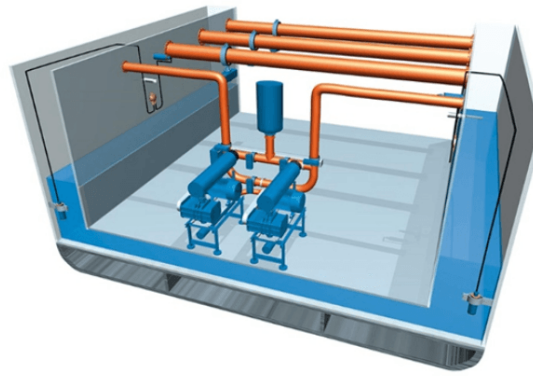


Figure 2.8: Active tank system, source:www.hoppe-marine.com

### 2.5.2. Gyrostabilizers

As early as 1904, Schlick [35] proposed the first gyrostabilizer for ships. Gyrostabilizers operate on the property of gyroscopes to resist rotational movements. 2.10 shows a clear picture on how such a system looks like. Although seeming promising at first, early devices did not succeed to become the industries standard for roll control devices. This was caused by two major problems. Firstly the size of the gyroscopes and the cor-

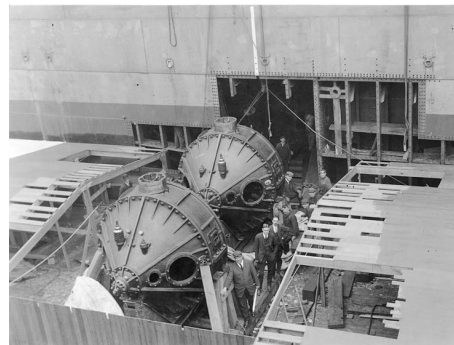


Figure 2.9: 2 Gyroscopes installed on the USS Henderson in 1917, source:US Navy Historical Center, Dept. of the Navy, Washington D.C

responding weight led to problems for this method. The loads on deck were too big. Secondly, according to Perez and Steinmann [31], the gyroscopes were unable to maintain performance over an extended envelope of sea states and sailing conditions. In their paper they re-investigated the possibility of using gyroscopes

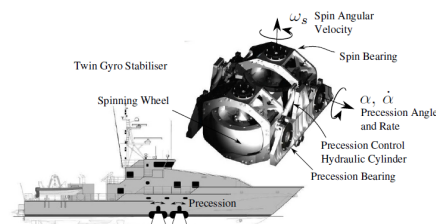


Figure 2.10: Example of Halycon's twin gyro stabilizer, source: Perez and Steinmann [31]

for roll compensating. They justify this by stating that developments in different areas such as materials, design methods, increase in computational power etc. have led to new possibilities in this field. In the linear performance case study they show that using a twin gyro stabilizer with a total weight of 3.7% of the ship displacement can reduce roll motions significantly, mainly at the natural frequency of the vessel. As with the anti-roll tanks, there is a negative roll-reduction at lower frequencies which means an increase in the motion amplitude. As Perez [27] discusses, performance in a regular sea is merely the upper bound of performance. In irregular sea-states the performance can be significantly worse. Saturation can occur when the maximum

precession angle is reached. In that specific situation the twin gyro stabilizer shows a major decrease in performance. Perez and Steinmann [31] suggest constrained optimized control to deal with this problem. This imposes that the problem remains that performance is variable in irregular seas.

### 2.5.3. Moving mass roll control

Various articles report on Cremieu being one of the first to implement a moving mass roll control system on a vessel. The 10-ton mass he used was based on a curved rail and damped by submersing it in a viscous fluid. This passive system, at least in theory, compensates the roll motions in the same way a passive tank does. The motion of the moving mass lags the roll motions of the vessel it is on while the natural period of the system should be of the same order of the vessel. Although this method is promising in theory, the execution was below average. The mass hit the ship sides resulting in massive shocks. In literature, a great deal has been

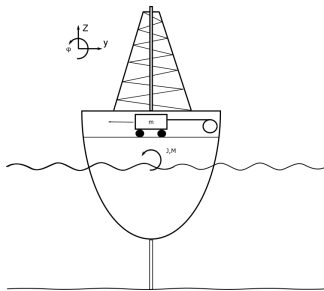


Figure 2.11: Simplified front view of drillship with ballast train

written on the subject of roll control, however most papers do not focus on using an actual mass, but on using a moving mass system to model the moving CoG of the anti-roll tank. Treacle et al. [41], St Jago [39] and Habing [8] have described doing simulations with a moving mass control system. Significant roll reductions, up to 50%, can be achieved for vessels with a long natural period, such as the Huisman Drillship. Habing [8] has found by doing simulations in Orcaflex that for a simple barge. The results are not as promising due to the high natural frequency these vessels possess. This agrees with results that other researchers have found.

Treacle et al. [41] have found in their paper, that using a mass as small as 0.5% to 1% of ship displacement can achieve a reduction in roll motion of 85% in regular waves at a period equal to the natural period of the vessel.

At around the same time as Treacle et al. [41] investigated this subject Koike and Saeki [13] were working on a similar topic. Koike and Saeki [13] investigated a, what they call, hybrid anti-roll system. It consists of a mass spring damping system combined with a control system to compensate the roll motions of a high speed survey vessel. They also conclude that a small mass can include tremendous reductions in roll motions for the vessel they have tested it on.

Next to hybrid systems, passive-controlled stabilizers have been mentioned in literature, for instance by Nonweiler et al. [24] who controlled stiffness and damping, rather than actively moving the control weight.

On the subject of roll control, by a moving mass, for twin-hull shaped vessels not much literature is found. However, St Jago [39] has created a model for motion control on a SWATH, a vessel concept designed by Huisman equipment for fast installation of wind turbines in wind farms. In 2.12 the Wind Turbine Shuttle is shown.

This thesis differs from the other motion control studies due by the fact that for this twin hull vessel, second-order wave effects play an important role for motions in contrary to the case for regular mono-hulls.

Using a moving weight control system, is advantageous comparing it to anti-roll tanks since there are no free surface effects present to degrade performance Smith and Thomas III [37]. Due the density of the solid mass, which will probably exceed the density of water, the moving weight system will very likely to occupy less space than an equivalent anti-roll tank. However some researcher state that using such a system can be dangerous, and that an equally effective u-tank can be designed with the same weight.

### 2.5.4. Other control systems

In literature some other systems are proposed, such as bilge keels, rudder-roll control, using fins to control vessel motions. This thesis work will be limited to systems that can be used at zero-forward speed. Therefore



Figure 2.12: Render of wind turbine shuttle

rudder-control as in Amerongen et al. [1] and fin control are ignored as well as the bilge keels, since they will impose a whole set of different issues that are unwanted such as increased draft and increased sensitivity to underwater currents. Furthermore the focus on the project is on control systems rather than on hull design.

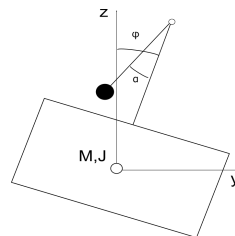


Figure 2.13: Double pendulum model

### 2.5.5. Conclusion

A sizable selection of articles have been written on the account of roll control systems. All authors agree that roll is the biggest and most unwanted motion of all the six DoF. Whatever control system is chosen, the working principle remains the same, that of the mathematically equivalent double pendulum, as shown in 2.13, say Smith and Thomas III [37], except for the gyroscopic systems, these kind of systems are producing an opposing force to the roll motion, regardless of frequency. A mass counteracts the roll motion of the vessel at the same frequency, but with a different phase, preferably a lag of  $90^\circ$ .

Choices between the different systems could be made based on costs, reliability, when can it be used; with forward speed, stationary or both, usability for heel compensation and cost reduction. Sellars and Martin [36] produced a paper for hands-on selection of a roll stabilization system mainly based on the economic feasibility of the different systems were Moaleji and Greig [22] approached this from a more technical point of view, as did Smith and Thomas III [37]. The mentioned motion control system above all seem to reduce the motion significantly, the choice for a roll control system therefore will be based the specific design requirements, such as deck space or a possibilities for anti-heeling.

## 2.6. Control strategy

Recent developments in the field of control theory have spiked the interest in roll control systems. In the period from the 60's, when Webster and Dogan [47] presented their work on roll control with modern control, until now, the focus on designing anti-roll devices has shifted to the field of controls and computational methods rather than just the mechanical designs of those systems. In many papers feedback control was used for the models. This type of control acts on movements of a system. Which means that a time-lag will always be present due to the physical nature of dynamic systems. To overcome this problem, a shift to the feedforward method of control could be made. In the field of roll control devices this would mean, using the waveheight or waveslope as an input for the controller instead of the roll angle of the vessel.

### 2.6.1. Feedback control

In various papers about roll control systems the control part have been treated varying in magnitude and complexity. Some authors like Treacle et al. [41], St Jago [39] use the relatively straightforward PID controller to compensate for roll motions. The choice for this type of controller is for simplicity, they state that better controller might exist, however controller selection is outside the scope of their research. For a long time the PID controller has been the industries standard of control due to the straight forward implementation. Minorsky [20] was the first one to describe such a controller by investigating how helmsman were able to keep their course. The control was based on the current course error, but also on the past error as well as the current rate of change. One could call this proportional, integral and derivative action, hence the name PID controller. Due to the nature of the physical system, some constraints needs to be put on the PID, hence the name constrained control.

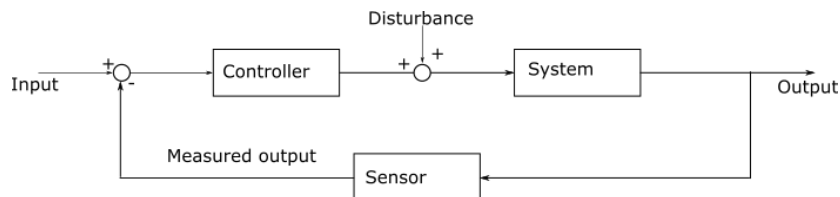


Figure 2.14: Common feedback control loop

The PID controller is a good example of a feedback controller, of which a schematic is depicted in 4.4. In roll control the input is usually zero, since roll is in principle an unwanted motion Kula [17]. The benefit of using such a feedback system, is that a change in system parameters, such as a changing GM or ship displacement, will not directly result in instability, which could be the case for feed-forward systems. PID control, or feedback controllers in general, tend to perform well in situations where the time constant of the actuator is considerably less than the time constant of the system to be controlled Moaleji and Greig [22]. If this would not be the case, the system would self-excite which could be catastrophic. This phenomenon is called wind-up in control terms.

With the offshore industry being a conservative industry as it is, some researchers have chosen to build on already existing PID controllers. Saari and Djemai [33] propose a system which consists of multiple PID controllers that are optimized around a linearized working point. A switching controller is used to switch between working points. Due to the nature of this system it the authors claim it is easy to implement in existing software. Koshkouei and Nowak [15] have proposed a similar system; a switched controller system based on SMC, which as they state yields a higher roll reduction, switched with PID control, based on performance. This type of control is what Moaleji and Greig [22] refers to as open-loop adaptive control, a controller is chosen based on predefined cases and control settings. Good knowledge of system and disturbances are therefore required.

Another approach which is used in various research on feedback control of roll motions, such as Fossen [5] is the LQR. This widespread controller is used for what is called "optimal" control in industry. Basically it can be seen as a method to design a state-feedback controller based on minimizing certain cost functions by certain weight factors determined by an engineer. The benefit of this method is that it can aid in the design of a cost-effective control method, which can be build on more than just stability, the disadvantage is that the design parameters have to be chosen, which will make designing an LQR an iterative process, based on the skill of the engineer. For more information on the LQR, Goodwin et al. [7] or any other standard control book can be issued. Since waves are considered a Gaussian process as described by Ochi and Sahinoglu [25], the wave dynamics need to be included in by means of a Kalman filter as described by Katebi et al. [12]. "If not included, the controller will increase the damping of the ships roll at the natural roll frequency, but since roll motion is a consequence of the combined sea disturbance and the response operator of the ship, significant roll motion is commonly found outside the region of natural roll and disturbance rejection of the control is adequate only if the disturbance spectrum is accounted for." Perez and Blanke [29]

### 2.6.2. Feedforward control

Simply speaking a feed-forward control system is a system which is controlled based on the input, the feed. In 2.15 a feed-forward scheme is depicted. The control is based on knowledge of the system. For that reason it is not very robust, the full scale system needs to behave as expected for the controller to function properly. With a system that is highly susceptible to changes in parameters, such as a drillship, other control strategies might prove to be a better option.

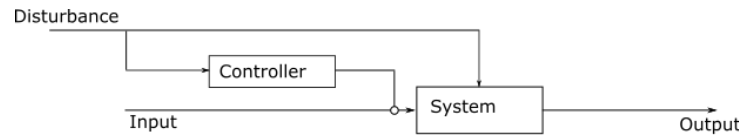


Figure 2.15: Common feed forward scheme

To account for this, different researchers have proposed the used of closed-loop adaptive control, since as Perez and Blanke [29] recognize, one of the key issues in roll motion control is the adaption to the changes in environmental conditions, especially for moving vessels, but different loads and wave conditions, make adaptive control also very feasible for seakeeping purposes. Amerongen et al. [1] used adaptive control techniques to accurately control a vessel in course keeping and course changing dynamics, and improved fuel efficiency by 2%. Moaleji and Greig [22] wrote a quite extensive section on adaptive control to apply on anti-roll tanks. He believes that a ship-tank system cannot efficiently be controlled using any feedback controllers, due to the fact that the time-constant of the actuators is high in comparison to the time-constant of the system to be controlled. Moaleji proposes two novel methods for roll-damping control. The first being a wave-prediction control, which in fact is a feedback control system, that deals with the tardiness of the pump system by predicting the waves in advance by means of an ARX-model. In 2.16 Verifying this by simulations, this method has proven to effectively stabilize roll motions, were other controllers such as PID did not prove to be effective due to the changes in model.

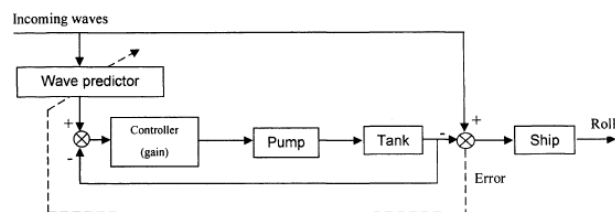


Figure 2.16: Wave prediction control scheme, source: Moaleji and Greig [22]

The second method that he proposes is what the author calls an inverse adaptive controller. This method aims to minimize the difference between the plant output and the filter's input as shown in 2.17. As the plant probably has some delay between input and output, this also needs to be taken into account for the model. Then using a least mean square fit as proposed by Levy [19], the inverse model is updated according to changing system parameters based on the measured error. Moaleji claims that the solution he proposes is able to adapt itself to variations in the plant transfer function without losing its roll reduction performance. Using simulations, Moaleji has proven this method to be the most robust stabilizing method, even exceeding the wave prediction control method.

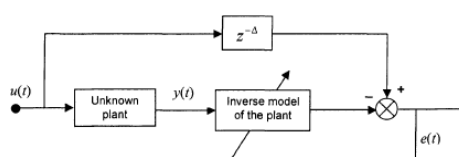


Figure 2.17: Inverse adaptive control scheme, source: Moaleji and Greig [22]

### 2.6.3. Filtering

For state estimation of roll angle and roll velocity, a filter needs to be implemented to filter the wave frequencies, drift or noise that might be present in the signal, as well as any other sensory noise that might be present in the signal. Different types of filters can be used for this purpose. The simplest one being a low-pass filter of which the name describes its function perfectly; only frequencies that are lower than a set value will be passed. Another filter which is commonly used in industry is the Kalman filter according to Perez and Blanke [29]. For example Bishop and Gary [2] describe the principles of such a filter in an understandable manner.

### 2.6.4. Conclusion

Many papers have been written on the subject of the control method for ship roll damping for different control systems. In general, the control strategies can be divided into 2 subcategories, feedback and feedforward control. Both can be divided in subcategories, like cascaded control and optimal control. Feedback control is stable and more robust than is feedforward control, however when properly designed, a feedforward should be faster by definition. One should however be take caution as modeling error can result in catastrophic results.

## 2.7. Computational methods

Different methods are used in literature to describe and model dynamic vessel behavior.

### 2.7.1. Frequency domain models

Common practice in the industry is to analyze the dynamic behavior of offshore structures in the frequency domain. With the assumption of a low wave-steepness, linear waves are assumed. Since ocean waves are not regular waves, it would not suffice to model them as regular waves. Newman [23] had proposed to model waves as a Gaussian meaning a sea state can be described by a superposition of sinusoidal components with random phases and amplitudes. While working in the frequency domain, most researchers assume linear behavior of the offshore structures. By that assumption, the output can also be described as a Gaussian process.

### 2.7.2. Time domain models

When nonlinear effects are of such magnitude that those cannot be neglected, in many instances a non-linear time-domain model is proposed. Such a model is able to cope with many nonlinearities such as viscous damping or radiation forces. Treacle III [42] first created a relatively simple 3-DoF nonlinear model in MOT-SIM to simulate the controlled moving-weight-ship system. Based on this model a classical PID controller was implemented. In a LAMP he implemented the same controller and simulated ship motions in six DoF to verify the results found in the basic model. The results do not match exactly which is attributed to the natural frequency of the servo mechanism. The method proposed by Treacle seems, although accurate, highly time consuming. Different other works, such as St Jago [39], Habing [8] and Taghipour et al. [40] have used time-domain simulations as a method for validation.

### 2.7.3. Hybrid frequency-time domain modeling

A relatively new trend in ship motion models is the use of a hybrid frequency-time domain model, as time-domain simulations with convolution terms are computationally demanding Taghipour et al. [40]. Different identification methods have been proposed in literature to describe the impulse response model for viscous damping, as proposed by Cummins [4]. In most simulation software, the method proposed by Ogilvie [26] is applied, which is in essence estimating the different coefficients for different frequencies. As Perez and Blanke [29] states, hydrodynamic codes based on potential theory compute the coefficients needed for a finite set of frequencies of interest. As these coefficients are frequency dependent, one could imagine why this method will not suffice for every different frequency in the spectrum. Using frequency dependent coefficients, has another downside, as Kristiansen et al. [16] states, it is not straightforward to implement in designing a control system. Taghipour et al. [40] compares different method of identification of the convolution terms in the Cummins equation. Taghipour compares three different methods, focused on the state-space description; impulse response curve fitting, realization theory and regression in the frequency domain. He has found that using these methods, computational time would be less as well as a significant save in memory use. He describes the realization as described by Kristiansen et al. [16] and Yu and Falnes [48] and the regression theory as equally accurate.

**2.7.4. Conclusion**

Choosing a computational method will depend on what the purpose of the model will be. For designing a controller, most authors in literature agree that a frequency domain method, if necessary completed with a state-space representation of the non-linear effects, would be the fastest method. However since not every effect will be captured, validation and verification by a non-linear time-domain simulation will be beneficiary.

# 3

## Analytic study: Dynamic roll compensation

### 3.1. Introduction

An analytic study is executed to compare different concepts of roll motion control as well as to get a feeling for the order of magnitude of roll reduction for regular waves. This study will serve as a justification for the use of an active roll control system as well as a base for validation of more complex models.

### 3.2. Ship modeling

The ship will be modeled in 1 DoF, the roll motion. The ship is modeled as a rigid body with mass  $M$  and mass moment of inertia  $J$ . Restoring forces and damping forces are present which are for this model linearly described as:

$$M_r = -C_{44}\phi \quad (3.1)$$

$$M_d = -B_{44}\dot{\phi} \quad (3.2)$$

Where  $C_{44}$  and  $B_{44}$  are coefficients which have been established by diffraction software. For respectively restoring and damping moments. The excitation can be split into two parts; Firstly, the static heeling moment is induced by moving a mass around by swiveling the on board crane. This moment will depend on the horizontal distance between CoG and the crane tip,  $d$ , as well as on the mass that will be lifted,  $m_{lift}$ .

$$M_{heel} = m_{lift}d \quad (3.3)$$

Secondly, a disturbing moment will act on the ship as a result of the regular wave. This harmonic moment will be described by:

$$M_{harmonic} = M_d \sin(\omega t + \epsilon) \quad (3.4)$$

In which the phase,  $\epsilon$ , is assumed to be equal to zero for regular waves.

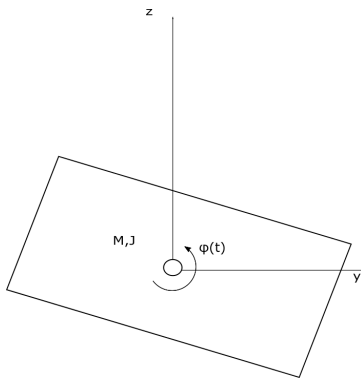


Figure 3.1: Ship model

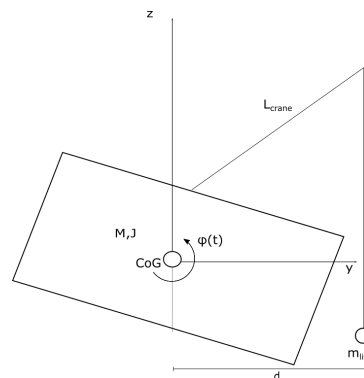


Figure 3.2: Ship model with crane

In 3.1 the simplified ship model is shown. In 3.2, the swiveling crane with mass is added.

What remains for the model are the radiation forces. These forces are a result of the changing fluid momentum as a result of the motion of the hull. Radiation forces proportional to acceleration are called added-mass, in this analytic study they are neglected. Proportional to velocity, the term radiation damping is used in industry. These coefficients are found by diffraction software for this simplified model. For now, non-linear viscous damping is not taken into account.

### 3.3. Modeling of moving mass control system

As found in chapter 2, most on board roll control systems designs are based on the principle of shifting the CoG. This will be modeled by a double pendulum fixed to the ship, with length  $l$ , which is at the endpoint fitted with a point mass. This mass can be controlled by a controlling moment  $M_{control}$  in the hinge of the double pendulum. The angle  $\alpha$  between the rod of length  $l$  and the  $z$ -axis should remain small, to be able to linearize the set of equations. The two rods are assumed rigid and mass less. The control system is modeled by a double pendulum, because:

1. The same mathematics can be re-used for describing the dynamics of the crane with mass attached.
2. No discontinuities have to be taken into account for end-stops of the moving mass. However, angles should remain small, since in reality, movement of the mass is limited, and the pendulum mass  $m$  should not gain too much height in relation to the ship.

In 3.3 this control system is schematically displayed.

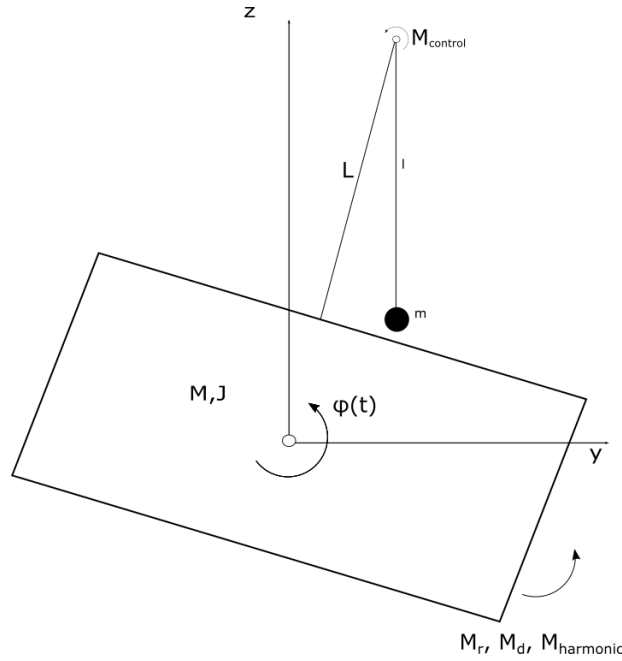


Figure 3.3: Model of ship and control system

#### 3.3.1. Modeling method

With all parameters defined, the equations of motion can be derived. A suitable and elegant method that is used is the Lagrangian method. The Lagrangian is defined by:

$$\mathcal{L} = \mathcal{K} - \mathcal{P} \quad (3.5)$$

Where  $\mathcal{K}$  depicts kinetic energy, and  $\mathcal{P}$  the potential energy.  $Q$  is the generalized force vector. From this the EOM's can be derived by using Lagrange's equation:

$$\frac{d}{dt} \frac{\partial \mathcal{L}}{\partial \dot{q}_s} - \frac{\partial \mathcal{L}}{\partial q_s} = Q_s \quad (3.6)$$

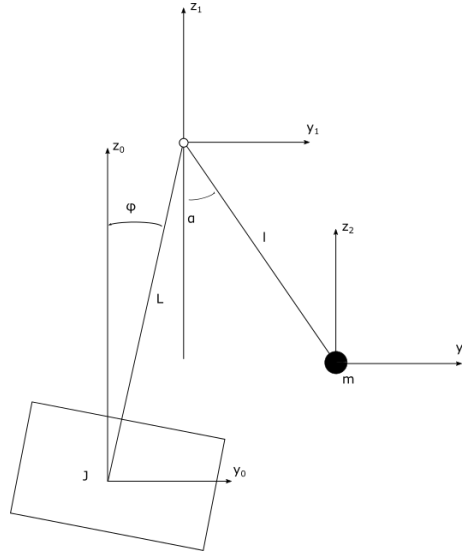


Figure 3.4: Coordinate system for Lagrangian derivation

In 3.4 a schematic drawing is shown of the analytic model. All moments will be interpreted as generalized forces in the derivation of the EOM. The added mass moment of inertia is included in  $J_s$ .

In general kinetic energy is given by:

$$\mathcal{K} = \sum_{s=1}^N \frac{1}{2} m_s v_s^2 \quad (3.7)$$

and potential energy by:

$$\mathcal{P} = \sum_{s=1}^N m_s g h_s \quad (3.8)$$

The next step is to derive the generalize coordinates by using trigonometry.

$$y_0 = z_0 = 0 \quad (3.9)$$

$$y_1 = -L \cdot \sin(\phi) \quad (3.10)$$

$$z_1 = \cos(\phi) \cdot L \quad (3.11)$$

$$y_2 = -L \cdot \sin(\phi) + \sin(\alpha) \cdot l \quad (3.12)$$

$$z_2 = \cos(\phi) \cdot L - \cos(\alpha) \cdot l \quad (3.13)$$

As both  $\alpha$  and  $\phi$  are functions of time, the time derivatives of the above coordinates, i.e. the relevant velocities, can be calculated as follows:

$$\dot{y}_0 = \dot{z}_0 = 0 \quad (3.14)$$

$$\dot{y}_2 = -L\dot{\phi} \cos(\phi) + \dot{\alpha} \cos(\alpha) l \quad (3.15)$$

$$\dot{z}_2 = -\dot{\phi} \sin(\phi) L + \dot{\alpha} \sin(\alpha) l \quad (3.16)$$

Using this results an expression for kinetic and potential energy can be derived:

#### Kinetic Energy

$$\mathcal{K} = \frac{1}{2} m (\dot{y}_2^2 + \dot{z}_2^2) + \frac{1}{2} J_s \dot{\phi}^2 \quad (3.17)$$

$$\mathcal{K} = \frac{1}{2} \dot{\phi}^2 (mL^2 + I_{xx}) - \cos(\phi + \alpha) mL \dot{\phi} \dot{\alpha} + \frac{1}{2} ml^2 \dot{\alpha}^2 \quad (3.18)$$

### Potential Energy

$$\mathcal{P} = mgz_2 \quad (3.19)$$

$$\mathcal{P} = mg(\cos(\phi) \cdot L - \cos(\alpha) \cdot l) \quad (3.20)$$

Using Lagrange's equations (3.6) The following the non-linear EOM's have been derived:

$$(mL^2 + I_{xx})\ddot{\phi} - \cos(\phi + \alpha)mL\ddot{\alpha} + \sin(\phi + \alpha)mL\dot{\alpha}^2 - mgL\sin(\phi) = M_{harmonic} - M_{heel} - C_{44}\phi - B_{44}\dot{\phi} \quad (3.21)$$

$$ml^2\ddot{\alpha} - \cos(-\phi + \alpha)mL\dot{\phi} + mL\sin(\phi + \alpha)\dot{\phi}^2 + mgl\sin(\alpha) = M_{control} \quad (3.22)$$

It is convenient for frequency domain calculations to linearize the given system. Taking only first order terms into account, the following EOM's are found in matrix form:

$$\begin{bmatrix} (mL^2 + I_{xx}) & -mLL \\ -mLL & ml^2 \end{bmatrix} \cdot \begin{bmatrix} \ddot{\phi} \\ \ddot{\alpha} \end{bmatrix} + \begin{bmatrix} B_{44} & 0 \\ 0 & 0 \end{bmatrix} \cdot \begin{bmatrix} \dot{\phi} \\ \dot{\alpha} \end{bmatrix} + \begin{bmatrix} -mgL + C_{44} & 0 \\ 0 & mgl \end{bmatrix} \cdot \begin{bmatrix} \phi \\ \alpha \end{bmatrix} = \begin{bmatrix} M_{harmonic} - M_{heel} \\ M_{control} \end{bmatrix}$$

### 3.3.2. Model verification

As a quick verification, the angles  $\alpha$  and  $\phi$  can be set equal to zero. As a result, respectively the first and second equations should take the form of a single pendulum system. For this set of equations this turns out to be the case. To verify the ship model, a quick check is performed on the natural frequencies of the system. Natural frequencies of a mass spring system can be found by solving:

$$\det(-\omega_n^2 \mathbf{M} + \mathbf{K}) = 0 \quad (3.23)$$

Which means that roll damping is neglected for now. This results in:

$$\det \begin{bmatrix} -mgL + C_{44} - (mL^2 + J_s)\omega_n^2 & mL\omega_n^2 \\ mL\omega_n^2 & mgL - ml^2\omega_n^2 \end{bmatrix}$$

This will lead to 2 values of  $\omega_n$ . The values for  $C_{44}$  and  $I_{xx}$  of Wang [44] are used which are calculated by the use of diffraction software:

$$I_{xx} = 8.61 * 10^9 \text{ kgm}^2, C_{44} = 9.83 * 10^8 \text{ Nm/rad} \quad (3.24)$$

Wang [44] has measured the natural frequency of the Huisdrill to be equal to 18.7 s, or about  $0.34 \frac{\text{rad}}{\text{s}}$

To check if at least the ship model of the Huisdrill is in compliance with this, the pendulum system is neglected. Leading to:

$$I_{xx}\ddot{\phi} + C_{44}\phi = 0 \quad (3.25)$$

Now the natural frequency is found as:

$$\omega_n = \sqrt{\frac{C_{44}}{I_{xx}}} = \sqrt{\frac{9.83 * 10^8}{8.61 * 10^9}} = 0.34 \text{ rad/s} \quad (3.26)$$

### 3.3.3. Conclusion

The natural frequency of the model corresponds to the measured value of the Huisdrill. In terms of verification, both systems can be both described as a single pendulum system which solutions are commonly found in literature. The mass and stiffness matrix are both symmetric which is as expected, the damping matrix is symmetric which is not necessary, but nevertheless convenient.

By validating the ship model, and verifying the double pendulum model, It will be assumed for now that the model can be used for initial estimation of control system performance.

## 3.4. Modeling of gyroscopic control system

The control moment of the gyroscopic control system is generated by conservation of angular momentum Perez and Steinmann [31]. For roll control a twin-gyroscopic system is best to be used, since this will prevent a pitching momentum. Then assuming constant spinning velocity  $\omega_{spin}$  of the gyroscopes, we are able to derive the roll EOM's.

### 3.4.1. Modeling method

Similar to the double pendulum model, the ship model with a gyroscope is found to be

$$J_s \ddot{\phi} + B_s \dot{\phi} + C_s \phi = M_{harmonic} - M_g - M_{heel} \quad (3.27)$$

This gyroscopic force is dependent on the precession rate  $\dot{\psi}$  and angle  $\psi$  which is the rotation of the twin gyroscope around the sway axis, as well as the angular momentum of the rotating object which is described by:

$$K_g = \omega_{spin} J_{spin} \quad (3.28)$$

The simplified gyroscopic model of Perez and Steinmann [31] will be adapted in this paper. It should be noted that the model is based on certain simplifications, such as the neglecting of the moment of inertia of the gyro for the roll motion. For one-degree of freedom for the the vessel and the a model of the gyroscope this will lead to a non-linear second-order system in which n is the number of spinning discs. In 3.5 a schematic

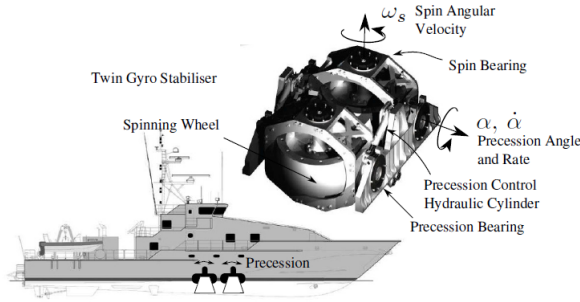


Figure 3.5: Model of ship and gyro control system Perez and Steinmann [31]

is shown of the gyroscopic control system. The roll angle vector is perpendicular to the spin and precession vector. A torque  $T_{precess}$  can be applied to control the roll movements of the vessel. The equations for the ship combined with the above system are as follows:

$$I_{xx} \ddot{\phi} + B_{44} \dot{\phi} + C_{44} \phi = M_{harmonic} - nK_g \dot{\psi} \cos(\psi) - M_{heel} \quad (3.29)$$

$$J_g \ddot{\psi} + C_g \dot{\psi} + B_g \psi = K_g \dot{\phi} \cos(\psi) + T_{precess} \quad (3.30)$$

In matrix notation:

$$\begin{bmatrix} I_{xx} & 0 \\ 0 & J_g \end{bmatrix} \cdot \begin{bmatrix} \ddot{\phi} \\ \ddot{\psi} \end{bmatrix} + \begin{bmatrix} B_{44} & nK_g \cos(\psi) \\ -K_g \cos(\psi) & B_g \end{bmatrix} \cdot \begin{bmatrix} \dot{\phi} \\ \dot{\psi} \end{bmatrix} + \begin{bmatrix} C_{44} & 0 \\ 0 & C_g \end{bmatrix} \cdot \begin{bmatrix} \phi \\ \psi \end{bmatrix} = \begin{bmatrix} M_{harmonic} - M_{heel} \\ T_{precess} \end{bmatrix}$$

When the cosine term is linearized:

$$\cos(\psi) \approx 1 \quad (3.31)$$

The linearized matrices are given below:

$$\begin{bmatrix} I_{xx} & 0 \\ 0 & J_g \end{bmatrix} \cdot \begin{bmatrix} \ddot{\phi} \\ \ddot{\psi} \end{bmatrix} + \begin{bmatrix} B_{44} & nK_g \\ -K_g & B_g \end{bmatrix} \cdot \begin{bmatrix} \dot{\phi} \\ \dot{\psi} \end{bmatrix} + \begin{bmatrix} C_{44} & 0 \\ 0 & C_g \end{bmatrix} \cdot \begin{bmatrix} \phi \\ \psi \end{bmatrix} = \begin{bmatrix} M_{harmonic} - M_{heel} \\ T_{precess} \end{bmatrix}$$

### 3.4.2. Model verification

The mass and stiffness matrices are symmetric, which is as expected. The damping matrix is not, but that is merely a choice of roll angle, and second to that not a requisite.

To verify the ship model, a quick check is performed on the natural frequencies of the system. Using:

$$\det(-\omega_n^2 \mathbf{M} + \mathbf{K}) = 0 \quad (3.32)$$

Which means that roll damping is neglected for now. This results in two uncoupled equations. If we calculate the natural frequency for the ship again, using the same parameters, which are used before the natural frequency turns out to be:

$$\omega_n = \sqrt{\frac{C_{44}}{I_{xx}}} = \sqrt{\frac{9.83 * 10^8}{8.61 * 10^9}} = 0.34 rad/s \quad (3.33)$$

Which is what it should be.

### 3.4.3. Conclusion

The simplified model used by Perez and Steinmann [31] is shortly explained in this section. It will be used for base calculations of roll control systems with a gyroscope, the model seems to be a good approximation at first.

### 3.5. State-space description

The properties of the proposed control systems should be investigated, properties such as stability, controllability, observability and robustness are of interest before designing a control system. From earlier model tests, for the moving mass system, NMP behavior was detected. This should be taken into account in controller design and parameter choice.

For control purposes, the systems are represented in state-space, as shown in 3.6. Where  $\mathbf{A}$ ,  $\mathbf{B}$ ,  $\mathbf{C}$  &  $\mathbf{D}$  rep-

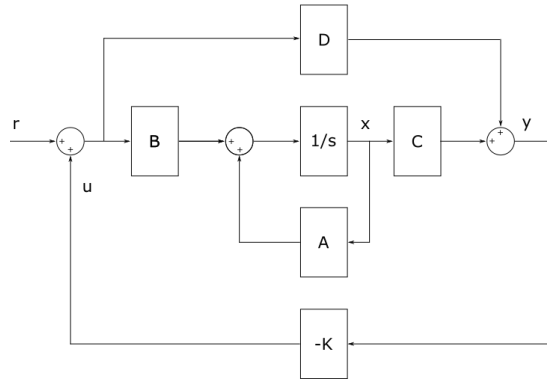


Figure 3.6: State space with output feedback scheme

resent system matrices and where  $\mathbf{K}$  represents the output controller.

Now if we choose the state vector as:

$$x_{dp} = \begin{bmatrix} \phi \\ \alpha \\ \dot{\phi} \\ \dot{\alpha} \end{bmatrix} \quad (3.34)$$

An the input vector as:

$$u_{dp} = \begin{bmatrix} (M_{harmonic} - M_{heel}) \\ M_{control} \end{bmatrix} \quad (3.35)$$

We can represent the double pendulum system as:

$$\dot{x}_{dp} = \mathbf{A}x_{dp} + \mathbf{B}u_{dp} \quad (3.36)$$

$$y_{dp} = \mathbf{C}x_{dp} + \mathbf{D}u_{dp} \quad (3.37)$$

With:

$$\mathbf{A} = \begin{bmatrix} \mathbf{0} & \mathbf{I} \\ \mathbf{M}^{-1}\mathbf{K} & \mathbf{M}^{-1}\mathbf{C} \end{bmatrix}, \mathbf{B} = \begin{bmatrix} \mathbf{0} \\ \mathbf{M}^{-1}\mathbf{F} \end{bmatrix}, \mathbf{C} = \mathbf{I}_{4 \times 8}, \mathbf{D} = \mathbf{0} \quad (3.38)$$

With  $\mathbf{M}$ ,  $\mathbf{C}$  and  $\mathbf{K}$  being the mass, damping and spring matrices, and  $\mathbf{F}$  being the forcing vector of the system. Represented in state-space form this will be:

$$\begin{bmatrix} \dot{\phi} \\ \dot{\alpha} \\ \ddot{\phi} \\ \ddot{\alpha} \end{bmatrix} = \begin{bmatrix} 0 & 0 & 1 & 0 \\ 0 & 0 & 0 & 1 \\ \frac{mgL - C_{44}}{I_{xx}} & -\frac{mgL}{I_{xx}} & -\frac{B_{44}}{I_{xx}} & 0 \\ \frac{L(mgL - C_{44})}{I_{xx}} & -\frac{L(mgL + I_{xx})}{I_{xx}} & -\frac{LB_{44}}{I_{xx}} & 0 \end{bmatrix} \cdot \begin{bmatrix} \phi \\ \alpha \\ \dot{\phi} \\ \dot{\alpha} \end{bmatrix} + \begin{bmatrix} 0 & 0 \\ 0 & 0 \\ \frac{1}{I_{xx}} & \frac{L}{I_{xx}} \\ \frac{L}{I_{xx}} & \frac{(L^2 m + I_{xx})g}{I_{xx}^2 m} \end{bmatrix} \cdot \begin{bmatrix} (M_{harmonic} - M_{heel}) \\ M_{control} \end{bmatrix} \quad (3.39)$$

And:

$$y_{dp} = [\mathbf{I}_{4 \times 4}] \cdot \begin{bmatrix} \phi \\ \alpha \\ \dot{\phi} \\ \dot{\alpha} \end{bmatrix} \quad (3.40)$$

Using a similar method, such a state-space representation can also be created for the gyroscopic system, using the following state vector:

$$x_g = \begin{bmatrix} \phi \\ \psi \\ \dot{\phi} \\ \dot{\psi} \end{bmatrix} \quad (3.41)$$

The state equations for the gyroscopic system are described by:

$$\begin{bmatrix} \dot{\phi} \\ \dot{\psi} \\ \ddot{\phi} \\ \ddot{\psi} \end{bmatrix} = \begin{bmatrix} 0 & 0 & 1 & 0 \\ 0 & 0 & 0 & 1 \\ -\frac{C_{44}}{I_{xx}} & 0 & -\frac{B_{44}}{I_{xx}} & -\frac{nK_g}{I_{xx}} \\ 0 & -\frac{C_g}{J_g} & \frac{K_g}{J_g} & -\frac{B_g}{J_g} \end{bmatrix} \cdot \begin{bmatrix} \phi \\ \psi \\ \dot{\phi} \\ \dot{\psi} \end{bmatrix} + \begin{bmatrix} 0 & 0 \\ 0 & 0 \\ \frac{1}{I_{xx}} & 0 \\ 0 & \frac{1}{J_g} \end{bmatrix} \cdot \begin{bmatrix} M_{harmonic} - M_{heel} \\ T_{precess} \end{bmatrix} \quad (3.42)$$

And:

$$y_g = [\mathbf{I}_{4 \times 4}] \cdot \begin{bmatrix} \phi \\ \psi \\ \dot{\phi} \\ \dot{\psi} \end{bmatrix} \quad (3.43)$$

### 3.6. Estimation of parameters for Huisdrill P10000 case study

In order to be able to apply a realistic numeric study on this model, parameters should be derived. As there is very little to no information on both models, a study on parameter magnitude is done for both models.

#### 3.6.1. Double pendulum model parameters

Choosing the double pendulum model enables the possibility to approximate a curved track as well as a flat trajectory for the moving mass. However choosing this model will add an additional natural frequency to the system, the pendulum length should therefore be carefully chosen, as  $\omega_n = \sqrt{\frac{g}{l}}$ . In this report a pendulum with the same natural frequency of the vessel is chosen, as this will represent a passive anti-roll tank most accurately.

With a maximum trajectory length  $b$  of 39m (the vessel breadth), the circle equation can be used to derive the height of the pendulum at the end stops, as we do not want the pendulum mass to go overboard. In 3.7 this is explained graphically

$$y^2 + (z - l)^2 = l^2 \quad (3.44)$$

It turns out to be that the height  $h$  is about 2.2m at the end stops, which is a reasonable for a curved track

In 3.1 the vessel parameters for roll are shown, in 3.2 are listed.

Parameter	Value	Unit	Description
$m_{ship}$	5.19e7	kg	Based on Wang [44]
$I_{xx}$	8.61e09	$kgm^2$	Based on Wang [44]
$B_{44}$	3e7	$Nms/rad$	Based on Wang [44]
$C_{44}$	9.83e8	$Nm/rad$	Based on Wang [44]

Table 3.1: Ship and general parameters

#### 3.6.2. Gyroscopic model parameters

The gyroscopic parameters are based on the weight of the gyroscope. In different papers, for example Perez and Steinmann [31], a gyroscope with a weight of approximately 3.5 % of the ship displacement is proposed.

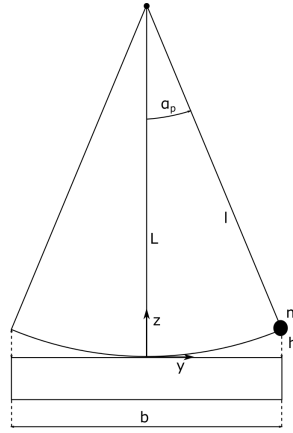


Figure 3.7: Schematic of pendulum length and angle derivation

Parameter	Value	Unit	Description
l	84.37	m	Based on natural frequency of the vessel
L	l+1	m	Based on natural frequency of the vessel
m	0.01M <sub>s</sub>	kg	Initial value is 1% of ship displacement.

Table 3.2: Moving mass parameters

Further specifications are usually not given. Therefore for an initial design some parameters are to be estimated. It should be kept in mind that this is an initial estimation, the definite sizing of the gyroscopic system is part of the design process, and therefore more or less a choice.

As stated before, the angular momentum is calculated by:

$$K_g = \omega_{spin} J_{spin} \quad (3.45)$$

This parameter should be maximized, since it depicts the coupling between the different systems as is shown in equation 3.31. In this expression:

$$J_{spin} = \frac{\pi \rho h D^4}{32} \quad (3.46)$$

And  $\omega_{spin}$  is the angular velocity in  $\frac{rad}{s}$ . The volume of the disc is based on the mass, and is given by:

$$V_{disc} = \frac{\pi D^2 h}{4} \quad (3.47)$$

$$m_{disc} = \rho_{steel} \frac{\pi D^2 h}{4} \quad (3.48)$$

For basic design, it will be assumed that normal construction steel is used, with density  $\rho_{steel}$  of  $7800 \text{ kg/m}^3$  and an elastic stress  $\sigma_{max} = 250 \text{ MPa}$ , is used for the gyroscope discs.

As can be seen from the equations, the design of such a gyroscope is mainly dependent on available space and the properties of the materials which are used for the discs.

When the above equations are rewritten, the following result is obtained.

$$h = \frac{4m_{disc}}{\pi D^2 \rho_{steel}} \quad (3.49)$$

If  $m_{disc}$  is taken as  $\frac{1}{2} M_g$ , when two discs of equal size are assumed together with a massless frame.

If the mass and material is known, it is a design choice how to dimension the gyroscopic discs. In this case study:

$$h = 4m, D = 6m \quad (3.50)$$

Now with:

$$\sigma_{max} = \frac{1}{4} \omega_{spin}^2 D^2 \rho_{steel} \quad (3.51)$$

Where  $\sigma_{max}$  is the elastic limit of steel. The maximum angular velocity is found as  $60 \frac{rad}{s}$ . Finally, the angular momentum  $K_g$  is estimated as:

$$K_g = 2.36 \cdot 10^8 \quad (3.52)$$

When it is assumed that the gyroscopic discs rotate around their CoG,  $C_G$  should equal 0.  $J_g$  can be calculated by the standard formula for the moment of inertia for a cylinder;

$$J_g = \frac{m_{disc}}{12} (\frac{3}{4} D^2 + h^2) \quad (3.53)$$

$B_g$  is assumed to be zero, i.e. the friction in the bearings is neglected.

A spring constant can be introduced for the gyroscope by choosing the height of the center of rotation of the gyroscope. It turns out to be beneficial to have such a constant to let the angle  $\psi$  of the gyroscope return to 0 without having to control for this. In 3.8 it can be seen how the moments change when there is a rotation. For small angles a spring constant is based on the change in volume and thus mass. This constant  $C_g$  is found to be  $5e5(Nm/rad)$

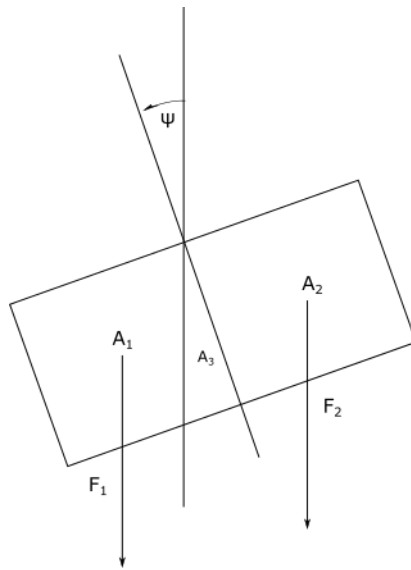


Figure 3.8: Explanation pendulum effect

Parameter	Value	Unit	Description
$m_g$	$9.1 \cdot 10^5$	$kg$	Mass of gyroscope
$J_g$	$3.26 \cdot 10^6$	$kgm^2$	Mass moment of inertia around the precession angle
$J_{spin}$	$3.97 \cdot 10^6$	$kgm^2$	Mass moment of inertia of a single spinning wheel around it's center.
$B_g$	0	$Nms/rad$	Gyroscope damping constant due to friction in the precession bearing.
$C_g$	$2.5e5$	$Nm/rad$	Gyroscope spring constant
$\omega_{spin}$	60	$rad/s$	Angular velocity of gyroscope
$K_g$	$2.36 \cdot 10^8$	$kgm^2/s$	Gravity constant

Table 3.3: Gyroscope parameters

## 3.7. System properties

Now that the parameters are estimated, checks can be done on the control properties of both systems.

### 3.7.1. Pole-zero plots

In figure 3.9 the pole-zero map of the vessel is shown. As there are no poles in the real positive domain, the system is stable for these parameters as follows from common control theory.

In figure 3.10 the pole-zero map of the ship with pendulum is drawn. It can be seen that this system is again stable. The imaginary part of the poles is shifted to just above and just below the original placement. This will lead to 2 resonance peaks just below and just above the original peak. 2 new resonance peaks are formed, at different frequencies from the original ship system.

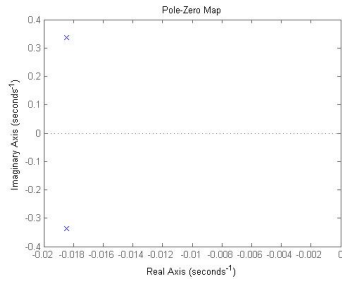


Figure 3.9: Pole plot Huisdrill P10000

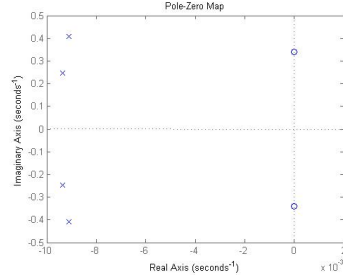


Figure 3.10: Pole plot Huisdrill P10000 with double pendulum

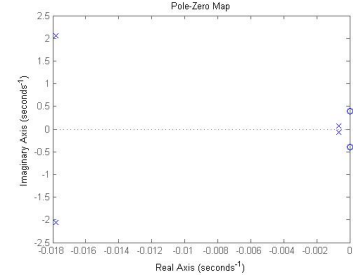


Figure 3.11: Pole plot of Huisdrill P10000 with gyroscope

In figure 3.11 the poles and zero's are shown of the ship with the gyroscopic damping system. The system is again stable and non minimum phase behavior is not present.

### 3.7.2. Bode plot

A bode plot is the frequency characteristic of a given system. It is given in terms of magnitude and phase. The bode-plots given, show the vessel's roll angle of the vessel on the y-axis and the environmental moment on the vessel on the logarithmic x-axis. In figure 3.12, the roll-roll frequency characteristic of the vessel without any form of compensation is shown.

In figure 3.13 the roll motion of the Huisdrill is shown when the double pendulum system is present. Two resonance peaks are now present were in the original system there was only one. By inspecting this plot, it is apparent that the model does not accurately approximates the sliding mass model, as 2 new natural frequencies appear. This is due to the 'spring' force introduced by the pendulum dynamics, a sliding mass would not introduce this behavior, except for when a spring is added.

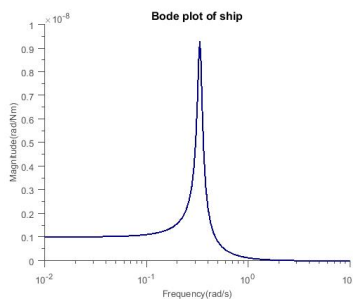


Figure 3.12: Bode plot of Huisdrill P10000 roll motion without additional compensation systems

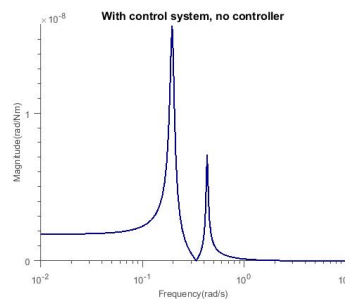


Figure 3.13: Bode plot of Huisdrill P10000 roll motion with the double pendulum compensation systems

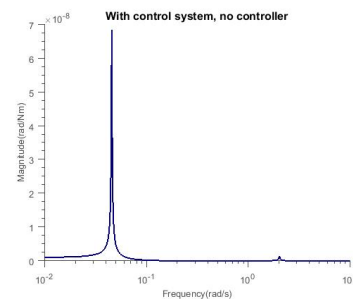


Figure 3.14: Bode plot of Huisdrill P10000 roll motion with a gyroscopic compensating system

### 3.7.3. Controllability

Controllability of a system is an important property in control system designs. A check commonly used is to verify if the controllability matrix is full rank. This matrix for LTI-systems is in general calculated by:

$$W_r = [B \quad AB \quad A^2B \quad \dots \quad A^{n-1}B] \tag{3.54}$$

For the double pendulum system this leads to:

$$W_{r,dp} = \begin{bmatrix} 0 & 0 & 0 & 1 \\ 0 & 0 & 1 & -\frac{B_{44}}{I_{xx}} \\ 0 & 1 & -\frac{L^2 gm}{I_{xx}} - \frac{Lmg}{I_{xx}} - \frac{g}{l} - \frac{C_{44}}{I_{xx}} + \frac{B_{44}^2}{I_{xx}^2} & -\frac{L^2 gm}{I_{xx}} - \frac{Lmg}{I_{xx}} - \frac{g}{l} - \frac{C_{44}}{I_{xx}} + \frac{B_{44}^2}{I_{xx}^2} \\ 1 & -\frac{B_{44}}{I_{xx}} & -\frac{L^2 gm}{I_{xx}} - \frac{Lmg}{I_{xx}} - \frac{g}{l} - \frac{C_{44}}{I_{xx}} + \frac{B_{44}^2}{I_{xx}^2} & \frac{B_{44}(2L^2 mg I_{xx} + 2mg l I_{xx} + g I_{xx}^2 + 2C_{44} l I_{xx} - B_{44}^2 l)}{I_{xx}^3 l} \end{bmatrix} \quad (3.55)$$

And for the the gyroscopic system this gives:

$$W_{r,g} = \begin{bmatrix} 0 & 0 & 0 & 1 \\ 0 & 0 & 1 & -\frac{B_g}{J_g} - \frac{B_{44}}{I_{xx}} \\ 0 & 1 & \frac{B_g}{J_g} + \frac{B_{44}}{I_{xx}} & -\frac{K_g^2 n}{I_{xx} J_g} - \frac{B_g B_{44}}{I_{xx} J_g} - \frac{C_g}{J_g} - \frac{C_{44}}{I_{xx}} + \left(\frac{B_g}{J_g} + \frac{B_{44}}{I_{xx}}\right)^2 \\ 1 & \frac{B_g}{J_g} + \frac{B_{44}}{I_{xx}} & -\frac{K_g^2 n}{I_{xx} J_g} - \frac{B_g B_{44}}{I_{xx} J_g} - \frac{C_g}{J_g} - \frac{C_{44}}{I_{xx}} + \left(\frac{B_g}{J_g} + \frac{B_{44}}{I_{xx}}\right)^2 & -\frac{\xi}{I_{xx}^3 J_g^3} \end{bmatrix} \quad (3.56)$$

with:

$$\xi = -2B_g I_{44}^2 J_g K_g^2 n - 2B_{44} I_{44} J_g^2 K_g^2 n + B_g^3 I_{44}^3 + B_g^2 B_{44} I_{44}^2 J_g + B_g B_{44}^2 I_{44} J_g^2 - 2B_g C_g I_{44}^3 * J_g - B_g C_{44} J_g^2 J_g^2 + B_{44}^3 J_g^3 - B_{44} C_g I_{44}^2 J_g^2 - 2B_{44} C_{44} I_{44} \quad (3.57)$$

As both matrices have rank 4(full rank), it can be concluded that both systems are controllable by full state feedback.

### 3.7.4. Verification

To verify if the linearization step was allowed, a quick check can be performed. Remembering the criterion for linearization; small angles of  $\phi$  are required. Using a wave amplitude of  $9.93 \cdot 10^6 Nm$ , found by the use of diffraction software for the natural frequency, it is found that the assumption of small angles of  $\phi$  is valid for all frequencies of the uncompensated ship, since -161dB is a magnification of  $8.9 \cdot 10^{-9}$ . With the given moment for the resonance frequency, this leads to an angle of 0.09 rad, or 5.1 degrees, which is acceptable for this assumption.

As a last check to verify if the combined system behaves as it should, a pendulum with the same natural frequency as the vessel is tested. With the pendulum of length of 84.37 m, the two systems should cancel each others movement. As is shown in 3.13 this is indeed the case at the natural frequency of  $0.34 \frac{rad}{s}$ . The amplification at this frequency is  $5 \cdot 10^{-25}$ . It is shown however, that this behavior comes at a cost of amplification at different frequencies. Therefore the controller should be designed in such a way that the curve is flattened, and that peaks are not near common excitation frequencies as found in a wave-spectrum.

## 3.8. Controller design

Remembering the general state-space feedback scheme depicted in figure 3.6 an update state-space scheme can be derived now. As the roll angle is preferably zero, the reference input is always zero, as well as matrix **D**. The output  $u_2$  of controller **K** is for now defined as  $M_{control}$  and  $T_{precess}$  for respectively the double pendulum and gyroscopic control system. A graphical representation of this is found in figure 7.8. In this figure  $u_1$  is the disturbance, described earlier as  $M_{harmonic} - M_{heel}$ .

As

$$\mathbf{C} = \mathbf{I} \quad (3.58)$$

And

$$u_2 = M_{control}, u_2 = T_{precess} \quad (3.59)$$

For respectively the double pendulum system, and the gyroscopic control system.

A controller is to be designed for types of control systems. Loop shaping is used to create a favorable open loop frequency domain response. The open loop response  $L(j\omega)$  is defined as the product of the system with the controller, so that:

$$L(j\omega) = H(j\omega)C(j\omega) \quad (3.60)$$

With  $H(s)$  being the transfer function from control input to output  $\alpha$  (the angle of the pendulum with the z-axis). The sensitivity function is defined as:

$$S(j\omega) = \frac{1}{1 + L(j\omega)} \quad (3.61)$$

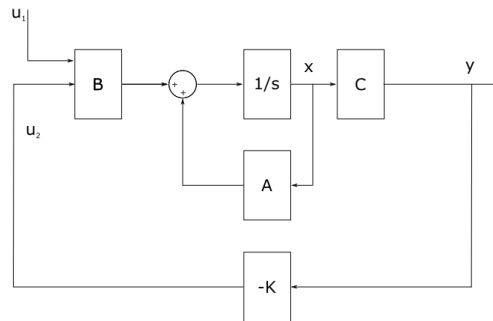


Figure 3.15: State space with output feedback scheme

And the complementary sensitivity function:

$$T(j\omega) = \frac{L(j\omega)}{1 + L(j\omega)} \quad (3.62)$$

The sum of  $S(j\omega)$  and  $T(j\omega)$  should be 1. From control theory, it follows that for disturbance rejection at low frequencies,  $S(j\omega)$  should be small, where  $T(j\omega)$  should be close to 1 meaning the loop gain  $L(j\omega)$  should be high in the low frequency region. In the crossover region, where  $L(j\omega)$  crosses 0 dB, or 1 a filter should be used to damp resonant modes as well as a good phase margin (PM). At high frequencies,  $T(j\omega)$  should be small, and  $S(j\omega)$  should be close to 1 to decrease sensitivity for high frequency sensor noise. The process of loop shaping is a process of trial and error.

### 3.8.1. Double Pendulum Controller

The goal of adding the control system is to add damping to the system in order to reduce roll motions and thereby increasing workability of the vessel. Therefore the aim is to remove resonance peaks from the response curve, i.e. flattening the curve. It is observed if 3.12 and 3.13 are compared that there is no real improvement, except for the damping at natural frequency of the vessel. This comes at the cost of adding an additional peak. This fact is what caused the design of Cremieu to fail in practice, while in theory significant reductions were achieved. An active controller can overcome is needed to mitigate this behavior.

In 3.17 the designed controller is shown as a Bode magnitude characteristic. It is tuned in such a way that  $L(s)$ , shown in 3.16 is nearly flat for low frequencies. The controller consists of 2 lag-compensators in series with a notch filter. The notch filter is used to damp the resonance peaks. The 2 lag-compensators are used to decrease sensitivity to high frequency noise. Mathematically the controller is described as:

$$K(s) = K_p \frac{s^2 + 2\beta_1\omega_1 s + \omega_1^2}{s^2 + 2\beta_2\omega_2 s + \omega_2^2} \frac{1}{\tau_1 s + 1} \frac{1}{\tau_2 s + 1} \quad (3.63)$$

In 3.18 three different bode plots of transfer functions from disturbing moment to roll angle are shown. It can be seen that for low frequencies the magnification of the disturbing moment is increased by adding a control system. This is due to the fact that the pendulum angular velocity is controlled to be 0, leading to no active correction on the roll angle of the vessel, only to damping. For heeling this unwanted, meaning that this controller is unfit for that purpose. At intermediate frequencies, the controller shows great improvement compared to the original system, as there is a much lower resonance peak. At higher frequencies, the active control shows behavior which is less favorable. This should not be an issue as the wave-spectrum does not contain waves of such high frequencies. Expressed in RRR, which is explained later, there is a reduction of a staggering 84% or 16dB.

In 3.19 the response to an initial angle  $\phi$  of 0.1 rad or 5.7 deg is plotted for 3 different systems. It should be noticed that adding the control system, with no additional control actually decreases the system performance. Safety measures should therefore be in place, in case the control system fails. The uninterrupted line shows the response of the system with an active controller. It is obvious significant improvement in response

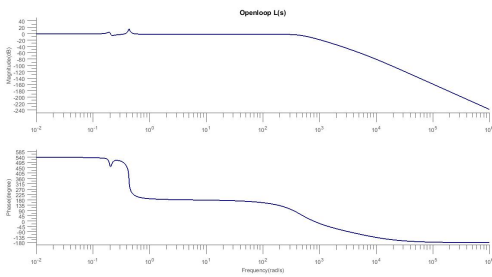


Figure 3.16: Open loop Bode plot

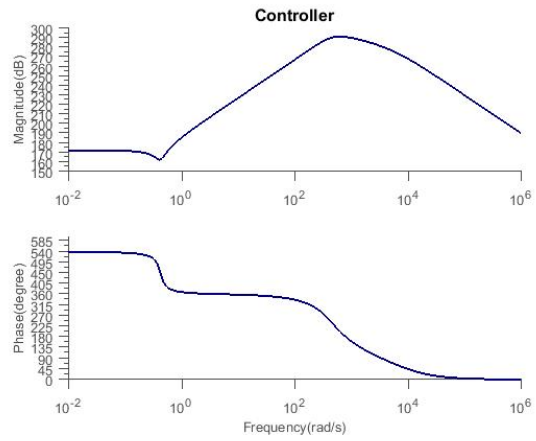


Figure 3.17: Controller Bode plot

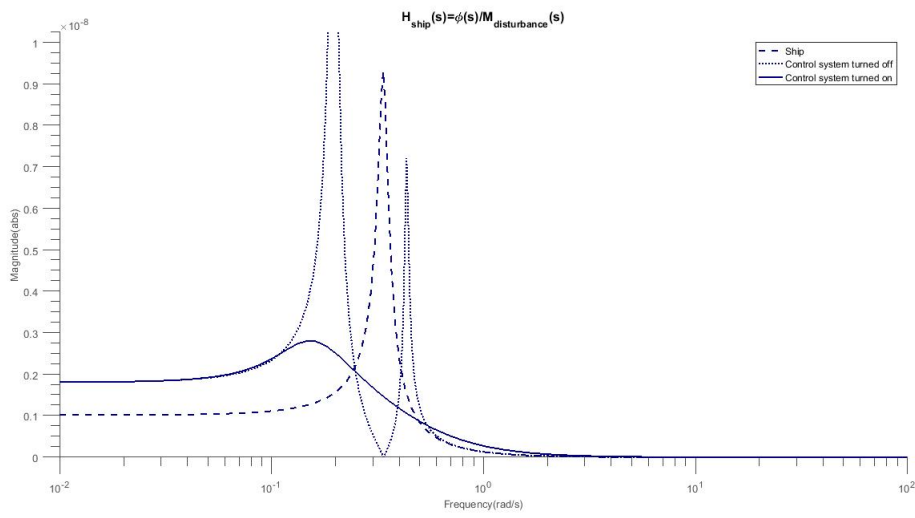


Figure 3.18: Bode plot of controlled and uncontrolled frequency response

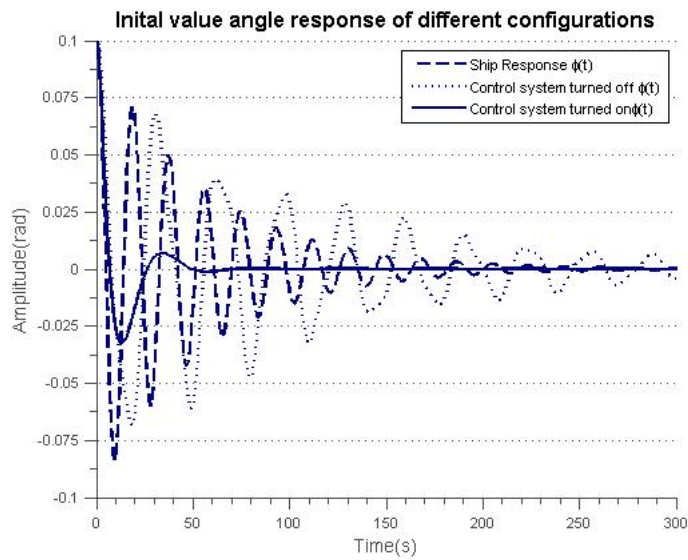


Figure 3.19: Initial value response to an angle of 0.1 rad

time is obtained using the proposed controller. Equilibrium is achieved well below 100 seconds, where the ship without any control is still oscillating after 250 seconds.

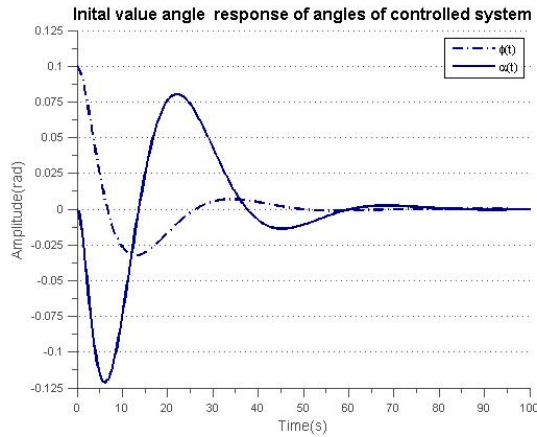


Figure 3.20: Open loop Bode plot

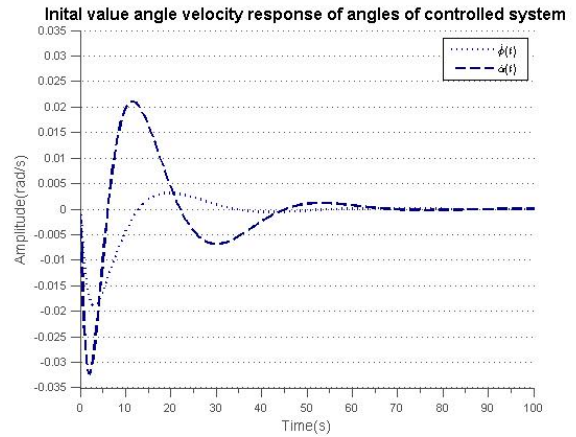


Figure 3.21: Controller Bode plot

In 3.20 the angle of the pendulum and that of the vessel are shown in one plot. It is seen that due to a shift in phase, both systems are damped. A similar result is seen in 3.21 for the velocity response to the initial displacement. Both angle and velocity return to zero quite nicely. No additional integral action required as there is no steady state error due to the inherently stable system around  $\phi = 0rad$  as there is no external moment acting on the vessel.

Remembering equation 3.12 a non-linear expression for the horizontal distance between the *CoG* of the vessel and the *CoG* of the pendulum mass was derived. Under the assumption of small angles, this may be linearized. The deviation is thus expressed as:

$$d = -\phi * L + \alpha * l \tag{3.64}$$

The result for an initial angle of  $0.1rad$  is shown in 3.23. This is an important result as the maximum deviation should not exceed half of ship breadth at any time. As is seen from the graph, for the initial value response, this is not the case for the initial value of  $0.1rad$ .

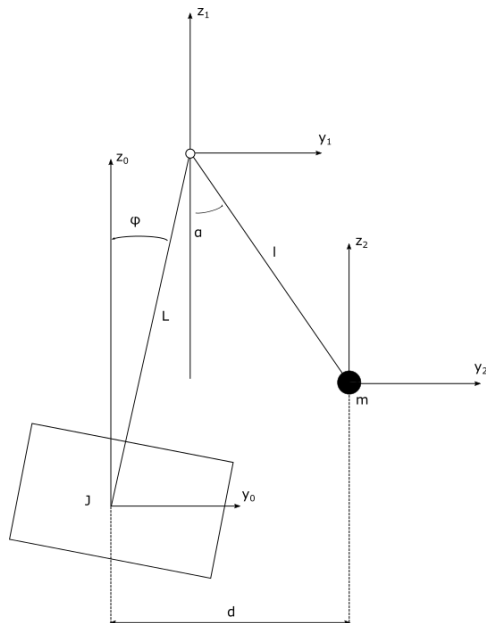


Figure 3.22: Schematic for deviation explanation

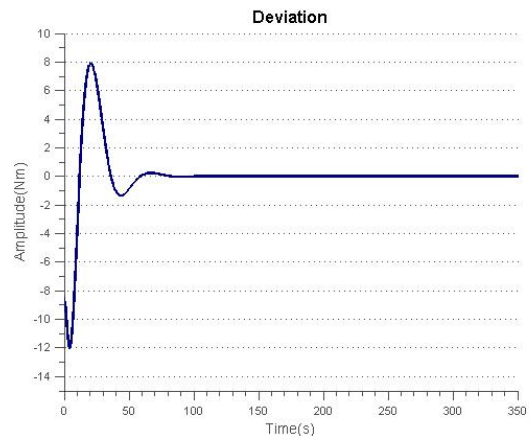


Figure 3.23: Initial value response plot

As a conclusion to the controller design of the double pendulum system a time domain simulation is

plotted. The forcing function in this case is:

$$M_{harmonic} = 9.93e6 * \sin(0.34t) \quad (3.65)$$

Which indeeds corresponds to the frequency and moment amplitude at the natural frequency of the vessel. Initial conditions are 0. Looking at 3.24 it can be observed that angles  $\phi$  and  $\alpha$  increase the first 50 seconds after which a steady state response is achieved. As with the initial value response,  $\alpha$  lags  $\phi$  by which means the ship roll motion is damped. In 3.25 the time domain response to the same forcing function is plotted.

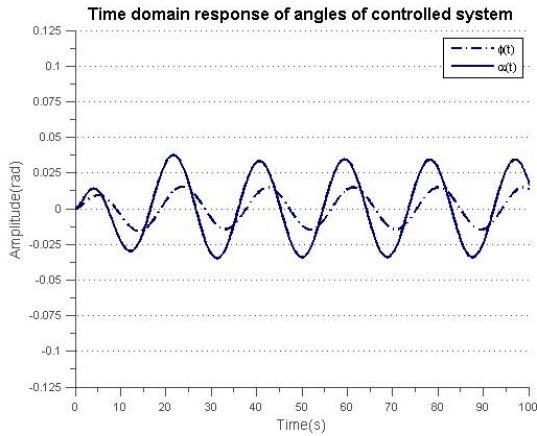


Figure 3.24:  $\alpha$  and  $\phi$  as a function of time

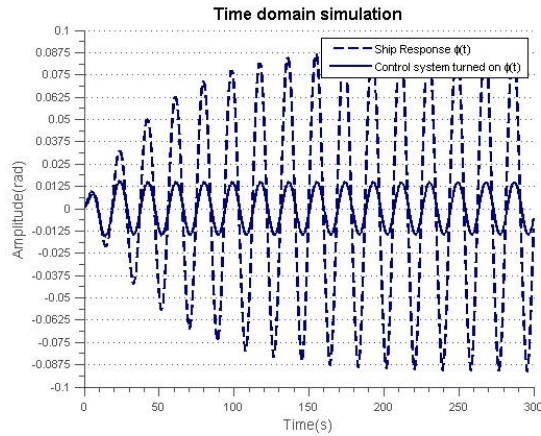


Figure 3.25: Huisdrill P10000 with and without active control

After steady state is reached, the angle  $\phi$  of the uncontrolled ship has an amplitude of about  $0.09 \text{ rad}$ , were the ship with controller does not exceed a maximum angle of  $0.02 \text{ rad}$ . This corresponds to the 80% reduction found by comparing the Bode-plots of both systems.

### 3.8.2. Gyroscope control

As well as for the double-pendulum control-system, the goal of adding a twin disc gyroscope is to add damping to the ship roll motion. Designing a highly advanced controller is not the scope of this research, first a PID-controller is implemented. For the gyroscopic control system, the well known PID-controller is implemented. In the classical form the PID-controller is known in the Laplace domain as:

$$u_2(s) = K_{p,g}e(s) + \frac{1}{s}K_{i,g}e(s) + \frac{K_{d,g}s}{\tau_{d,g}s + 1}e(s) \quad (3.66)$$

Where  $e(s)$  is the error signal. As there is no reference input, the error signal can, depending on the user's choice be  $\phi(t)$  (the ship roll angle) or  $\psi(t)$  (the precession angle). By definition of a PID-controller, the controlling torque is applied based on the error in angle, velocity or accumulated position error of the chosen angle. The time constant  $\tau$  is present to reduce the impact of high frequency noise for the derivative term in the *PID* controller by not increasing the magnification at higher frequencies.

In 3.27 the frequency characteristic of the ship-gyroscope system is shown as a Bode-plot. Compared to the Bode plot of just the ship, shown in 3.26, three things stand out; a second resonance peak is formed, a negative resonance is present and the phase diagram has 3 jumps instead of one. This second peak is formed due to the fact that there is a small spring constant, which makes the system more or less behave like the double-pendulum control system. The main difference here is the difference in frequencies. The first natural frequency is very low, where the second peak is at about 3 rad/s. This might induce strange behavior of the combined-ship gyro system with no active control.

The main goal as stated above is to add damping to the system. Therefore it is interesting to design just a derivative controller at first. By root locus methods, the gain is found to be  $2.43e74$ . A time constant  $\tau$  of 0.1 is found by inspecting the bode-plot of the combined system. A derivative controller is created using this parameters. A bode plot of this controller is found in 3.29

The new system behavior is plotted together with the old system in 3.28. It is shown that improvements are significant. One major flaw in using only derivative control is the fact that there is no 'price' put on large angles of  $\psi$ . As a result, the precession angle  $\psi$  may become very large which is unwanted mainly due to two

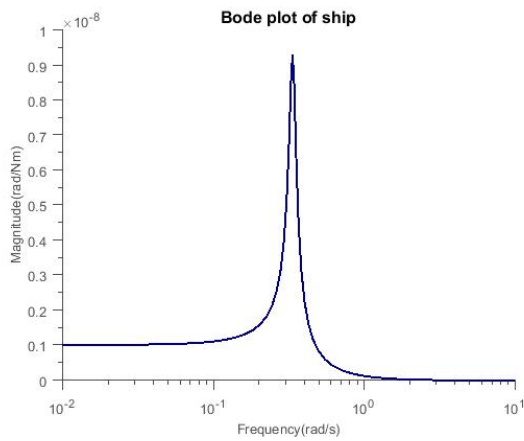


Figure 3.26: Huisdrill bode plot, no control system

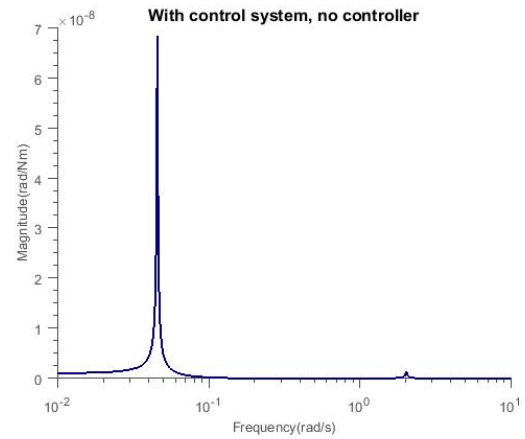


Figure 3.27: Bode plot of Huisdrill roll motion with the gyroscopic control system

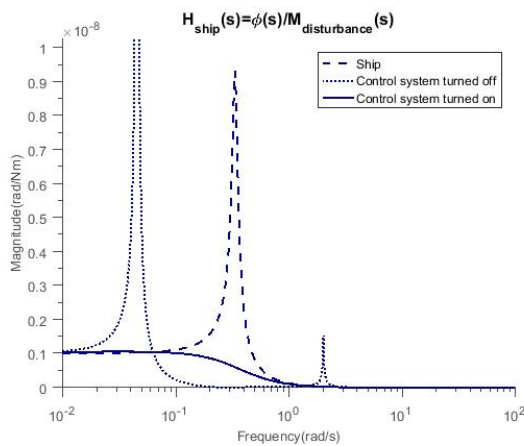


Figure 3.28: Bode plot of controlled and uncontrolled response

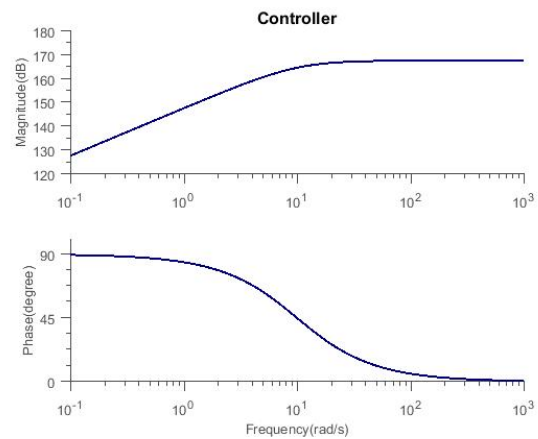


Figure 3.29: Controller for gyroscopic control system

reasons. It is unwanted to reach such big angles for the twin-disc gyroscope, secondly for large angles, the linearization does not hold, thereby producing results which may not be accurate.

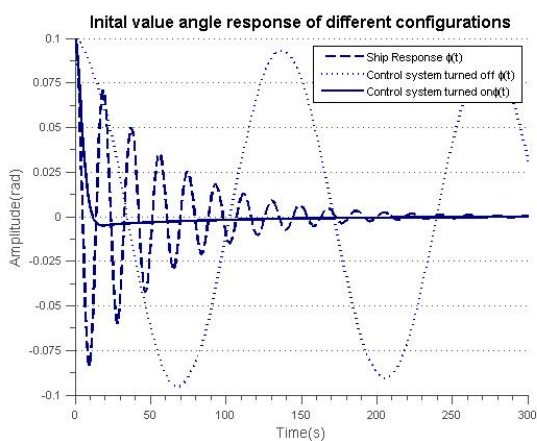


Figure 3.30: Initial value response of three different systems

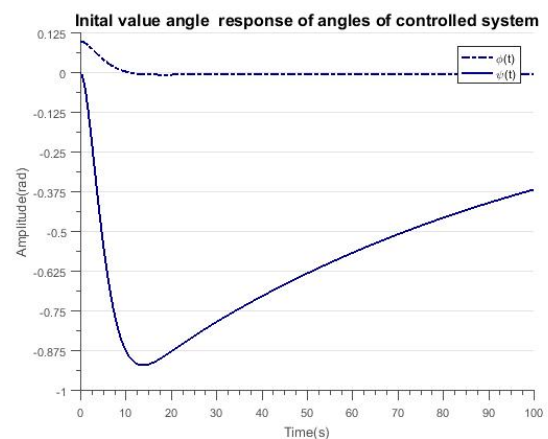


Figure 3.31: Initial value angle response of roll and precession angle

In 3.30 the initial value response of roll angle  $\phi$  for the 3 different cases is shown. As was expected from the Bode-characteristic, the controlled system shows improved dynamics. Within 20 seconds equilibrium is

reached. There is only little overshoot and no oscillation. The ship with a gyroscopic system were the precession angle is not controlled shows doubtful behavior. The two resonance frequencies seen in the Bode-characteristic show in the initial value response, were the high frequency is damped out quickly, the low frequency oscillation does damps very slowly and even after 300 seconds no significant reduction in amplitude is present. In 3.31 the precession and roll angle are shown in one plot. The precession angle reaches -1 rad or 57.3 degrees after which it slowly reaches 0 rad. An angle of +/- 1 rad is obviously not small enough for the linearization condition to hold. For the above-mentioned reasons, a new controller with a proportional action is introduced. With:

$$K_p = 1e7, K_d = 1e8 \tag{3.67}$$

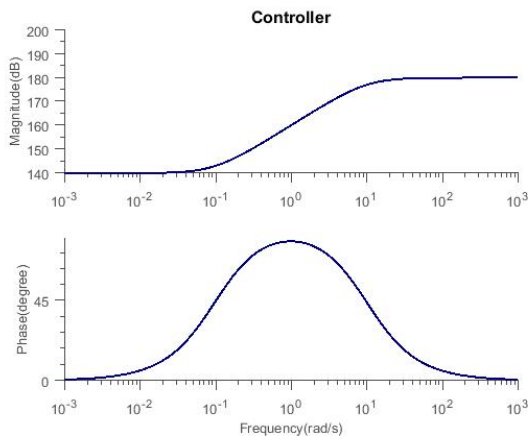


Figure 3.32: Bode plot of PD-controller

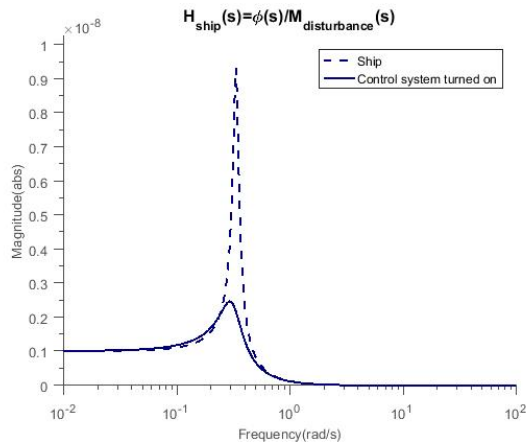


Figure 3.33: Initial value angle response of roll and precession angle

In 3.32 there is a bode plot of the new controller. The results of integrating this controller are shown in 3.33. Compared with the derivative only control, there is a small resonance peak. However comparing the characteristic with the original ship, it is observed that the peak is significantly reduced. This will cause the initial value response and the time domain simulations to show improved behavior.

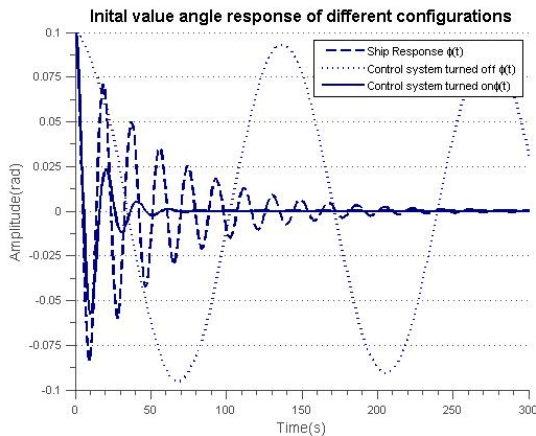


Figure 3.34: Initial value response of three different systems

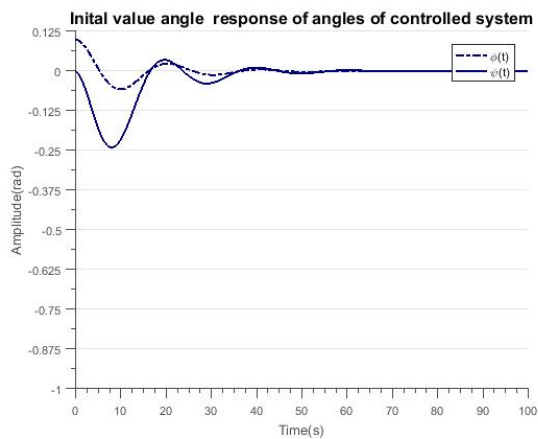


Figure 3.35: Bode plot of controlled vs uncontrolled system

Viewing 3.35 this is indeed the case. Within 60 seconds, equilibrium is reached, where the ship without any additional control systems took 250 systems to achieve the same equilibrium.

### 3.9. Conclusion

Both systems prove to be able to realize significant reductions in roll for excitations at the natural frequency as well as for the initial value response. For the test-case of the Huisdrill p10000 reductions in roll at natural frequency of 80% for the double pendulum system, and 93% have been achieved. The time needed for the

vessel to be at rest after an initial angle of 0.1 deg has been reduced from 250 to about 70 seconds for the double pendulum model and 60 for the gyroscopic control system. For low frequencies, which are of interest for the static heel compensation, it is seen from the Bode-plots, that both control systems prove not to be of much help for compensating for static heel reduction. From the physical nature of the double pendulum model, it could be stated that that model can be used for heel compensation, were the gyroscope would have to keep spinning around the precession angle to compensate for the heel. Therefore this research will continue by expanding the double-pendulum model as the RRR of 80% is promising as well.

It should however be noted that, however the reductions in theory are promising, more extensive calculations are to be made to investigate the behavior in irregular waves.

# 4

## Analytic study: Static Heel

### 4.1. Introduction

In the previous section it was concluded that using the model combined with a controller based on the angle  $\alpha$  of the pendulum with the z-axis could not lead to any significant results for static heel compensation. Therefore in this chapter a second, more elementary model is proposed to model the static heeling of the vessel and to design a fit controller.

### 4.2. Ship Modelling

In the previous chapter a double pendulum model was derived for the dynamic behavior of the double pendulum model as schematically depicted in 4.1. We recall the heeling moment as:

$$M_{heel} = m_{lift}d \quad (4.1)$$

Where  $d$  is the distance between the *CoG* of the vessel and the *CoG* of the load in the sway direction, or the radius. This heeling moment will result in a heeling angle which is to be counteracted by the moving mass system. Remembering the linearized *EoM*'s as derived in the previous chapter:

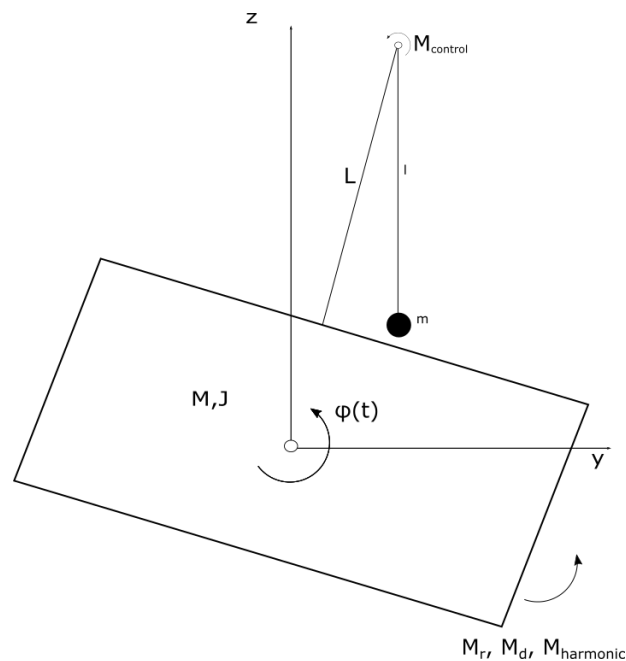


Figure 4.1: Model of ship and control system

$$\begin{bmatrix} (mL^2 + I_{xx}) & -mL \\ -mL & mL^2 \end{bmatrix} \cdot \begin{bmatrix} \ddot{\phi} \\ \ddot{\alpha} \end{bmatrix} + \begin{bmatrix} B_{44} & 0 \\ 0 & 0 \end{bmatrix} \cdot \begin{bmatrix} \dot{\phi} \\ \dot{\alpha} \end{bmatrix} + \begin{bmatrix} -mgL + C_{44} & 0 \\ 0 & mgl \end{bmatrix} \cdot \begin{bmatrix} \phi \\ \alpha \end{bmatrix} = \begin{bmatrix} M_{harmonic} - M_{heel} \\ M_{control} \end{bmatrix}$$

For the swiveling crane it can be assumed that the motions are significantly slow to be able to neglect acceleration coupling and the acceleration of the moving mass. This will greatly reduce the complexity of the model since a *SDoF* model can be used. As no dynamics of the pendulum are taken into account, it can be assumed that the mass will be at the position it is commanded whenever it should be, assuming no lag. By this assumption, we can model a controlling moment acting directly in the ship roll *DoF*. The *EoM* reduces to:

$$J_s \ddot{\phi} + B_s \dot{\phi} + (C_s - mgL)\phi = M_{heel} - M_{control} \quad (4.2)$$

Where the controlling action is now acting "directly" on the vessel. This is an assumption which St Jago [39] and Treacle et al. [41] have made in their respective papers.

### 4.3. Heeling moment modeling

An assumption of the model is that the moment induced by the swiveling crane is of low speed, low acceleration and of no specific frequency. To simulate one swiveling moment, from centerline to most outward position, a ramp function is used as the input, physically representing a linearly increasing load, which will become constant when the maximum radius is reached on which the crane can safely operate. Some simplifications are used to assess the forcing function of the swiveling crane. For example the shifting *CoG* of the structural weight of the crane is neglected. In 4.2 the heeling moment is plotted as a function of time. The maximum loading moment is based on the radius of the crane multiplied added with half vessel breadth (the crane is usually placed on the side of the vessel) with the total load acting on the crane tip. The values found in table 4.1 follow from a Huisman crane specification document. The value is used to define an order of magnitude for the crane induced load. In formula form:

$$M_{heel} = (r + 1/2b)m_{lift} \quad (4.3)$$

Parameter	Value	Unit	Description
r	19	m	Radius of crane@250mt
$m_{lift}$	250	mt	Safe working load
$m_{lift}$	519	mt	Compensation weight
$\omega_{s,max}$	0.2	rpm	Maximum swiveling velocity@250mt
$M_{heel}$	$9.4e7$	Nm	Maximum heeling moment induced by crane

Table 4.1: 250 mt crane parameters

The swiveling velocity is to be translated to a linear velocity in yaw direction. In figure 4.3 it can be observed that the velocity will follow a sinusoidal function as the crane rotates. For the simplified input signal, the average velocity of this movement will be taken as the ramp rate for the input signal. With an angular velocity of  $0.2rpm$ , the time the crane tip needs to move from center line to most outward position equals 75s. The radius  $r$  at that point is  $19m$  leading to a translational velocity of about  $0.2533m/s$

### 4.4. Controller design

A 1-*DoF* system is best described directly written as a transfer function in the Laplace domain.

$$G(s) = \frac{\phi(s)}{M_{heel}(s)} = \frac{1}{I_{44}s^2 + B_{44}s + (C_{44} - mgL)} \quad (4.4)$$

With the controller:

$$C(s) = M_{control}(s) = mgl\alpha(s) \quad (4.5)$$

To reduce static heel, a feedback controller is to be designed based on the roll angle error of the vessel  $\phi$ . So the set point of  $\alpha$  is set to be proportional to  $\phi$ .

$$\alpha(s) = K_p\phi(s) \quad (4.6)$$

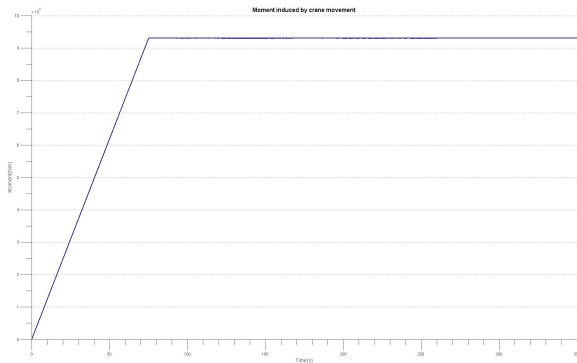


Figure 4.2: The forcing moment induced by the swiveling motion of the crane

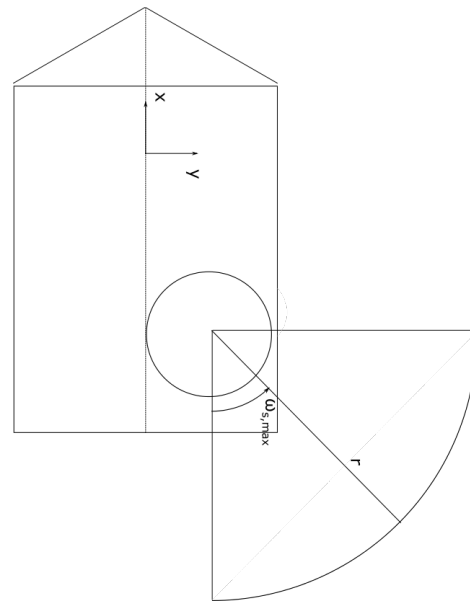


Figure 4.3: How the crane swiveling motion translates to a movement in sway direction

Substituting (4.6) in (4.5) gives:

$$C(s) = mglK_p\phi(s) \tag{4.7}$$

This is visualized in 4.4 As we want the roll moment to be 0 Nm, the input is equal to 0. The transfer function of the system with feedback control:

$$H(s) = \frac{G(s)}{1 + G(s)C(s)} \tag{4.8}$$

or

$$H(s) = \frac{\phi(s)}{M_{heel}(s)} = \frac{1}{I_{xx}s^2 + B_{44}s + (C_{44} - mgL + mglK_p)} \tag{4.9}$$

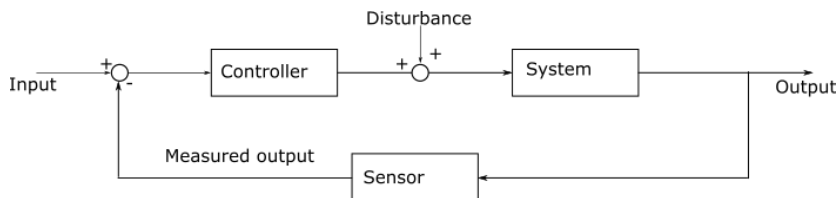


Figure 4.4: Common feedback control loop

In 4.5 the response to the forcing function shown in 4.2 of both the controlled and uncontrolled vessel. It should be kept in mind that the model is linearized, and that moving the mass in excess of 19.5 meters outside the centerline will not be possible, as the mass will not be able to travel outside the ships outer borders. Tuning the gain will therefore be done carefully based on those 2 constraints. In 4.5 the gain is chosen to be 1. This results in a nice reduction of steady state roll angle error. Increasing just the gain will decrease the steady state roll error according to the model, however a zero angle can not be achieved by means of this controller. This can be explained by means of the model. Transforming the transfer function to the frequency domain, by substituting  $s = j\omega$  in  $H(s)$ .

$$H(\omega) = \frac{1}{I_{xx}j\omega^2 + B_{44}j\omega + (C_{44} - mgL + mglK_p)} \tag{4.10}$$

As the quasi-static equilibrium is investigated, it is interesting to review  $|H(\omega)|$  for omega approaching 0. i.e.

$$\lim_{\omega \rightarrow 0} H(\omega) = \frac{1}{(C_s - mgL + mglK_p)} \tag{4.11}$$

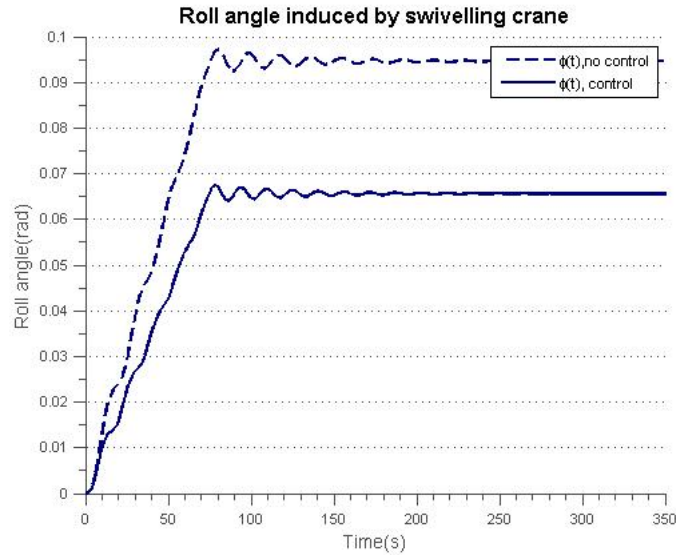


Figure 4.5: TD simulation of the controlled and uncontrolled ship

From the latter equation, it can be observed that by choosing a very high gain, the roll angle will become very small, however it will never be 0. A high gain can cause instability, and will not comply with the above mentioned-constraints. To overcome this problem, an integral action is required to control the steady state error. It should be maximized without becoming too high so that no integral wind-up will occur.

The maximum heeling moment the crane will induce can be fully compensated by shifting the pendulum mass to the most outer position it can reach. This will lead to a zero roll angle offset of the vessel. The controller will take the form of:

$$C(s) = mgl\phi(s)\left(K_p + \frac{K_i}{s}\right) \quad (4.12)$$

Rewriting  $H(s)$ :

$$H(s) = \frac{s}{(C_s - mgL + mglK_p)s + mglK_i} \quad (4.13)$$

From this it follows from this, that for  $s$  approaching 0,  $H(s)$  will be approaching 0 as well, which is the goal of the heel compensation. If the heeling moment shown in 4.2 is applied to the system with the new controller, the results are promising. The response to this heeling moment is shown in 4.6 It should be noted that, imple-

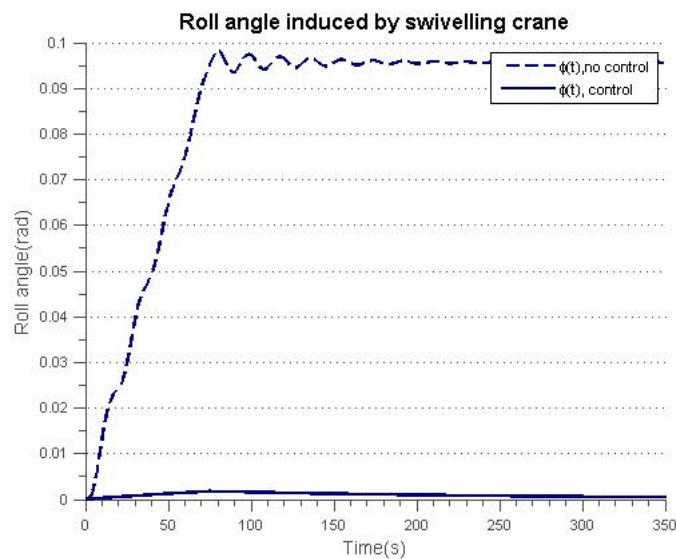


Figure 4.6: TD simulation of the controlled (PI-controller) and uncontrolled ship

menting this controller should be done with caution, as the constraints are not automatically met. It should be kept in mind, that it is not possible to increase  $\alpha$  by too much. By making a simple moment equilibrium, it is clear that the compensating moment is limited to  $1/2bm$ . The parameters used for this controller are  $K_p = 10^2$ , and  $K_i = 10^{-1}$ . The system remains stable for this combination of parameters.

## 4.5. Conclusion

Creating a simplified model for the static heel compensation of the Huisdrill P10000 has led to very promising results. Using a mass which is feasible for dynamic roll compensation, the heel moment induced by the crane can be almost completely counteracted for this example case. This design should however be checked in the time domain, and preferably be done using constraint control, as this model can not be used to limit the angle  $\alpha$  of the pendulum, so that the mass will not go "overboard".



# 5

## Analytic study: Combined static & dynamic behavior

### 5.1. Introduction

The main interest of this research is to investigate how the ballast train system can be used to compensate for heel as well as for dynamic loads on the vessel. In this chapter a combination of earlier found results is reviewed.

### 5.2. Mass size

From chapter 4 it followed that the compensation capacity for static heel is dependent on the horizontal distance outside the vessel *CoG* and the weight of the ballasting mass, so that:

$$M_{control}(s) = mgl\alpha(s) \quad (5.1)$$

Where the distance  $d = l\alpha(s)$  in this linearized model. With the 1% mass proposed in literature, and a distance limited to half ship breadth, this means the compensation would be limited. Since it is impossible to increase  $d$  outside the vessel limits, one could suggest to increase the mass of the ballast. As the control moment is linear with the mass of the ballast, this should result in a higher compensation. In 5.1 The controller moment is plotted as a function of  $d$  for three different sizes of the ballast train mass.

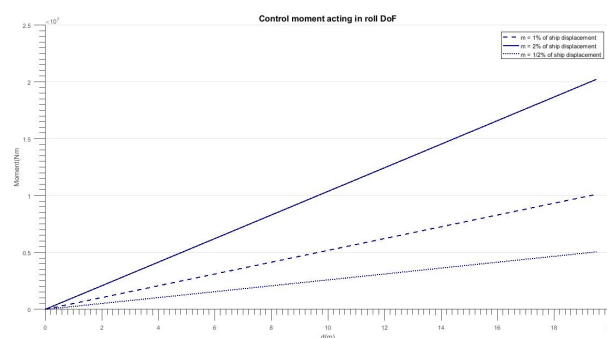


Figure 5.1: Control moment as a function of mass

In chapter 3 it was shown that the ballast mass would reach a position in exceedance of 10 m outside the vessel *CoG*. For the dynamic damping control, it more or less holds that the controlling moment is the product of the deviation and the mass, so increasing the mass would mean a lower deviation, without decreasing performance of the controller. For compensation purposes it is deemed beneficiary to increase the mass, so that compensation is possible for static heel as well as well as for harmonic excitation. One could however think of reasons to limit the mass of the ballast, such as:

- Increased deck loads, leading to specialized support structures
- Ship stability is decreased due to lower GM
- Higher actuator forces
- Higher friction of the ballast
- Higher power consumption due to repeated acceleration of a bigger mass

Integrating such a system in a vessel design is therefore not straight forward and potentially a safety risk. The weight of the mass should therefore be very carefully chosen.

### 5.3. Control strategy

With the mass of the ballast train chosen, the control strategy can be determined. In the previous two chapters, two different controllers are designed for the two different control goals, as the different controllers are unsuitable to properly control the vessel for the the other control situation. Although not straight forward in the frequency domain, in time domain, it is possible to introduce a third controller to control in what conditions the dynamic roll damping system should be active. This is controller is preferably build in the time domain to be able to add non-linear constraints to the control system. The main goal should be to compensate for the swiveling crane, to keep the vessel upright, and where possible to damp the roll motion. The decision to compensate for harmonic motions should be based on the sea-state and the amount of distance left to the side of the vessel. It is recommended to design such a controller.

### 5.4. Relation pendulum versus moving mass control system

Choosing for a double was done for numerous reasons. The question however raises, if it is justified to model the moving mass-system by the pendulum model. There are some properties that differ from model to model. For the static heel model, as dynamics of the control system are not taken into account, it is allowed to do so. The control moment is equal when:

$$d = l\alpha(s) \quad (5.2)$$

For small angles of  $\alpha$  and when the ballast is equal. However, when dynamics are of importance, such as when harmonic excitations is present, modeling the moving mass by the double pendulum system might not be completely accurate. Where the moving-mass system does not have the tendency to "return" to the centerline, the double-pendulum system does. This leading to a natural frequency introduced by the pendulum system. As we recall the natural frequency of a pendulum being:

$$\omega_n = \sqrt{\frac{g}{l}} \quad (5.3)$$

We can state that this linearized double-pendulum system properly models the moving-mass system, when the mass and natural frequency are equal. This brings us back to Koike and Saeki [13] who proposed a hybrid system, where a active control system was combined with a passive mass-spring system with a natural frequency equal to that of the vessel. With the natural frequency defined for the mass-spring system as:

$$\omega_n = \sqrt{\frac{k}{m}} \quad (5.4)$$

It can be concluded that the double-pendulum model accurately describes a moving mass system with a spring constant  $k = mg/l$  for small angles of  $\alpha$  and  $\phi$ .

### 5.5. Conclusion

Using a combined roll damping/heel compensation control system is very promising. It should however be kept in mind that the mass of the ballast can not be increased infinitely, the current model does not account for that. Controlling heel and motions at the same time should be controlled in a proper way. Hitting the end-stops can induce unstable dynamics of the system, which of course is to be avoided at all times.

Regarding the comparison between the moving mass system and the double pendulum model, it can be concluded that the double-pendulum model accurately describes a moving mass system with a spring constant  $k = mg/l$  for small angles of  $\phi$ .

# 6

## Performance of control system

### 6.1. Introduction

To investigate to what extent the added control system improves the vessel behavior, performance measurement characteristics should be investigated. Perez [28] has described several methods to do so, of which a few are used for this paper:

- Percentage Reduction of Roll at Resonance - RRR
- Percentage Reduction of Statistics of Roll - RSR
- Increase in Percentage of Time Operable - IPTO

#### 6.1.1. The Percentage Reduction of Roll at Resonance

*RRR* is a commonly used method to describe performance of the roll control system. Since in general damping is low for the roll motion of a vessel, a resonance peak will occur. The RRR is an expression for the reduction in magnitude of this peak. As the wave spectrum usually is defined as a whole spectrum of frequencies, this description does not suffice to describe the real roll control effect, and tends to overestimate the effect of the roll damping system. In equation 6.1 it is shown how RRR is calculated.

$$RRR = \frac{|H_{ol}(j\omega) - H_{cl}(j\omega)|}{|H_{ol}(j\omega)|} \Big|_{\omega=\omega_n} = 1 - \frac{H_{cl}(j\omega)}{H_{ol}(j\omega)} \Big|_{\omega=\omega_n} = 1 - \frac{\phi_{cl}(j\omega)}{\phi_{ol}(j\omega)} \Big|_{\omega=\omega_n} \quad (6.1)$$

The roll reduction over full range of frequencies is described as:

$$RR(\omega) = 1 - \frac{\phi_{cl}(j\omega)}{\phi_{ol}(j\omega)} = 1 - |S(j\omega)| \quad (6.2)$$

With  $S(j\omega)$  being the sensitivity function, since:

$$S(j\omega) \triangleq \frac{\phi_{cl}(j\omega)}{\phi_{ol}(j\omega)} \quad (6.3)$$

Now taking into account the Bode's integral constraint or the 'waterbed' effect [Jigretski

$$\int_0^{\infty} \ln |S(j\omega)| d\omega = 0 \quad (6.4)$$

Which in fact states that if sensitivity to disturbance is reduced for a certain frequency range, it must be increased at another frequency range. One could imagine, that roll reduction at a certain frequency range must come at a cost of roll amplification at another range. Therefore, a frequency range must be defined for which roll reductions will be the most significant. It can be understood that the roll is to be reduced in the frequency range of the wave spectrum.

### 6.1.2. Percentage Reduction of Statistics of Roll

*RSR* is a more appropriate method to describe the achieved roll damping, as ocean waves are usually described as a superposition of waves with different amplitudes, frequencies, direction and phase. By multiplying the wave spectrum by the force RAO squared, this spectrum can be transformed to the motion response spectrum. Just as for the wave spectrum some statistical parameters are useful to compare:

**0th order moment**  $m_0$ , is also know as variance

**RMS value**  $\sqrt{m_0}$

**Most probable maximum** The expectation of the highest roll amplitude peak in a spectrum.

To calculate the reduction for those parameters, we use:

$$RSR = 100\left(1 - \frac{P_{cl}}{P_{ol}}\right) \quad (6.5)$$

Where  $P$  is the statistical parameter described above. As this reduction concerns the whole range of frequencies, it may be a more suitable predictor of roll reduction compared to the *RRR*.

### 6.1.3. RRO

*RRO* is the Reduction of Probability of Roll peak Occurence. In other words, the chance that in a given sea state the maximum roll amplitude will exceed a certain value. This value might help in predicting whether or not to produce, load & unload, and so on. The distribution of wave amplitude is best described by a Rayleigh probability density function. 6.1 visualizes this phenomena, quite well. To obtain a reduction percentage in chance that a roll angle will be exceeded for the controlled versus the uncontrolled vessel, the chance of exceedance has to be calculated for both systems. This chance can be expressed as:

$$P(\phi_a > \phi_e) = \int_{\phi_e}^{\infty} \frac{\phi_a}{m_r^0} \exp \frac{-\phi_a^2}{2m_r^0} d\phi_a = \exp \frac{-\phi_e^2}{2m_r^0} d\phi_a \quad (6.6)$$

where  $\phi(a)$  is the maximum amplitude of roll in a realization and  $\phi(e)$  is the maximum roll angle of interest. Similar to earlier reductions, the reduction in probability of roll peak occurance is calculated as:

$$RRO(\phi_e) = 100\left(1 - \frac{P(\phi_{a,cl} > \phi_e)}{P(\phi_{a,ol} > \phi_e)}\right) \quad (6.7)$$

For further reference on this subject, see Perez [27], Journee et al. [11] or any other standard issue textbook on oceanwaves and/or ship hydrodynamics.

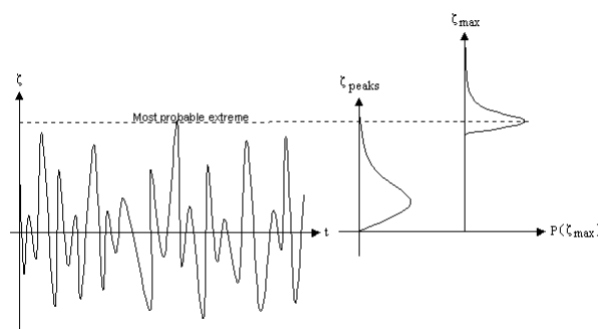


Figure 6.1: Probability distributions for short and long term Journee et al. [11]

### 6.1.4. Increase in Percentage of Time Operable

*IPTO* is a more practical view of the performance of the roll control system. Perez [28] has written a quite extensive chapter about the subject. Depending on what is intended task of the vessel operability limits are conceived. One could think of:

- Motion sickness Incidence at bridge
- Bow slamming
- Deck wetness

These limits may sound a bit vague, however, they are usually directly derived from movements, velocities and accelerations. As one could imagine, high accelerations could induce sea sickness. In this report, this will not be thoroughly evaluated. The general idea is that many indicators are reviewed and weighted to calculate the *IPTO* number.

## **6.2. Conclusion**

There are numerous methods to measure the improvement of adding a control system to a vessel to decrease roll motions. The *RRR*, a commonly used measure is a parameter used by many companies that deliver gyro stabilizers for yachts is actually not really suitable to properly determine performance. For this paper, reduction of roll statistics, *RSR*, is more useful, as it describes the reduction in a seastate. For operability calculations, the increase in percentage of time operable *IPTO* can be a useful parameter.



## 4-Dof model reviewed in frequency domain

### 7.1. Introduction

So far the model has been limited to a 1-*DoF* for ship motions. In chapter 3 the behavior of the example vessel due to a harmonic motion was described for only the roll *DoF* for the controlled and uncontrolled system. In chapter 4 the results of using a controller to compensate for a static heeling moment were presented. In chap 5 the effects and limitations of compensating for heel and dynamic loading are treated. This chapter however, will treat the dynamic response of the example vessel to a wave spectrum, and as there is coupling between the different *DoF*'s, in multiple degrees of freedom.

### 7.2. Reference frames

Perez [28] has written a paper to deal once and for all with the ambiguity of reference frames. He has defined the north-east-down, geometric, body-fixed and hydrodynamic frame. For the current paper the hydrodynamic or h-frame is most important, as the interest lies in computing forces and motions of the vessel. The specifications are similar to the reference frame introduced in 2.4.1 with the difference of the z-axis being defined downwards positive. The origin of the h-frame moves with the average velocity of the vessel in the x-y plane, 0 for this report. The origin is at the height of the mean water level. This reference frame proposed by Perez is used to describe the oscillatory motions. In 7.1 the reference frame proposed by Journee is shown. In 7.2 the frame used for the frequency domain study is shown.

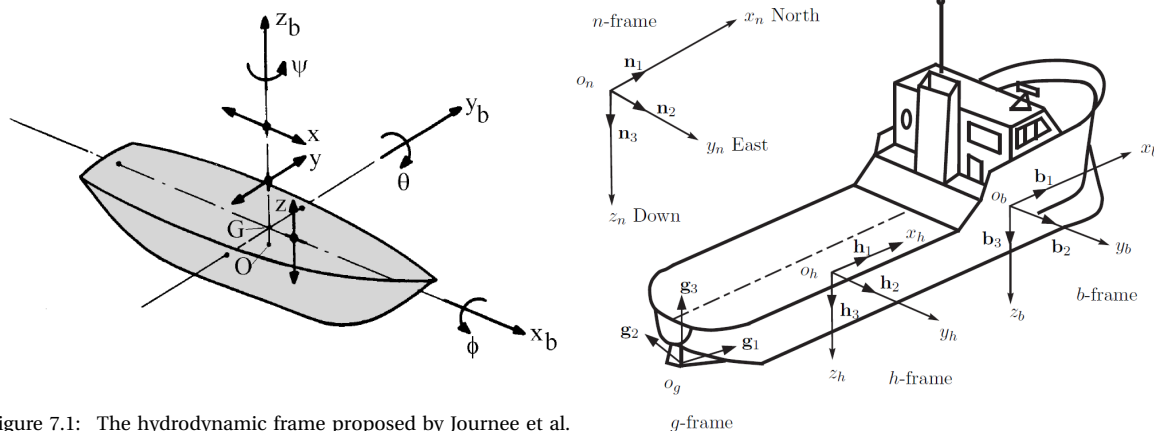


Figure 7.1: The hydrodynamic frame proposed by Journee et al. [11]

Figure 7.2: Reference frame as proposed by Perez [28]

### 7.3. Wave spectra

In previous chapters, the disturbance introduced by the waves was modeled as regular harmonic waves that produced a moment acting on the vessel described in the form of:

$$M_{harmonic} = M_a \sin(\omega t + \epsilon) \tag{7.1}$$

Ocean waves are in general however not accurately described by this representation, as everyone who has seen the ocean waves will know.

#### 7.3.1. Statistical description

In literature, the sea elevation  $\zeta$  at a position is usually described as superpositioned waves, with different (random) frequencies, phases, amplitudes and directions. All characteristics are random in magnitude. In 7.4 this is illustrated. Assuming that the average of  $\zeta$  is not changing over time,  $\zeta(x, y, t)$  can be described as a stationary stochastic process. With this assumption, a spectral density function is used to statistically describe the ocean waves. In other words, the distribution of wave energy over frequency is described by such a function. In 7.3 it is seen how a realization of waves is translated into a spectral density function. In

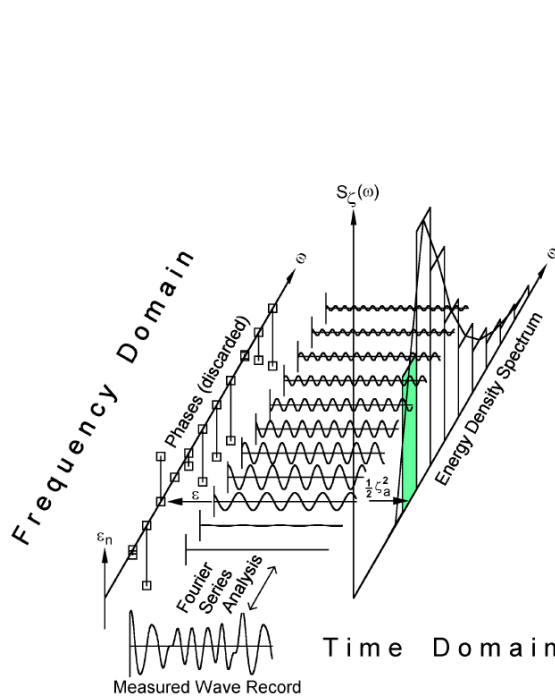


Figure 7.3: How a wave spectrum is obtained Journee et al. [11]

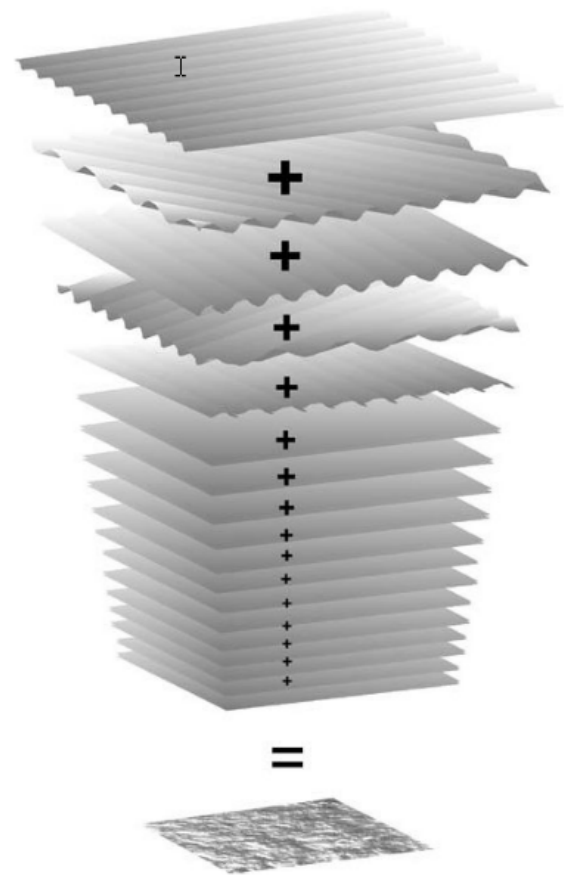


Figure 7.4: Irregular waves with directionality

literature, Perez [27], Journee et al. [11], Holthuijsen [9] and many others, statistics of wave periods are used to describe the wave spectrum, with an important parameter to describe the seastate being the n-th order moment of the unidirectional spectrum  $S_\zeta \zeta$ .

$$m_\zeta^n = \int_0^\infty \omega^n S_\zeta \zeta(\omega) d\omega \tag{7.2}$$

For Gaussian processes it holds that the average wave period

$$T_1 = 2\pi \frac{m_\zeta^0}{m_\zeta^1} \tag{7.3}$$

And the significant wave height

$$H_s = 4\sqrt{m_\zeta^0} \quad (7.4)$$

Which is also known as  $H_{1/3}$ , the average height of the highest  $\frac{1}{3}$  peaks in a realization or measurement.  $T_1$  and  $H_s$  are parameters used to define a sea-state.

### 7.3.2. Standard Wave Spectra

When wave buoys are present, a spectrum can be determined. Researchers in the past have attempted to create a standard form of the wave spectrum. Some commonly used spectra are the Brettschneider, Pierson-Moskowitz, JONSWAP and the ITTC(Modified Pierson-Moskowitz) wave spectra. The JONSWAP spectrum was developed in collaboration with the TU Delft, mainly focusing on fetch limited waves, as can be found in the North sea. The goal of this report however is to investigate the possibility of roll compensation in a swell sea, meaning that waves have been fully developed, and can be assumed to be unidirectional. Therefore the modified Pierson-Moskowitz spectrum is used, which is more suited for open seas. This spectrum is described by:

$$S_{\zeta\zeta}(\omega) = \frac{173H_s^2}{T_1^4\omega^5} \exp\left(-\frac{692}{T_1^4\omega^4}\right) [m^2 s] \quad (7.5)$$

This spectrum will however not suffice to accurately describe the situation were swell is present together with locally generated wind waves. For that scenario, a spectrum with 2 peaks is necessary. As swell wave compensation is the scope of this paper, locally generated waves are neglected. In 7.5 and 7.6 the PM wave spectrum is drawn for different versions of  $H_s$  and  $T_1$ . For modeling swell waves, a PM wave spectrum with

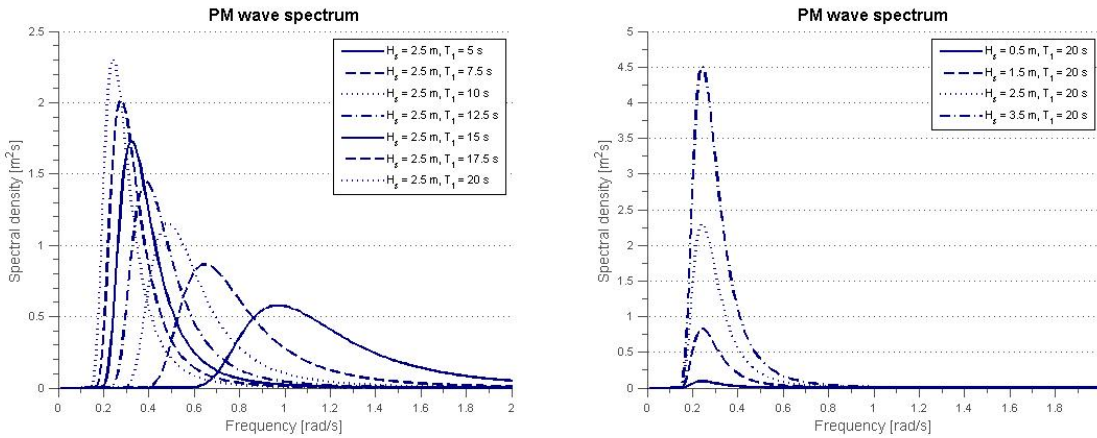


Figure 7.5: Pierson Moskowitz spectrum for different values of  $T_1$  Figure 7.6: Pierson Moskowitz spectrum for different values of  $H_s$

$H_s$  of 1.5 m and a  $T_1$  of 20 seconds is chosen. This represents long waves in relatively mild sea state. In 7.7 this spectrum is shown.

## 7.4. Ship modeling

In addition to the roll motion, in this chapter, the heave, sway and yaw are added to the model. The main reason for this is the coupling with the roll motion. To neglect this coupling might result in non-realistic results of roll reduction. The *EOM*'s of the new model can be written in the following form, based on Newton's second law:

$$\mathbf{M} \cdot \ddot{\mathbf{x}} = \vec{\mathbf{F}} \quad (7.6)$$

$$\ddot{\mathbf{x}} = \begin{bmatrix} \ddot{y} \\ \ddot{z} \\ \ddot{\phi} \\ \ddot{\psi} \\ \ddot{\alpha} \end{bmatrix} = \begin{bmatrix} \text{Sway} \\ \text{Heave} \\ \text{Roll} \\ \text{Yaw} \\ \text{Pendulumangle} \end{bmatrix} \quad (7.7)$$

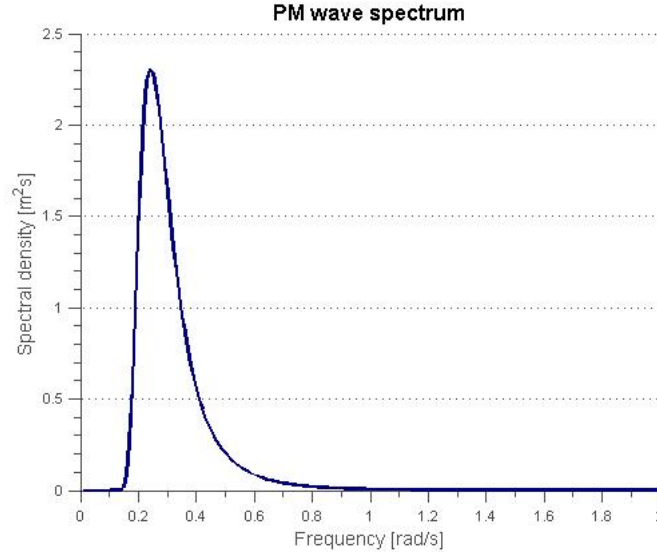


Figure 7.7: Pierson Moskowitz spectrum for west-African swell

In some literature the mass matrix  $\mathbf{M}$  is written in 4-DoF. As for some motions, there is no coupling with the roll motion, these DoF will be neglected in this model. An additional DoF is added to account for the pendulum angle as is done in chapter 3. This will result in the following mass matrix where the pendulum origin is at the vessel CoG:

$$\mathbf{M} = \begin{bmatrix} m_{ship} + m & 0 & 0 & -m_{ship}y_g & 0 \\ 0 & m_{ship} + m & -m_{ship}z_g & m_{ship}x_g & 0 \\ 0 & -m_{ship}z_g & I_{xx} & -I_{xz} & 0 \\ -m_{ship}y_g & m_{ship}x_g & I_{zx} & I_{zz} & 0 \\ 0 & 0 & -mL & 0 & ml^2 \end{bmatrix} \quad (7.8)$$

Where  $x_g, y_g, z_g$  are the distances to the CoG in respectively the x,y and z direction. In many models, these distances are chosen to be 0. Furthermore  $I_{xz}$  and  $I_{zx}$  are in many applications not known, or small and thus assumed 0. The force vector  $\vec{\mathbf{F}}$  consists of first order wave excitation forces and moments as well as hydromechanic forces and moments. Second-order wave forces are neglected. The hydromechanic forces can be divided in: viscous forces, which are assumed to be linear. Radiation forces will result in two main actions on the vessel.

- Added mass, forces proportional to accelerations
- Potential damping, forces proportional to velocities

Hydrostatic forces or restoring forces enable the ship to be stable. They are proportional to movement. Just as in the 1-DoF model, a damping and a stiffness matrix can be created for the model of the Huisdrill P10000. It is outside the scope of this paper to derive the matrices following from the forces described. For symmetric vessels, the added mass matrix for a 6-DoF model is in general given by:

$$\mathbf{A}(\omega_e) = \begin{bmatrix} a_{11}(\omega_e) & 0 & a_{13}(\omega_e) & 0 & a_{15}(\omega_e) & 0 \\ 0 & a_{22}(\omega_e) & 0 & a_{24}(\omega_e) & 0 & a_{26}(\omega_e) \\ a_{31}(\omega_e) & 0 & a_{33}(\omega_e) & 0 & a_{35}(\omega_e) & 0 \\ 0 & a_{42}(\omega_e) & 0 & a_{44}(\omega_e) & 0 & a_{46}(\omega_e) \\ a_{51}(\omega_e) & 0 & a_{53}(\omega_e) & 0 & a_{55}(\omega_e) & 0 \\ 0 & a_{62}(\omega_e) & 0 & a_{64}(\omega_e) & 0 & a_{66}(\omega_e) \end{bmatrix} \quad (7.9)$$

(Perez and Blanke [29]) For the system in this paper surge and pitch are not taken into account, and were the pendulum angle DoF is added this will become:

$$\mathbf{A}(\omega_e) = \begin{bmatrix} a_{22}(\omega_e) & 0 & a_{24}(\omega_e) & a_{26}(\omega_e) & 0 \\ 0 & a_{33}(\omega_e) & 0 & 0 & 0 \\ a_{42}(\omega_e) & 0 & a_{44}(\omega_e) & a_{46}(\omega_e) & 0 \\ a_{62}(\omega_e) & 0 & a_{64}(\omega_e) & a_{66}(\omega_e) & 0 \\ 0 & 0 & 0 & 0 & 0 \end{bmatrix} \quad (7.10)$$

Similarly for the velocity proportional radiation forces of a symmetric vessel:

$$\mathbf{B}(\omega_e) = \begin{bmatrix} b_{22}(\omega_e) & 0 & b_{24}(\omega_e) & b_{26}(\omega_e) & 0 \\ 0 & b_{33}(\omega_e) & 0 & 0 & 0 \\ b_{42}(\omega_e) & 0 & b_{44}(\omega_e) & b_{46}(\omega_e) & 0 \\ b_{62}(\omega_e) & 0 & b_{64}(\omega_e) & b_{66}(\omega_e) & 0 \\ 0 & 0 & 0 & 0 & 0 \end{bmatrix} \quad (7.11)$$

Restoring forces on a vessel act on the heave, roll and pitch motion. Furthermore there is a pitch-heave coupling which is not taken into account for calculations. The stiffness matrix will therefore take the following form:

$$\mathbf{C} = \begin{bmatrix} 0 & 0 & 0 & 0 & 0 \\ 0 & c_{33} & c_{34} & 0 & 0 \\ 0 & c_{43} & c_{44} - mgL & C_{46} & 0 \\ 0 & 0 & 0 & 0 & 0 \\ 0 & 0 & 0 & 0 & mgl \end{bmatrix} \quad (7.12)$$

What remains is the first order wave force. This is assumed to be harmonic, or a summation of harmonics for irregular waves. Combining this information all of the above, will yield the following *EoM*:

$$(\mathbf{M} + \mathbf{A}(\omega_e))\ddot{\mathbf{x}} + \mathbf{B}(\omega_e)\dot{\mathbf{x}} + \mathbf{C}\mathbf{x} = \mathbf{F}_{harmonic}(\omega_e, \epsilon_e) \quad (7.13)$$

Now assuming:

$$\mathbf{F}_{harmonic}(\omega_e, \epsilon_e) = \mathbf{F}_a e^{i\omega_e t} \quad (7.14)$$

Substituted and divided by  $e^{i\omega_e t}$  this yields:

$$(-\omega_e^2(\mathbf{M} + \mathbf{A}(\omega_e)) + j\omega_e\mathbf{B}(\omega_e) + \mathbf{C})\mathbf{x} = \mathbf{F}_a \quad (7.15)$$

## 7.5. From wave spectrum to ship response spectrum

Now the wave input spectrum is known, as well as the the *EoM* of the improved model, the step that remains is how to transform the input spectrum to a response spectrum of the vessel, to research how vessel behavior improves by adding a the double pendulum control system. In offshore engineering it is common practice to use the motion *RAO* to relate the wave input spectrum to a vessel output spectrum. To do so, it is assumed that the amplitude of the forcing function is proportional to the wave height. i.e.  $F_a \propto \zeta_a$ . The second assumption is that the output frequency will equal the input frequency, so that:

$$\zeta(t) = \zeta_a e^{i\omega_e t} \quad (7.16)$$

$$F(t) = F_a e^{i\omega_e t} \quad (7.17)$$

$$x(t) = x_a e^{i\omega_e t} \quad (7.18)$$

Substituting this in (7.15) and dividing by  $e^{i\omega_e t}$  the *RAO* can be found.

$$\mathbf{RAO}(\omega_e) = \left| \frac{\mathbf{x}_a}{\zeta_a} \right|_{(\omega_e)} = \frac{\mathbf{F}_0}{(-\omega_e^2(\mathbf{M} + \mathbf{A}(\omega_e)) + j\omega_e\mathbf{B}(\omega_e) + \mathbf{C})} \quad (7.19)$$

With  $\mathbf{F}_0 = |\mathbf{F}_a/\zeta_a|$  being the force *RAO*. Using the *RAO* the response spectrum can be produced for each degree of freedom using the following relation:

$$S_{r,i}(\omega_e) = |\mathbf{RAO}_i(\omega_e)|^2 S_{\zeta}, i(\omega_e) \quad (7.20)$$

Now when the output spectrum is known, statistical parameters such as the n-th order moment can be readily derived. For the given system, a set of 4 spectra will needed to investigate the roll response spectrum to different excitation spectra.

## 7.6. Parameters

The test case for this frequency domain study is the Huisdrill P10000 as is mentioned before. Using diffraction software, The matrices  $\mathbf{M}$ ,  $\mathbf{A}$ ,  $\mathbf{B}$  and  $\mathbf{C}$  are found. Damping matrix  $\mathbf{B}$  and added mass matrix  $\mathbf{A}$  are frequency dependent. The infinite frequency added mass matrix is used, so that  $A_\infty = \lim_{\omega \rightarrow \infty} A(\omega)$ , to eliminate frequency dependency from the equations. The damping matrix  $\mathbf{B}$  is captured at a frequency of  $0.333 \text{ rad/s}$  close to the frequency of interest, the natural frequency. In the diffraction model, *CoG* of the vessel is assumed to be in the following position:

$$\{x_g, y_g, z_g\} = \{84.527, 0, 13.315\} \quad (7.21)$$

$I_{xz}$  and  $I_{zx}$  are assumed to be zero, as well as  $I_{xy}$  and  $I_{yx}$ . The resulting mass matrix for the vessel without control system:

$$\mathbf{M} = \begin{bmatrix} 5.19e7 & 0 & -6.91e8 & 4.39e9 \\ 0 & 5.19e7 & 0 & 0 \\ -6.91e8 & 0 & 8.61e9 & -4096 \\ 4.39e9 & 0 & -4096 & 1.16e11 \end{bmatrix} \quad (7.22)$$

The resulting mass matrix for the vessel with control system:

$$\mathbf{M}_{control} = \begin{bmatrix} 5.24e7 & 0 & -6.91e8 & 4.39e9 & 0 \\ 0 & 5.24e7 & 0 & 0 & 0 \\ -6.916e8 & 0 & 1.23e10 & 4.10e3 & -3.74e9 \\ 4.39e9 & 0 & 4.10e3 & 1.16e11 & 0 \\ 0 & 0 & -3.74e9 & 0 & 3.78e9 \end{bmatrix} \quad (7.23)$$

The added mass matrix is equal for both systems, with the only difference being the size, and is given by:

$$\mathbf{A} = \begin{bmatrix} 9.23e6 & 0 & 2.67e7 & 5.18e7 & 0 \\ 0 & 5.38e7 & 0 & 0 & 0 \\ 2.48e7 & 0 & 1.52e9 & 3.3e8 & 0 \\ 5.18e7 & 0 & 3.1e8 & 1.49e10 & 0 \\ 0 & 0 & 0 & 0 & 0 \end{bmatrix} \quad (7.24)$$

The linearized damping matrix is given by:

$$\mathbf{B} = \begin{bmatrix} 1.10e6 & 0 & 1.78e5 & 9.44e5 & 0 \\ 0 & 2.17e7 & 0 & 0 & 0 \\ 2.27e5 & 0 & 1.62e5 & 3.74e6 & 0 \\ 1.07e6 & 0 & 3.7e6 & 1.01e8 & 0 \\ 0 & 0 & 0 & 0 & 0 \end{bmatrix} \quad (7.25)$$

The last matrix to be defined is the stiffness matrix. This is different for the controlled and uncontrolled system. The stiffness matrix without any controller:

$$\mathbf{C} = \begin{bmatrix} 0 & 0 & 0 & 0 \\ 0 & 5.21e7 & -3.50e2 & 0 \\ 0 & -3.50e2 & 9.83e8 & -2.29e3 \\ 0 & 0 & 0 & 0 \end{bmatrix} \quad (7.26)$$

And for the ship with control system:

$$\mathbf{C}_{control} = \begin{bmatrix} 0 & 0 & 0 & 0 & 0 \\ 0 & 5.21e7 & -3.50e2 & 0 & 0 \\ 0 & -3.50e2 & 5.48e8 & -2.29e3 & 0 \\ 0 & 0 & 0 & 0 & 0 \\ 0 & 0 & 0 & 0 & 4.30e8 \end{bmatrix} \quad (7.27)$$

The forcing vector is defined as:

$$\mathbf{F} = \begin{bmatrix} F_{a,2} \\ F_{a,3} \\ F_{a,4} \\ F_{a,5} \\ M_{control} \end{bmatrix} \quad (7.28)$$

## 7.7. Controller implementation

To be able to compare the controlled and uncontrolled system, the controller is to be implemented. For reasons mentioned before, it is convenient to create a state space representation of the system to implement the controller using Matlab. The matrices are defined by:

$$\mathbf{A} = \begin{bmatrix} \mathbf{0} & \mathbf{I} \\ M^{-1}C & M^{-1}B \end{bmatrix}, \mathbf{B} = \begin{bmatrix} \mathbf{0} \\ M^{-1}F \end{bmatrix}, \mathbf{C} = \mathbb{1}, \mathbf{D} = 0 \quad (7.29)$$

With the state vector chosen as for the system without control system:

$$\mathbf{x} = [y \quad z \quad \phi \quad \psi \quad \dot{y} \quad \dot{z} \quad \dot{\phi} \quad \dot{\psi}]^T \quad (7.30)$$

And for the system with control system:

$$\mathbf{x} = [y \quad z \quad \phi \quad \psi \quad \alpha \quad \dot{y} \quad \dot{z} \quad \dot{\phi} \quad \dot{\psi} \quad \dot{\alpha}]^T \quad (7.31)$$

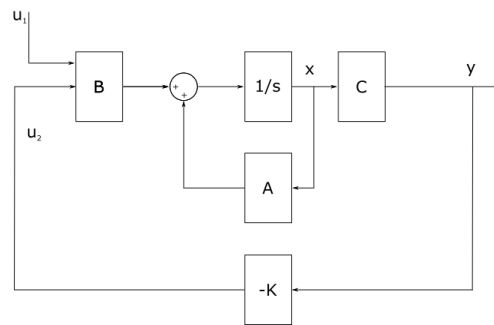


Figure 7.8: State space with output feedback scheme

## 7.8. Results

Using the same feedback scheme as for the analytic model, the system is defined. With the state-space system, the transfer function from input(force) to output(motion) can be calculated for all inputs and outputs of the system, i.e.

$$H_i(\omega_e) = \frac{y_i(\omega_e)}{u_i(\omega_e)} \quad (7.32)$$

The main interest is in the transfer functions that relate some input to the roll output, as the goal of the control system is to add roll damping to the system. In figures 7.9 to 7.12 The following transfer functions are therefore assessed:

- sway-roll
- heave-roll
- roll-roll
- yaw-roll

If this is re-written, we can use it to find to motion *RAO* for the different *DoF*'s.

$$y_i(\omega_e) = H_i(\omega_e) u_i(\omega_e) \quad (7.33)$$

To find the *RAO*, this is to divided by the input wave-spectrum  $\zeta(\omega_e)$

$$RAO_i(\omega_e) = \left| \frac{H_i(\omega_e) u_i(\omega_e)}{\zeta(\omega_e)} \right| = FRAO_i(\omega_e) H_i(\omega_e) \quad (7.34)$$

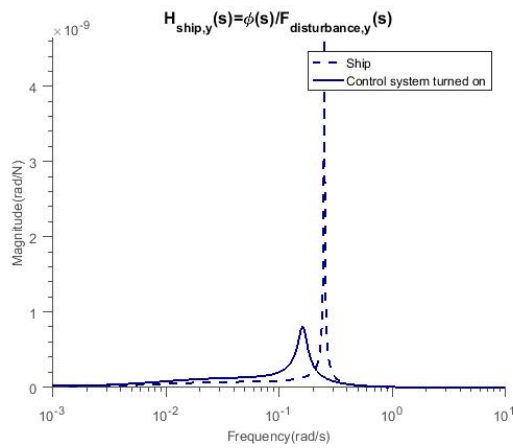


Figure 7.9: Transfer function from sway force to roll angle

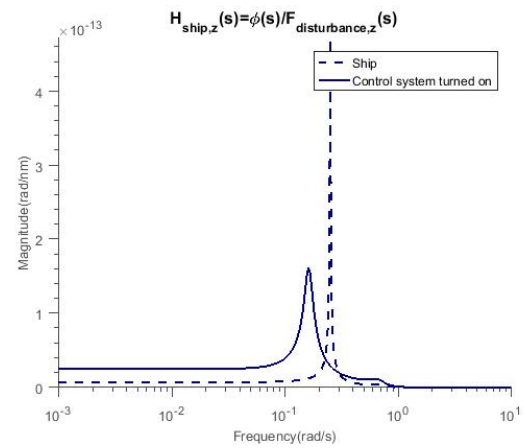


Figure 7.10: Transfer function from heave force to roll angle

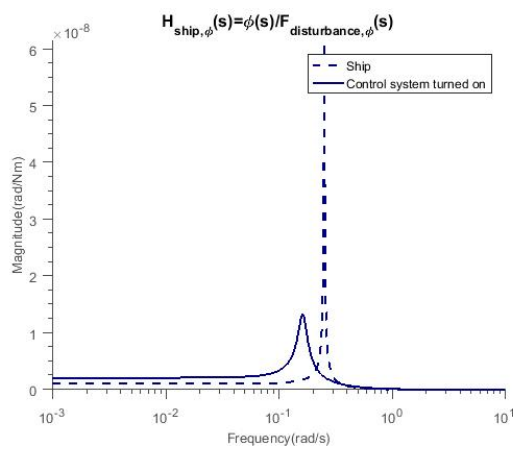


Figure 7.11: Transfer function from roll moment to roll angle

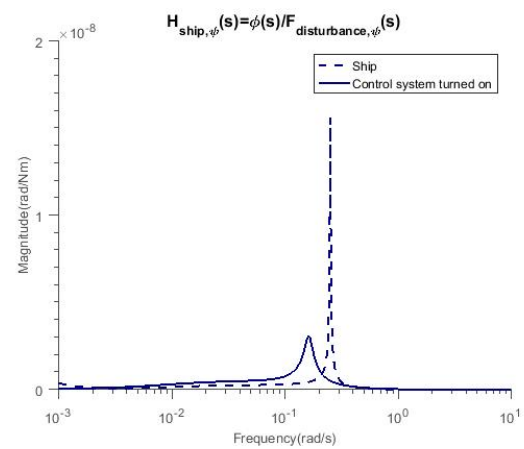


Figure 7.12: Transfer function from yaw moment to roll angle

It is observed that using the same controller as was designed for the analytic model similar results are obtained for all different *DoF*'s, and more importantly, the result for the roll transfer function shows the same characteristics as did the dynamic single *DoF* model; degraded performance for lower frequencies, a resonance peak which is lower in magnitude, and which is also found at a lower frequency than for the model which is not controlled. Model data obtained by means of diffraction software is used to calculate the force *RAO* or the *FRAO* for the Huisdrill p10000. The *FRAO* for beam seas, the angle of incidence is 90 degrees, is calculated as:

$$FRAO_i(\omega_e) = \left| \frac{u_i(\omega_e)}{\zeta(\omega_e)} \right| \quad (7.35)$$

Where  $u_i$  is a moment or force, and  $\zeta$  is the wave height. In 7.17 the *FRAO* relating the roll moment to the wave height is shown. It can be observed that those forces are not constant over the range of frequencies. Similar graphs could be made for the other *DoF*'s present in this model. With the *FRAO*'s known, the *RAO*'s can be calculated. In 7.13 to 7.16 these *RAO*'s are shown.

It is notable that with the exception of heave all *RAO*'s seem to have been improved. This behavior for the heave motion is due to the unfortunate combination of excitation forces at the frequency of the resonance peak of the vessel heave-roll transfer function. The response spectrum of the vessel motions is calculated by:

$$S_{r,i}(\omega_e) = \left| \frac{y_i}{\zeta_i}(\omega_e) \right|^2 S_{\zeta,i}(\omega_e) \quad (7.36)$$

As is found in many standard textbooks, such as: Journée et al. [11], Perez [27] This motion spectrum can be used to quantitatively describe the improved behavior in irregular waves. To do so the  $n$ -th order moment spectra needs to be calculated. These moments are calculated in an equivalent manner for response spectra

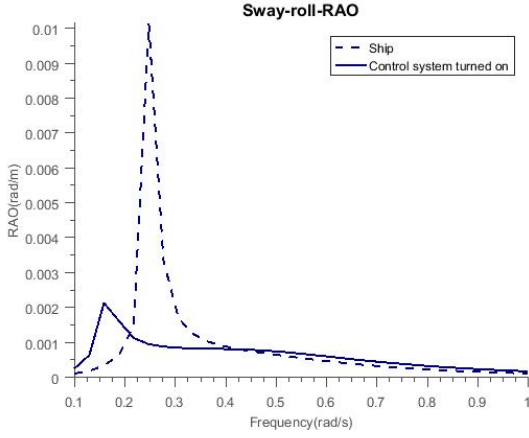


Figure 7.13: RAO sway to roll

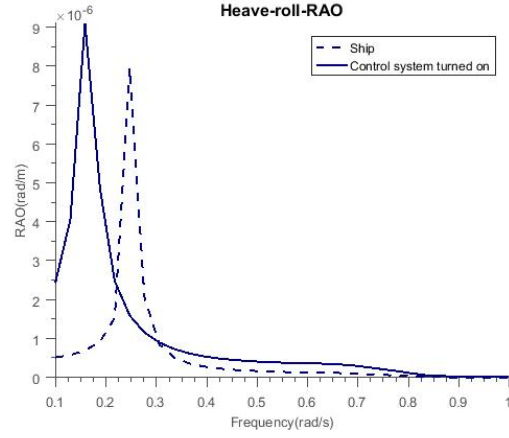


Figure 7.14: RAO heave to roll

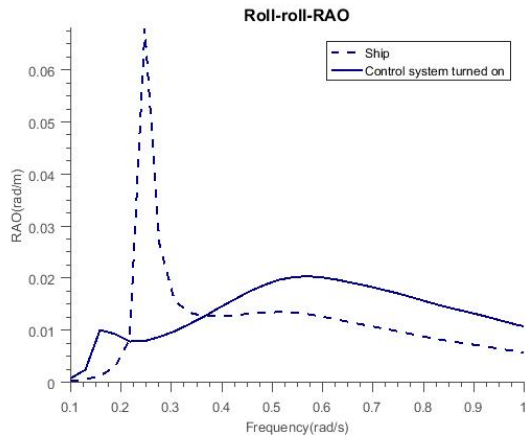


Figure 7.15: RAO roll to roll

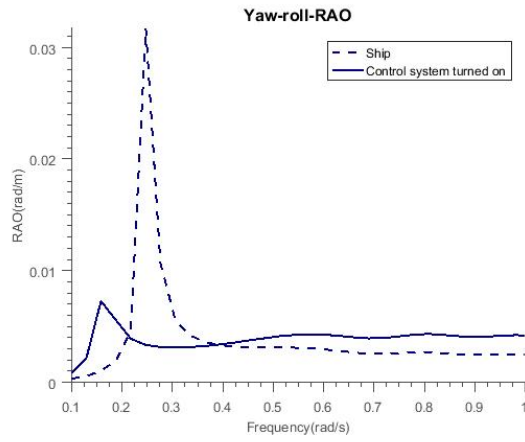


Figure 7.16: RAO yaw to roll

as they are for the excitation spectra;

$$m_{r,i}^n = \int_0^\infty \omega_e^n S_{r,i\zeta\zeta}(\omega_e) d\omega_e \quad (7.37)$$

Relevant output spectrum characteristics are the significant amplitude, which is defined equivalently to the significant wave amplitude, namely the average of the highest  $\frac{1}{3}$  amplitudes:

$$y_{r,1/3,i} = 2\sqrt{m_{r,i}^0} = 2RMS_i \quad (7.38)$$

Statistical parameter overview								
	Sway		Heave		Roll		Yaw	
	no control	control	no control	control	no control	control	no control	control
$m_{r,i}^0 (rad^2)$	9.81e-5	4.66e-6	5.82e-11	1.8836e11	4.80e-3	5.97e-4	9.69e-4	6.60e-5
$m_{r,i}^1 (\frac{rad^2}{s})$	2.48e-5	1.25e6	1.4495e11	3.98e-12	1.3e-3	2.27e-4	2.46e-4	2.0e-5
$y_{r,1/3,i} (rad)$	0.0198	0.0043	1.53e-5	8.68e-6	0.1384	0.0489	0.0622	0.0162
$RMS_i (rad)$	0.0099	0.0022	7.63e-6	4.34e-6	0.0692	0.0244	0.0311	0.0081
$T_{r,i}^1 (s)$	24.87	23.33	25.22	29.71	24.00	16.52	24.72	20.62

Table 7.1: Key characteristics wave output spectrum for  $H_s = 1.5m$ ,  $Tp = 20s$ 

Furthermore a mean period can be directly derived from the spectral moments, with the most important

one being:

$$T_{1,r,i} = 2\pi \frac{m_{r,i}^0}{m_{r,i}^1} \quad (7.39)$$

In table 7.1 an overview is given of those characteristics. With the statistics defined, the *RSR* (reduction of statistics of roll) can be calculated, to assess the performance of the roll damping device. The reduction rate is calculated for the *RMS* value,  $y_{\frac{1}{3}}$  as well as for  $m_0$  for all different output spectra.

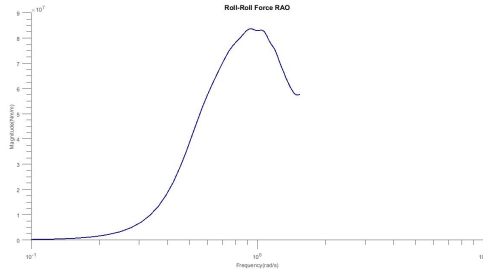


Figure 7.17: Moment RAO: roll moment/wave height

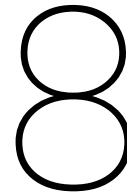
Reduction of Statistics of Roll				
	Sway	Heave	Roll	Yaw
$RSR_{m_{0,r,y}}$ (%)	95	67	87	93
$RSR_{RMS}$ (%)	78	43	65	74
$RSR_{y_{\frac{1}{3}}}$ (%)	78	43	65	74

Figure 7.18: Reduction of Statistics of Roll for  $H_s = 1.5m$ ,  $T_1 = 20s$

In 7.18 these results are presented. It can be observed that the reductions in the 0th-order spectral moment are significant, up to 95% for the Sway to roll spectrum. More interesting to compare are the reduction in *RMS* and  $y_{\frac{1}{3}}$ . Those reductions are as can be seen related, since the *RMS* value is linearly related to the value of  $y_{\frac{1}{3}}$ . In the three different cases, a reduction is noticed, where the reduction for sway is the highest in magnitude. As the transfer of roll to roll is the most significant, the reduction of 65% is a nice result as well and corresponds to results that have been found in literature. As is stated in 6.1, this reduction is lower than the reduction rates which have been found for irregular waves.

## 7.9. Conclusion

Significant reductions in *RMS*-values are found for the ship with the double-pendulum control system installed and active. The most important parameter, the reduction in *RMS* for roll-roll is 65%. A result worth mentioning is the lack of improvement in the Heave-roll *RAO* which is attributed to the unfortunate combination of hull characteristics and ship dynamics with the active controller. As this *RAO* is small in magnitude compared to the other *DoF*'s, this is not considered a problem. In the end, it can be concluded that regarding to the results of this model, significant improvements of vessel behavior can be achieved using the ballast train.



# Time domain study

## 8.1. Introduction

As a conclusion to this research a linear time domain study is conducted on the example case of the Huisdrill P10000. Movements as a result to a time domain simulation of the Pierson Moskowitz wave-spectrum of the P10000 are calculated to investigate time domain behavior.

## 8.2. Frequency study limitations

Studying vessel movements in the frequency domain study provides some benefits, it is fast, and gives in most cases good insight into system properties, and is therefore a proper domain for controller design. There are however some things that can not be fully covered in the this domain, and therefore this time domain simulation is executed. The added value will be the simulation of vessel behavior as a reaction on an irregular wave-spectrum realization to compare control system performance with the uncontrolled situation. Power consumption and controller torque for the controlled situation can be easily derived as an output from the Simulink model.

## 8.3. Model

Ship motions are assessed within a linear framework. Which means that added mass and damping are linearized. The control system dynamics are also regarded linear, as the expected angles are of such low magnitude so that linearization is allowed. The method used to simulate is again by representing the *Eom* by a set of state-space equations. Were the the respective **A**,**B**,**C**& **D**-matrices are calculated by:

$$\mathbf{A} = \begin{bmatrix} \mathbf{0} & \mathbf{I} \\ \mathbf{M}^{-1}\mathbf{C} & \mathbf{M}^{-1}\mathbf{B} \end{bmatrix}, \mathbf{B} = \begin{bmatrix} \mathbf{0} \\ \mathbf{M}^{-1}\mathbf{F} \end{bmatrix}, \mathbf{C} = \mathbb{1}, \mathbf{D} = 0 \quad (8.1)$$

With the state vector chosen as for the system without control system:

$$\mathbf{x} = [\phi \quad \dot{\phi}]^T \quad (8.2)$$

And for the system with control system:

$$\mathbf{x} = [\phi \quad \alpha \quad \dot{\phi} \quad \dot{\alpha}]^T \quad (8.3)$$

Matrix **M**,**A**,**B** & **C** are derived earlier in 3 and are to be found in that chapter. In 8.1 the scheme for Simulink is shown.

## 8.4. Time Record generation

To compare the controlled and uncontrolled Huisdrill P1000, a time record is to be generated which is statistically indistinguishable from the original signal used to create the wave spectrum. In 8 it was argued that the the wave elevation  $\zeta$  at position  $(x, y)$  at a time  $t$  was reached by super positioning all the different wave heights of the individual waves at that place and moment.

$$\zeta(t) = \sum_{n=1}^N \zeta_{a,n} \cos(k_n x - \omega_n t + \epsilon_n) \quad (8.4)$$

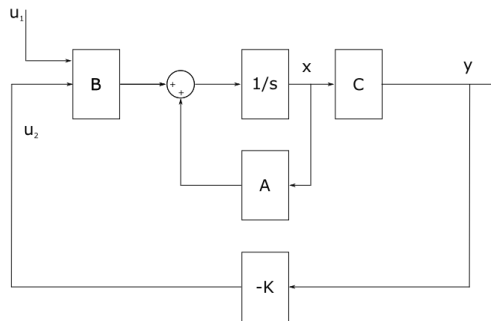


Figure 8.1: State space with output feedback scheme for Simulink

As it is impossible to create infinitely many waves, the spectrum is to be divided into  $N$  bins of equal length  $\Delta\omega$ . The amplitudes follow from the fact that the area under the curve of the selected interval is equal to the variance of the wave component. Journee et al. [11] Leading to:

$$\zeta_{a,n} = \sqrt{2\zeta(\omega)\Delta\omega} \quad (8.5)$$

Where:

- $\zeta_a$  = wave amplitude
- $\omega_n$  = wave frequency
- $k_n$  = wave number
- $N$  = total number of frequencies
- $\epsilon_n$  = phase lag

The wave number  $k_n$  can be related to the frequency of the wave  $\omega_n$  by means of the dispersion relationship. When obtaining the wave-spectrum all data regarding phase angles  $\epsilon_n$  has been forgotten. New values are randomly selected between 0 and  $2\pi$ . With all this information a new statistically equal wave record is created. It should be noted, that statistically equal does not mean the same. This principle is nicely illustrated in 8.2. Difficulties regarding this approach is that one can not know if the spectrum is "correct", a few high peaks

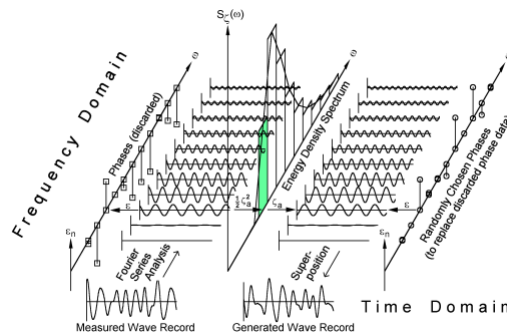


Figure 8.2: Wave record creation Journee et al. [11]

following each other at the beginning of the time series can yield a different result than when the peaks are more equally distributed in time.

With the wave height record defined, a translation from the wave height record to the forcing record is to be made. This is relatively straight forward achieved by multiplying the wave elevation by the force *RAO* for

the given frequency and *DoF* leading to:

$$F_w(t) = \sum_{n=1}^N \frac{F_{n,a}}{\zeta_{n,a}} \zeta_{n,a} \cos(\omega_n t + \epsilon_n + \epsilon_{F\zeta}) \tag{8.6}$$

Where

- $F_a$  = the force amplitude
- $\epsilon_{F\zeta}$  = the phase shift between force an elevation

To decrease calculation times  $N = 20$ , so the wave spectrum is divided into 40 bins of length  $\Delta\omega$ . In 8.3 the stars are plotted on the borders of the bins. In 8.4 1 realization of the PM wave-spectrum is visualized. The

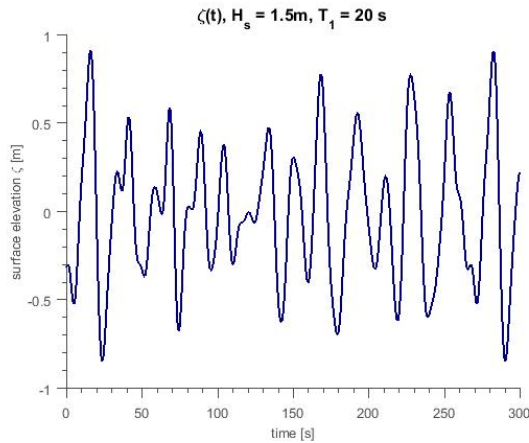
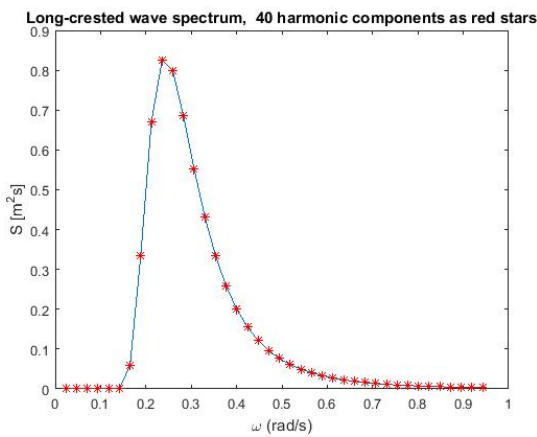


Figure 8.3: Wave spectrum divided in 40 bins  $H_s = 1.5m, T_1 = 20s$  Figure 8.4: A realization of the wave spectrum in 8.3

parameters are randomly generated. To be able to compare the controlled and uncontrolled, the randomly generated wave spectrum is the same each time it is generated. As shortly mentioned above, running a simulation on just one simulation is neither good or bad. However some spectra can induce bigger responses than others. To investigate this, different realizations of the PM spectrum are simulated to find a maximum roll amplitude which makes sense from the statistical point of view. It is of no use to show every individual realization is this report as they all look similar

## 8.5. Results

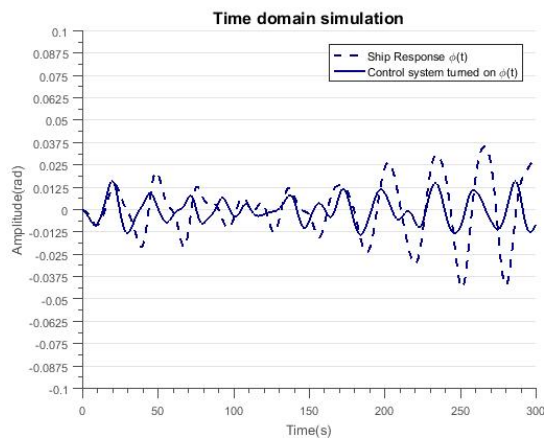


Figure 8.5: Roll response to irregular waves 1

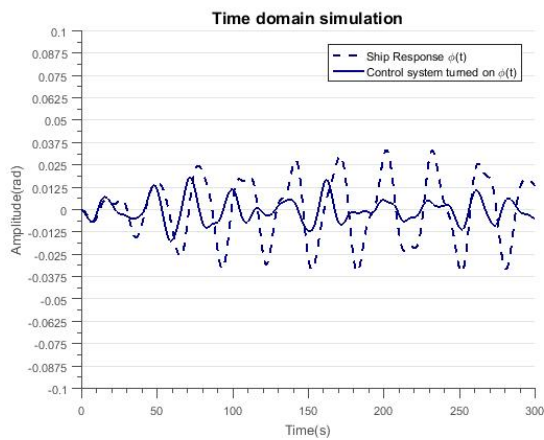


Figure 8.6: Roll response to irregular waves 2

### 8.5.1. Motion response

After simulating the model response to the different realizations of the wave spectrum, the roll response can be plotted. In 8.5 the time domain response is shown to the excitation of 8.4. In 8.6 the resulting roll motions of the Huisdrill p10000 are shown to another realization of the wave spectrum. In both plots, the dotted line is the roll angle  $\phi$  of the Huisdrill without any control system as a function of time(s), the uninterrupted line is the model with an active control system. It can be immediately observed that adding control reduces the roll amplitude of the vessel, also in irregular waves. In 8.7 the roll angle of the ship is plotted together with the angle of the pendulum with the z-axis,  $\alpha$ . As for the regular waves the angle  $\alpha$  lags the angle  $\phi$ , however the phase difference is such that compensation is achieved. In 8.8 the horizontal distance between the pendulum and ship *CoG* is shown. This distance does not exceed 2.5 m in amplitude in this relatively mild sea state with  $H_s = 1.5\text{ m}$  and  $T_1 = 20\text{ s}$  for the 300 s simulation.

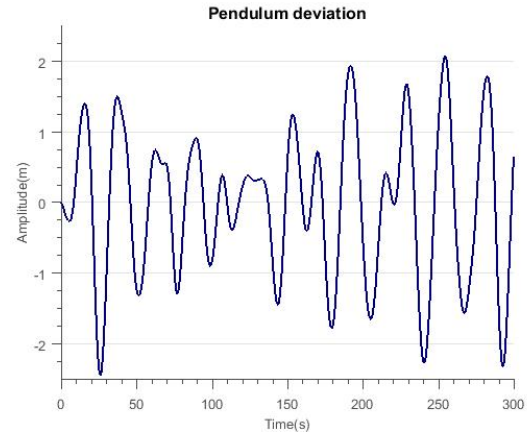
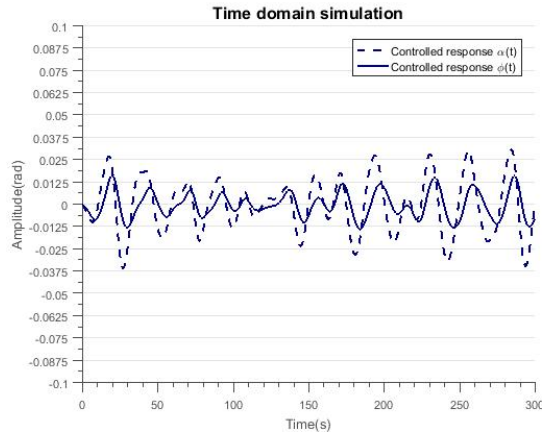


Figure 8.7: Roll and pendulum angle response in irregular waves    Figure 8.8: Pendulum deviation response to irregular waves

### 8.5.2. Extreme Wave Amplitude

Each realization might result in a different maximum wave amplitude. For different applications it can be useful to determine what is the most probable maximum amplitude which the drillship will encounter in a certain sea state. In literature, a distinction is made between short-and-long term wave-statistics. Short term statistics describe the distribution of amplitudes over 1 wave record, where the long-term statistics describe the distributions of maxima over a number of statistical equal wave records. This is nicely illustrated in 8.9 which is taken from Journee et al. [11] For a sea state with  $H_s = 1.5\text{ m}$  and  $T_1 = 20\text{ s}$ , simulated for 3600 s, the

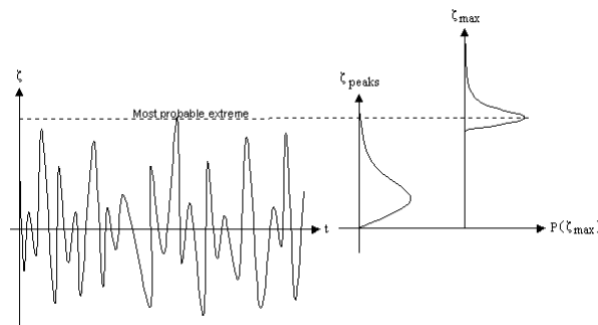


Figure 8.9: Probability distributions for short and long term Journee et al. [11]

maximum amplitude is calculated 10000 times for the controlled and uncontrolled ship. The resulting histogram consisting of 50 bins can be found in 8.10. From the shape it can be seen that this shape looks similar to the Weibull curve found in 8.9 for extreme value distribution. The most probable value for the roll angle is equal to 0.018 rad for the controlled system, and equals to about 0.037 for the ship without the control system

installed. With

$$RSR = 100(1 - \frac{P_{cl}}{P_{ol}}) \tag{8.7}$$

The RSR of the most probable maximum equals 59.9% for the given sea state. Next to the magnitude of the most probable peak, it is also worth noticing that the spread of maxima is much higher for the uncontrolled situation, meaning that much higher roll amplitudes can be possible.

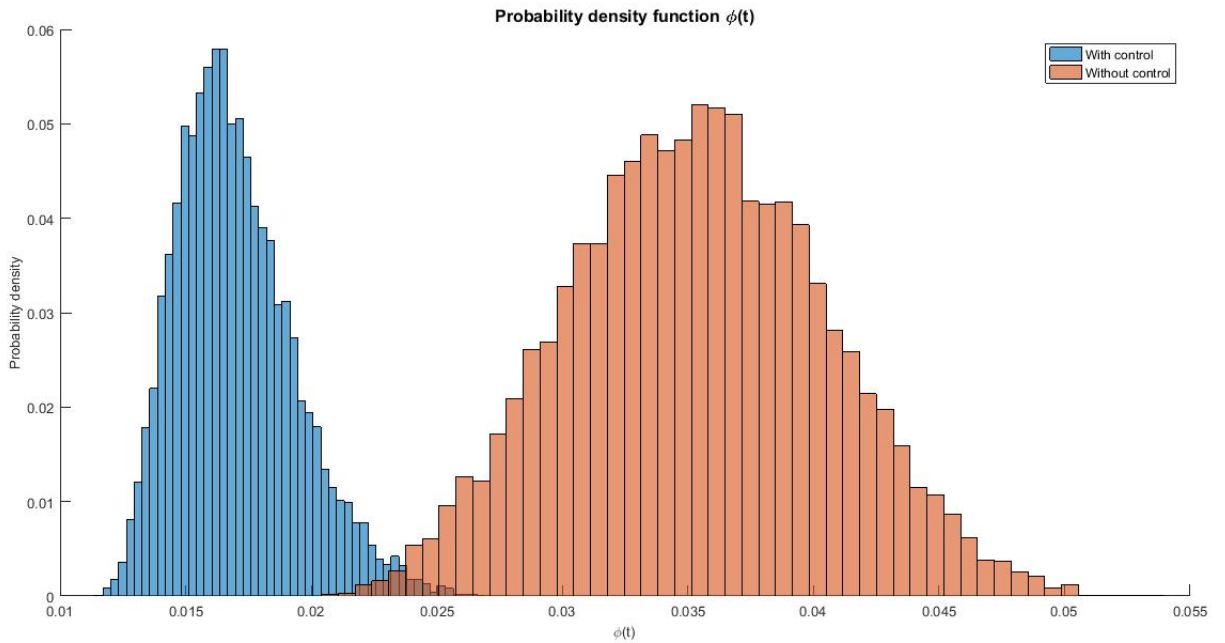


Figure 8.10: Histogram of maximum roll angle

### 8.5.3. Different seastates

In the previous section it was discussed how the results were obtained for one sea state. It might also be interesting how the the most probable maximum roll angle relates to different values of  $H_s$  and  $T_1$ . In 8.11

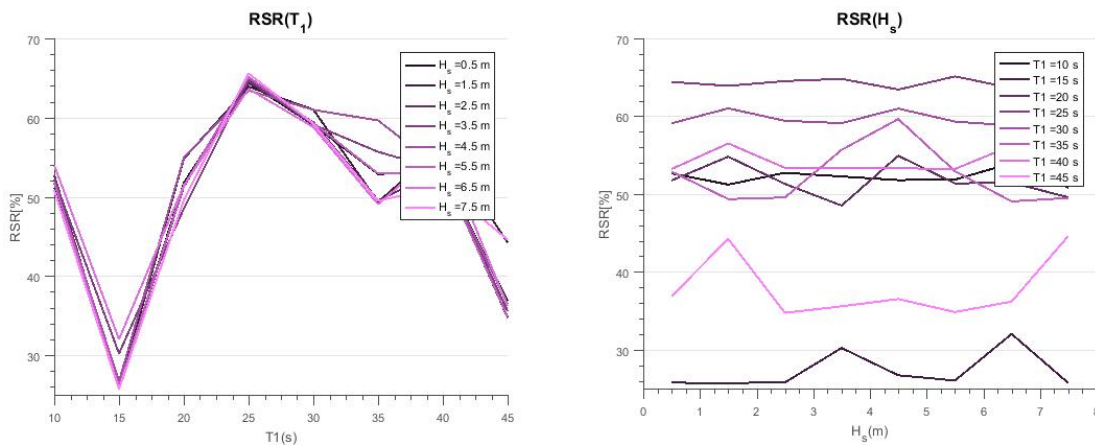


Figure 8.11: Reduction in Most probable maximum of a given seastate as a function of  $T_1$

Figure 8.12: Reduction in Most probable maximum of a given seastate as a function of  $H_s$

the reduction in the most probable amplitude of roll is shown as a function of period  $T_1$ . Every data point is generated by simulating both systems for 3600 seconds, 1000 times. Different lines refer to different values of significant wave height,  $H_s$ . The RSR is low for a period  $T_1$  of about 15 seconds and high for a period of

25 seconds. This area is where the natural frequency of the controlled as well as the uncontrolled Huisdrill P10000 are. When the period becomes larger, reduction decreases. The designed controller improves system dynamics at intermediate frequencies, so for a wave-spectrum with low or high  $T_1$  the reduction will be lower. From 8.12 it is hard to draw conclusions, the expectation is that when more simulations are ran, the  $RSR$  will be independent from the  $H_s$ , in other words, all the lines will be horizontal. It should be kept in mind that for high values of  $H_s$  roll angles will become of such magnitude that linearization will be questionable. The

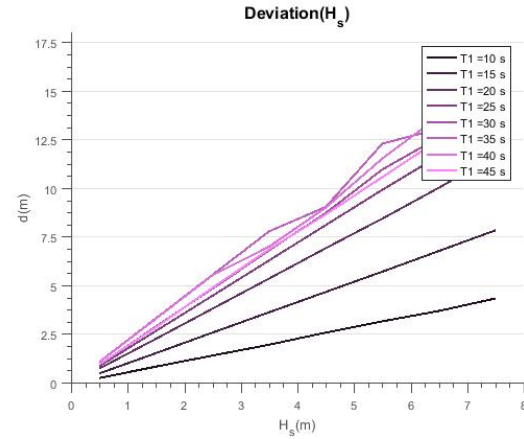
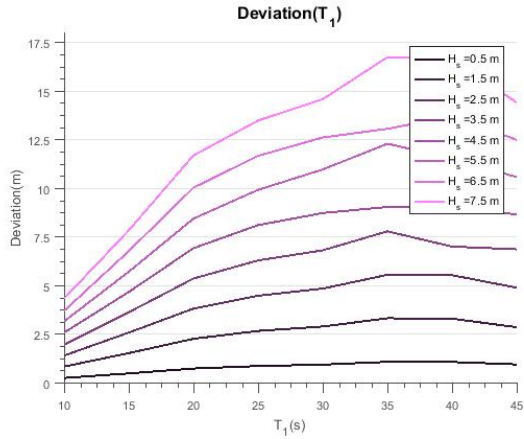


Figure 8.13: Most probable maximum deviation of the pendulum as a function of  $T_1$

Figure 8.14: Most probable maximum deviation of the pendulum as a function of  $H_s$

trend in 8.14 is clearly linear. With increasing significant wave heights, the most probable maximum deviation increases proportional. For 8.13 the relation is less obvious, from  $T_1 = 10s$  until  $T_1 = 25s$  the most probable maximum deviation increases linearly for all different wave heights, however for longer periods, the deviation more or less remains the same. This might be explained by the controllers lower gain at low frequencies. Reading 8.15 and 8.16 might require some additional information. The uninterrupted lines represent the

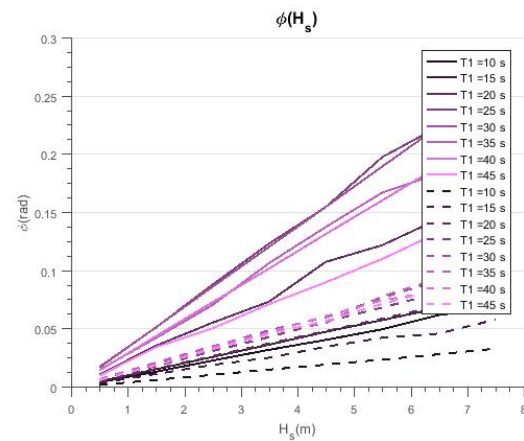
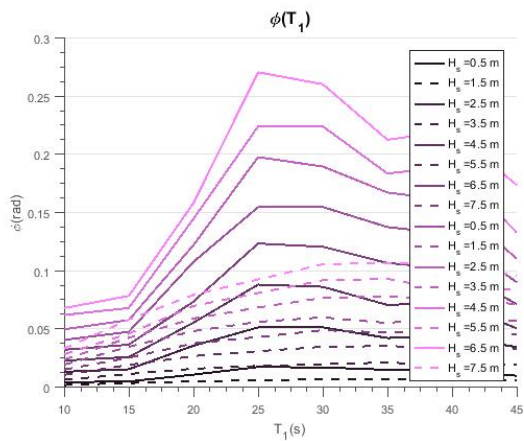


Figure 8.15: Most probable maximum roll angle as a function of  $T_1$

Figure 8.16: Most probable maximum roll angle as a function of  $H_s$

most probable roll angle of the vessel where no control systems are present, where the dotted lines symbolize the vessel with the double-pendulum control system. 8.15 shows that for all time periods simulated here, the roll angle of the controlled system is lower than for the vessel were no controller is installed. Worth noticing is the peak in roll angle for the uncontrolled vessel at  $T_1$  at around 25 seconds. This might be explained by the number of waves that are near the resonance frequency of the vessel. In 8.16 the relation between the significant wave height and the most probable maximum roll angle is shown. This relation is less complicated, and shows a linear trend. However one should be very cautious by interpreting those results as roll angles are exceeding values for which linearization is still allowed.

## 8.6. Non-linear Time Domain simulation

This Time Domain simulation is done based on the linearized model derived earlier in this report. Certain assumptions have been made that can, and sometimes will, influence the results that are found. For further research therefore, a more extensive non-linear time domain simulation can be done for an example vessel. In this section some non-linear effects are discussed, focusing on how they might produce different results from the results which are found using the frequency domain methods as well as the linear time domain simulation.

### 8.6.1. Non-linear equations of motion

The models in this paper are linearized at the working point, 0. This assumption is valid for angle around 0, so for small angles. Added mass and damping matrices are linearized as well. To investigate until what point these assumptions are valid a non-linear time domain simulation can be executed. It is not come to work with non-linearities in the frequency domain, although some researchers have tried to make this work. The main disadvantage of running a non-linear time-domain simulation is the required computing power and the required calculation time which goes hand in hand. However as was observed earlier, non-linear simulation will be needed when high values of  $H_S$  are simulated.

### 8.6.2. Non-linear wave loads

Non-linear wave loads, or second order wave drift forces can be categorized into 2 phenomena; the mean wave drift forces and the low-frequency drift forces. Both are as Journee et al. [11] states the result of non-linear behavior of structures in waves. In the current paper these effects are not assumed to be of low importance. A more thorough study could however take those into account to investigate how they can influence the roll motion behavior. For example, St Jago [39] has investigated the influence of this on a *SWATH* which is very susceptible to these kinds of loading due the the small water plane.

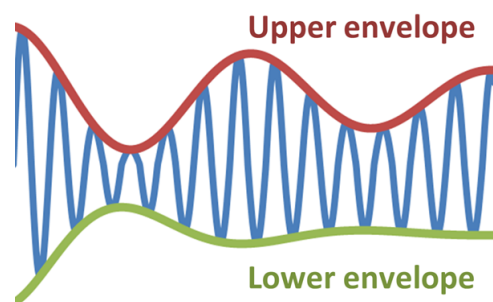


Figure 8.17: Visualization of wave envelope that might induce non-linear behavior

### 8.6.3. Control

The most interesting to investigate thoroughly in a non-linear time domain simulation is the control system part, mainly for two effects;

1. In the models used in this report, no constraints were put on any physical properties of the controller. However in reality, some parameters are limited by nature, or are designed to be limited. The most obvious parameter is the maximum deviation  $d$  the mass or pendulum is to obtain. This should not be exceeding half the vessel breadth in any situation. The controlled should be therefore designed in such a way that this cannot happen. The velocity and acceleration of the mass are not physically limited but are a matter of choice to a certain extent. The power which is limited by the vessel generator, which is the choice of a naval architect. It should however be kept in mind that it might not be worth consuming an amount of energy for stabilizing the vessel. This could also be incorporated in the non-linear control design.
2. Switched control In earlier chapters 2 different controllers were designed for 2 different purposes of control. In literature some examples show the possibilities of switched control Saari and Djemai [33]. In those papers, 1 main controller determined when to use which controller. In 5 it was argued that one should take grate care when using both controllers, as this might induce stable behavior. Installing such a main controller can overcome this problem.

## 8.7. Conclusion

In this chapter, a number of time domain simulations was ran to investigate the behavior of the Huisdrill P10000 with and without an active control system. The model derivation and process of obtaining the results were shown and plotted for one combination of significant wave height and time period, (1.5m,20s). For these parameters, the obtained reduction of most probable maximum wave height was 59.9% . Visual inspection showed that significant reduction in amplitudes was achieved for irregular waves. A histogram showed that the band of most probable roll amplitudes was much smaller for the controlled system. Later in the chapter the results of running multiple time domain simulations were presented. It was clear that the reduction was higher for seastates with a time period which was closer to the natural frequency of the Huisdrill, were the reduction was independent of the wave height. It followed from this section as well that the deviation of the pendulum as well as the roll angle linearly increased with the wave height. It should however being taken into account while interpreting those results, that for high values of  $H_s$ , the results might prove not to be accurate due to the linearization. In the final part the expected results of performing a non-linear time domain simulation are discussed: non-linear wave loads, controller restrictions and model linearization.

# Conclusion and recommendations

## 9.1. Conclusion

In the current paper, the performance of a gyroscope is compared with the performance of a moving mass, modeled as a double pendulum, for dynamic performance of a showcase vessel, the Huisdrill P10000. Results of this analytic study are promising, a reduction of more than 80% for both systems was achieved at the natural frequency of the Huisdrill. The decay time after a roll amplitude of 5.7 deg was reduced from about 250 seconds to 60 seconds for the gyroscope controller model and 70 seconds for the double-pendulum controller model. A static heel control system is modeled based on the double-pendulum equations. This proves to be able to compensate for the heeling moment depending on the weight at the crane tip as well as the weight and distance available to compensate. Combining the static and dynamic approach is possible with the note that there should be sufficient space for the mass to deviate after compensating for static heel.

In irregular waves the 4-*DoF* model shows good performance for the showcase of the Huisdrill P10000. The *RMS* value for the roll-roll motion was decreased by 65%. For other degrees of freedom, similar reductions were obtained. From this it can be included that for the given seastate, significant reductions can be achieved using the ballast train. In the time domain, it was shown that great reductions in most probable maximum of reduction of roll amplitude were achieved for time periods close to the natural frequency of the vessel. For no time period, reductions in performance were measured. It was found that the most probable maximum roll angle linearly increased with the wave height, as well as the most probable deviation did.

Interpreting the results of this study, it can be stated that both the gyroscopic control system as well as the double-pendulum system are able to introduce great reduction in dynamic roll motions. The main benefit of using the double-pendulum system is its ability to compensate for the heeling moment induced by the swiveling crane as well as compensating for the dynamic motions that a vessel will undergo offshore.

## 9.2. Recommendations

In a time limited study some questions will always go unanswered. Recommendations for further research are divided in three categories of research; controller design, model improvement & model testing.

### 9.2.1. Controller design

- It should be investigated how a controller can be implemented that is able to handle the combination of static heel and harmonic loads on the Huisdrill
- It might be interesting to investigate controller design when constraints are taken into account
- Power consumption for different controllers and control systems could be investigated

### 9.2.2. Model improvement

- The origin of the mass is now situated at the *CoG* of the vessel in rest. In real vessels this might not be the case. There it should be investigated how the vessel motion responses are influenced by this fact.
- The simulations in this report are done in Matlab, modeling the vessel in Orcaflex or Ansys Aqwa might reveal unexpected phenomena as less simplifications are applied

**9.2.3. Model testing**

- Even the best model remains an approximation of reality. For verification model tests or even full scale test should be executed.
- Area's of interest for these model tests are the sea states were roll angle becomes large,  $\phi > 0.1 rad$

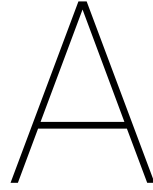
# Bibliography

- [1] J van Amerongen, VAN, and HR NAUTA LEMKE. Rudder roll stabilisation. 1982.
- [2] Greg Welch Bishop and Gary. An introduction to the kalman filter. 2006.
- [3] T. W. Chalmers. *The automatic stabilisation of ships*. Chapman & Hall, London :, 1931.
- [4] WE Cummins. The impulse response function and ship motions. Technical report, DTIC Document, 1962.
- [5] Thor I. Fossen. Handbook of marine craft hydrodynamics and motion control = vademecum de navium motu contra aquas et de motu gubernando, 2011.
- [6] William Froude. *On the rolling of ships*. Institution of Naval Architects, 1861.
- [7] Graham C. Goodwin, M. Seron, and Jose De Dona. Constrained control and estimation : and optimization approach, 2005.
- [8] R Habing. Roll damping to improve the operational limits of existing barge shaped vessels, 2016.
- [9] Leo H Holthuijsen. *Waves in oceanic and coastal waters*. Cambridge University Press, 2010.
- [10] Ing Fritz Horn. Zur theorie der frahmschen schlingerdämpfungstanks. In *Jahrbuch der Schiffbautechnischen Gesellschaft*, pages 453–480. Springer, 1911.
- [11] J. M. J. Journee, W. W. Massie, R. H. M. Huijsmans, Faculty of Mechanical Maritime Delft University of Technology, and Engineering Materials. *Offshore hydromechanics course OE4630*. TU Delft, Delft :, 3rd ed. edition, 2000.
- [12] MR Katebi, DK Wong, and MJ Grimble. Lqg autopilot and rudder roll stabilization control system design. 1987.
- [13] Y Koike and A Saeki. Application of hybrid anti-rolling system to actual ship. *JOURNAL-SOCIETY OF NAVAL ARCHITECTS OF JAPAN*, 185:111–118, 1999.
- [14] Umesh A. Korde. Active heave compensation on drill-ships in irregular waves. *Ocean Engineering*, 25(7): 541–561, 1998.
- [15] Ali J Koshkouei and Lukas Nowak. Stabilisation of ship roll motion via switched controllers. *Ocean Engineering*, 49:66–75, 2012.
- [16] Erlend Kristiansen, Åsmund Hjulstad, and Olav Egeland. State-space representation of radiation forces in time-domain vessel models. *Ocean Engineering*, 32(17):2195–2216, 2005.
- [17] KS Kula. An overview of roll stabilizers and systems for their control. *TransNav: International Journal on Marine Navigation and Safety of Sea Transportation*, 9, 2015.
- [18] BS Lee and D Vassalos. An investigation into the stabilisation effects of anti-roll tanks with flow obstructions. *International shipbuilding progress*, 43(433):70–88, 1996.
- [19] E. C. Levy. Complex-curve fitting. *IRE Transactions on Automatic Control*, AC-4(1):37–43, 1959.
- [20] Nicolas Minorsky. Directional stability of automatically steered bodies. *Naval Engineers Journal*, 32(2), 1922.
- [21] R. Moaleji. *Adaptive Control for Ship Roll Stabilization Using Anti-Roll Tanks*. University of London, 2007.

- [22] Reza Moaleji and Alistair R. Greig. On the development of ship anti-roll tanks. *Ocean Engineering*, 34(1):103–121, 2007.
- [23] J. N. Newman. *Marine hydrodynamics*, 1977.
- [24] TRF Nonweiler, PH Tanner, and P Wilkinson. Moving-weight ship stabilisers. In *Third Ship Control Systems Symposium, Univ., Bath, UK*, 1972.
- [25] Michel K. Ochi and Iordanis I. Sahinoglou. Stochastic characteristics of wave groups in random seas: Part 2 - frequency of occurrence of wave groups. *Applied Ocean Research*, 11(2):89–99, 1989.
- [26] T Francis Ogilvie. Recent progress toward the understanding and prediction of ship motions. In *5th Symposium on naval hydrodynamics*, volume 1, page 2.5. Bergen, Norway, 1964.
- [27] Tristan Perez. A review of geometrical aspects of ship motion in manoeuvring and seakeeping, and the use of a consistent notation. Technical report, Technical report. Marine System Simulator (MSS) Group, CeSOS, NTNU, 2005.
- [28] Tristan Perez. Ship motion control. course keeping and roll stabilization using rudder and fins. *Advances in Industrial Control*. Springer, 2005.
- [29] Tristan Perez and Mogens Blanke. Ship roll damping control. *Annual Reviews in Control*, 36(1):129–147, 2012.
- [30] Tristan Perez and Thor I. Fossen. Practical aspects of frequency-domain identification of dynamic models of marine structures from hydrodynamic data. *Ocean Engineering*, 38(2-3):426–435, 2011.
- [31] Tristan Perez and Paul D. Steinmann. Analysis of ship roll gyro-stabiliser control. *IFAC Proceedings Volumes*, 42(18):310–315, 2009.
- [32] PetroWiki. History of offshore drilling units, 2015.
- [33] Hammoud Saari and Mohamed Djemai. Ship motion control using multi-controller structure. *Ocean Engineering*, 55(2):184–190, 2012.
- [34] Turgut Sarpkaya and Michael Isaacson. *Mechanics of wave forces on offshore structures*. 1981.
- [35] E Schlick. The gyroscopic effect of flywheels on board ship. *Transactions of the Institute of Naval Architects*, 23:117–134, 1904.
- [36] Frank H Sellars and John P Martin. Selection and evaluation of ship roll stabilization systems. 1991.
- [37] TC Smith and WL Thomas III. A survey of ship motion reduction devices. Technical report, DTIC Document, 1990.
- [38] Dale Spencer. Bp energy outlook 2035. 2016.
- [39] R St Jago. Low frequency roll and pitch compensation for the wind turbine shuttle. 2011.
- [40] Reza Taghipour, Tristan Perez, and Torgeir Moan. Hybrid frequency-time domain models for dynamic response analysis of marine structures. *Ocean Engineering*, 35(7):685–705, 2008.
- [41] Thomas W. Treakle, Dean T. Mook, Stergios I. Liapis, and Ali H. Nayfeh. A time-domain method to evaluate the use of moving weights to reduce the roll motion of a ship. *Ocean Engineering*, 27(12):1321–1343, 2000.
- [42] Thomas W Treakle III. *A time-domain numerical study of passive and active anti-roll tanks to reduce ship motions*. PhD thesis, Virginia Polytechnic Institute and State University, 1998.
- [43] JH Vugts. *A Comparative Study on Four Different Passive Roll Damping Tanks*. Nederlands Scheepsstudiecentrum TNO, 1968.
- [44] Z Wang. Huisman model tests, 2008.

- 
- [45] P Watts. On a method of reducing the rolling of ships at sea. *Trans. INA*, 24, 1883.
- [46] P Watts. The use of water chambers for reducing the rolling of ships at sea. *Trans. of the Institution of Naval Architects*, 26, 1885.
- [47] William C Webster and P Dogan. The analysis of the control of activated anti-roll tanks. Technical report, DTIC Document, 1966.
- [48] Z. Yu and J. Falnes. State-space modelling of dynamic systems in ocean engineering. *JOURNAL OF HYDRODYNAMICS SERIES B -ENGLISH EDITION-*, 10(1):1–17, 1998.





# Research planning

## A.1. Overview

Date	Milestone	Deliverables
14-Nov	Start Thesis Research	Initial approval of topic
19-Dec	Kick-off meeting TU Delft	Thesis proposal is finished <ul style="list-style-type: none"><li>• Proposal report</li><li>• Proposal presentation</li><li>• Literature study halfway done</li></ul>
30-Jan	1st progress meeting	Literature study is finished <ul style="list-style-type: none"><li>• Presentation of Literature study results</li><li>• Report of literature study</li><li>• Definitive research plan</li></ul>
21-mar	2d progress meeting	Presentation and report updated with: <ul style="list-style-type: none"><li>• Analytic study</li><li>• Frequency domain model</li></ul>
24-Apr	3d progress meeting	<ul style="list-style-type: none"><li>• Control system design finished</li><li>• Time-domain model</li></ul>
19-jun	Green-light meeting	All analytic and numeric work is done. <ul style="list-style-type: none"><li>• Concept report is finished</li><li>• Concept presentation is given</li></ul>
03-Jul	Public presentation and defense	Report, code and presentation finished

Table A.1: Planning

## A.2. Gantt chart

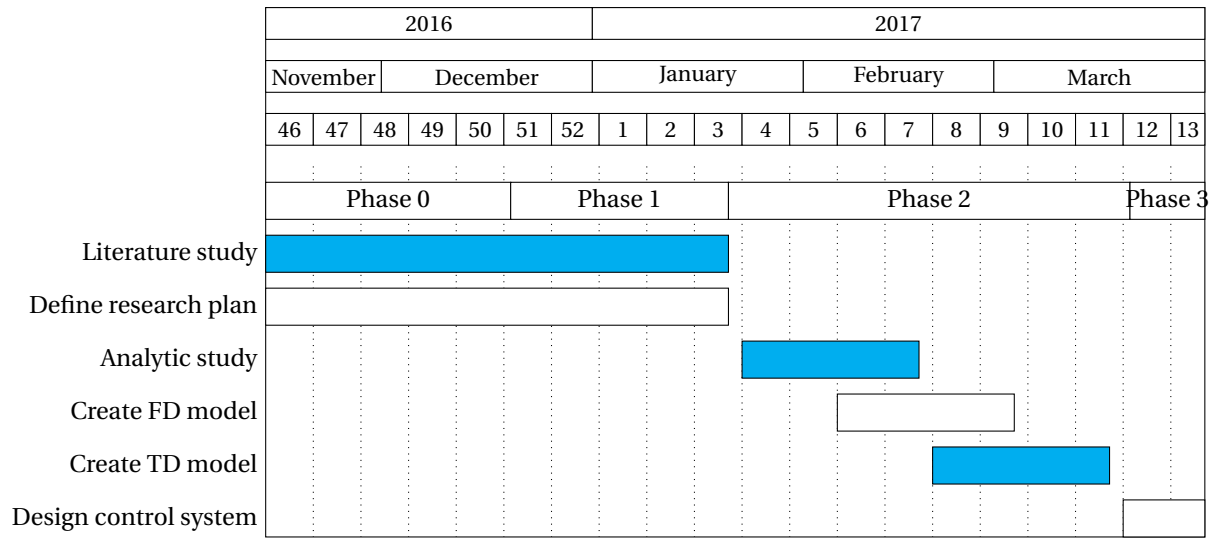


Figure A.1: Gantt Chart Nov-Mar

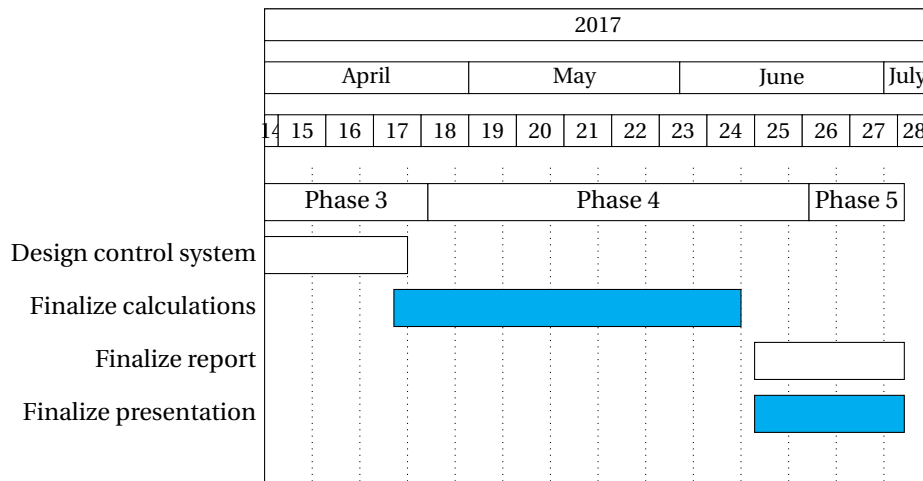


Figure A.2: Gantt Chart Apr-Jul

# B

## Minutes

### **B.1. Internal meeting 15-11-2016**

**Present** Ferdinand van Heerd, Matthijs Stofregen, Tong Mai, Zhuoyi Wang

#### **B.1.1. Project goals**

- Identify the nature of the problem
- Check if the project is feasible, if so, what are the limitations?
- Optimize the controller and control system

#### **B.1.2. Starting points**

- Swell conditions
- Drillship Huisdrill MKIII
- Mass used in the industry
- Actuators available to Huisman

#### **B.1.3. What does Huisman wants**

To know if a ballast train or similar concept is feasible, and under what conditions the use of such a system will be economic. A tool in the end would be nice.

#### **B.1.4. What does the TU wants**

Still unknown

#### **B.1.5. Leads**

- Taipei 101 earthquake resistance?
- Youtube video of roll compensation

## **B.2. Internal meeting 06-12-2016**

**Present** Matthijs Stofregen

### **B.2.1. feedback on report**

- Choice of control system should not be limited to ballast train. Other options should be checked for feasibility
- Process should be clear for presentation
- It should be investigated what Aqwa can and can not do

### **B.2.2. To do's**

**Anton-Jan** An updated report will be sent on 9-12-2016

**Anton-Jan** A report that is ready to send to the TU will be sent to Ferdinand van Heerd & Stofregen on 14-12-2016

**Anton-Jan** A clear flowchart is delivered on 9-12-2016

**Matthijs** Send Aqwa user manual

**Matthijs** Discuss off-days with HR

### **B.2.3. Ancillary matters**

- Tight schedule, but doable
- No delaying factors from Huisman
- Days at University should be mailed to Ferdinand and Matthijs

## **B.3. Kick-off meeting 20-12-2016**

**Present:** Prof. Dr. Ir. Huijsmans, Ir. Van Heerd

### **B.3.1. Received documents**

- Presentation 20-12
- Report phase 0

### **B.3.2. Points discussed**

- General introduction to project
- problem statement
- research goal
- research question
- research aim
- research approach
- progress literature study
- Planning

### **B.3.3. Points of attention**

- Think of using Matlab only model instead of a combination between Aqwa & Matlab
- Look into gyroscopic system. Will however probably not be used, since ballast train can also be used for heel compensation
- Verification and/or validation are very important. Think about how to do it.
- simple low pass filter will probably not suffice due to time lag in the system. Therefore think about implementing a more advanced filter like the Kalman filter.

### **B.3.4. To do's Prof. Huijsmans**

For the next meeting a committee will be formed. Prof. Huijsmans will assign a daily supervisor in the coming weeks.

### **B.3.5. Next meeting**

Next meeting will be in about 6 weeks. The literature study will be finished by then. An appointment is made with Monique Gazendam

## **B.4. Meeting 08-05-2017**

**Present:** Prof. Dr. Ir. Huijsmans, Ir. Van Heerd, Prof. Dr. Ir. van 't Veer

### **B.4.1. Received documents**

- Presentation 08-05
- Report 08-05

### **B.4.2. Points discussed**

- See presentation

### **B.4.3. Points of attention**

- Think about terminology DP and GM etc.
- Show understanding of system behavior in report (especially gyroscope)
- Colors of plot should be the same in each plot
- Vary Kg in gyroscopic control system
- Pictures presentation should be bigger
- Focus on FD model, little attention for TD model. Explain what non-linearities will be added, TD is just one showcase
- Bode plots not in dB

### **B.4.4. To do's Prof. Huijsmans**

For the next meeting a committee will be formed. Prof. Huijsmans will assign a daily supervisor in the coming weeks.

### **B.4.5. Next meeting**

Next meeting will be in about 6 weeks. The literature study will be finished by then. An appointment is made with Monique Gazendam

# C

## Huisman Model test

### C.1. Introduction

Huisman has investigated the possibilities for using an active anti-roll system before in 2008. This anti-roll study was based on the full scale drillship design; the Huisdrill. Model tests have been executed for three different loading conditions in the Delft water tank. A still from the movie is shown in C.1.



Figure C.1: Modeltests as performed by Huisman 2008

The 1:54 model is a representation of the Huisdrill. For this test, three loading conditions are defined for varying circumstances.

**LC1** Is the nominal case, based on which the controller is designed.

**LC2** Same vessel, with a lower GM and thus a higher natural roll period.

**LC3** Same vessel with a lower displacement.

In C.1 a more elaborate description is given of these loading conditions.

LC	Draft[m]	Displacement[mt]	GM[m]	Natural roll period[s]
LC1	11.8	52405	1.90	18.7
LC2	11.8	52405	1.25	24.7
LC3	8.1	29102	1.56	20.7

Table C.1: Regular waves(full scale values)

The slider mass is 300 metric tons for all the different tests. For each loading condition, three different tests are done:

- Decay tests
- Regular wave tests
- Irregular wave tests

In C.2 the test conditions for regular waves are shown. All tests are with a beam sea and soft mooring. The duration of the regular sea tests is 0.5 hour. In table C.3 the testing program for irregular waves is shown. These tests have to go on for 10800 seconds for statistical reasons. The mooring is again soft and the tests are done for beam seas.

#Test	LC	T[s]	H[m]
1	LC 1	16	5
2	LC 1	20	2.5
3	LC 2	25	4.6
4	LC 3	20	2.5

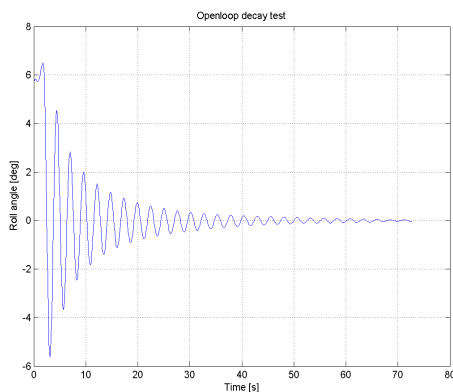
Table C.2: Regular waves(full scale values)

#Test	LC	T[s]	H[m]
5	LC 1	10	5
6	LC 1	16	5
7	LC 1	16	7.5
8	LC 1	20	2.5
9	LC 2	16	7.5
10	LC 2	20	2.5
11	LC 3	16	7.5

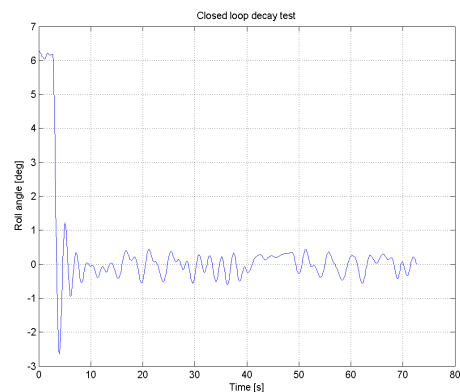
Table C.3: Irregular waves(full scale values)-JONSWAP spectrum;  $\gamma = 3.3$

### C.1.1. Results

As for example: Perez [28] and Moaleji [21] suggest, the highest damping can be achieved at natural frequency. In decay test, the ship will roll at the natural frequency, therefore it might be useful to investigate the dynamic behavior in a decay test. In C.2a a decay test is shown with the motion compensation system inactive. In C.2b the system is active. For the remaining load cases, similar graphs are presented in the model test report.



(a) Openloop decay test



(b) Closed loop decay test

Figure C.2: Decay tests LC1

When comparing the graphs, two things are worth paying attention to.

- The closed loop decay is much quicker compared to the open loop decay.
- The closed loop response does not approach zero.

The roll angle for the within 1deg within 5 seconds for the closed loop system, were the open loop system needs 15 seconds to so. This is an indication that the performance of the anti-roll system at the natural frequency is as expected. The inaccuracy of the closed loop response is accounted to the sensor noise close to the wave frequencies, which the executioner of the test had problems with to filter them out.

LC - Wave period - Wave height	Reduction of significant roll angle [%]	Maximum significant roll angle with system inactive [deg]	Maximum significant roll angle with system active [deg]
LC1-16s-5m	14.3	3.7	3.1
LC1-20s-2.5m	70.7	5.8	1.7
LC2-25s-4.6m	77.8	8.7	1.9
LC3-20s-2.5m	68.7	3.1	0.9

Table C.4: Performance regular waves

For regular waves, the results are shown in C.4 The wave-periods for the regular wave testing have been chosen very near to the natural roll period of the the ship in a specific load case. Reductions are therefore significant with the only exception being the first entry of the table with an excitation frequency below the natural frequency of the vessel. However no large improvements occur, the roll behavior does improve.

LC - Peak wave period - Significant wave height	Reduction of significant roll angle [%]	Maximum significant roll angle with system inactive [deg]	Maximum significant roll angle with system active [deg]
LC1-10s-5m	-3.8	1.8	1.9
LC1-16s-5m	29.2	2.8	1.9
LC1-16s-7.5m	29.0	3.9	2.7
LC1-20s-2.5m	61.5	2.8	1.1
LC2-16s-7.5m	17.2	2.6	2.1
LC2-20s-2.5m	25.8	1.1	0.8
LC3-16s-7.5m	15.1	1.9	1.6

Table C.5: Performance irregular waves

For irregular waves, the results are shown in C.5 for the 10s peak wave period, it can be seen that the behavior of the system is not improved, the contrary is true, however the roll angle is increased by 0.1 deg. One could argue that is not of utter importance. For all other combinations of significant wave height and peak period, the anti-roll system shows improvement, although not as high as is observed in the regular wave tests.

### C.1.2. Conclusion

The author has concluded that most improvement occurs at around the natural period, where the roll excitation are the largest. The regular wave response is close to what is predicted by the model, it is therefore concluded that the model is accurate. Since regular waves are not waves that are encountered at sea, it can be questioned the meaning of the given reductions in roll motions for regular waves. The designed controller, shows also robust behavior for the different load cases tested.





# Gyroscopes

<http://www.gyroscopes.org/math2.asp> Derivation Of The Equations Of Gyroscopic Motion by Robert M. Beal (May 2003) The equations appearing in this document were taken from various sections of the textbook Engineering Mechanics - Statics and Dynamics, Third Edition, by R. C. Hibbeler (ISBN 0-02-354140-7), primarily from chapters 20 and 21 of the Dynamics section; if the reader wishes to delve deeper into a topic or needs clarification on a part of this document, I refer you to Hibbeler's textbook. I have pieced together the equations, with occasional modifications and my own comments, to (hopefully) provide a smoothly flowing derivation of the equations of gyroscopic motion starting from the most basic equation of dynamics,  $F = ma$ , and proceeding uninterrupted to the stated goal.

We will start with Newton's well-known and accepted equation relating force ( $F$ ) to mass ( $m$ ) and acceleration ( $a$ ). For a particle, this is (bold type indicates a vector quantity):

$\Sigma F = ma$  This equation states that the sum of the external forces acting on a particle equals the particle's mass times its acceleration. Actually, Newton's original formulation related the external forces to the particle's linear momentum:

$\Sigma F = mv'$  Here,  $v$  is velocity,  $v'$  is the time rate of change of velocity ( $dv/dt$ ), and  $mv'$  is the time rate of change of linear momentum. If we chose a reference point  $O$  and  $r$  is a position vector to the particle, we can take the cross product of both sides of this equation to get an expression that relates the moment of the forces ( $M_o$ ) acting on the particle to the angular momentum ( $H_o$ ) of the particle with respect to the reference point  $O$ :

$r \times \Sigma F = r \times mv'$  Recognizing that  $r \times \Sigma F$  is the Sum of the Moments ( $\Sigma M_o$ ) of the forces acting on the particle about the reference point  $O$ , we can write:

$\Sigma M_o = r \times mv'$  Since the particle's angular momentum is  $H_o = r \times mv$ , if we take the time derivative of angular momentum, we have:

$d(H_o)/dt = d(r \times mv)/dt$   $H'_o = r' \times mv + r \times mv'$  Recognizing that  $v = dr/dt = r'$ , we have:

$H'_o = r' \times mr' + r \times mv'$  Since the cross product of two equivalent vectors is zero,  $r' \times mr' = m(r' \times r') = 0$ , therefore:

$H'_o = r \times mv'$  Substituting into the equation for the Sum of the Moments, we have:

$\Sigma M_o = H'_o$  That is, given a moving particle, the Sum of the Moments about a point  $O$  is equal to the time rate of change of the particle's angular momentum.

For a system of particles, we sum the moments of the forces of all the particles. In the following equation,  $S_f$  is the internal force acting on the  $i$ th particle due to all the other particles in the system:

$\Sigma_i [(r \times S_f)_i + (r \times S_f)_i] = \Sigma_i [H'_o]_i$  The internal forces cancel out because corresponding pairs of internal forces are equal in magnitude and opposite in direction, therefore,  $\Sigma_i (r \times S_f)_i = 0$ , and the resultant equation for a system of particles has the same form as the equation for a single particle:

$\Sigma [r \times S_f]_i = \Sigma [H'_o]_i$   $\Sigma M_o = H'_o$  In words, this states that the Sum of the Moments about point  $O$  due to the external forces acting on a system of particles is equal to the time rate of change of the angular momentum of the system of particles about this same reference point  $O$ .

We recognize that any solid body is a system of particles, so this equation applies to the analysis of a gyroscope.

What we need now is an expression for the angular momentum  $H_o$  or its time derivative  $H'_o$  that has attributes that we can physically measure such as mass, radius, angular velocity, and angular acceleration.

If we consider a particle in the body having an incremental mass  $Dm$  and having an angular velocity  $w$  with respect to reference point  $O$ , since  $v = w \times r$ , we can write:

$[DHo]_i = r \times Dm v_i$   $[DHo]_i = [r \times (w \times r)]_i Dm_i$  Summing all the incremental angular momenta for all the particles in the body, we have:

$\sum_i [DHo]_i = \sum_i [r \times (w \times r)]_i Dm_i$  If we let  $D$  approach 0, then  $D[Ho]_i$  and  $Dm_i$  become differentials, and we can replace  $\sum_i$  with integration. I will use  $\int$  instead of the usual integral sign simply because I don't have the usual integral sign available:

$\int r \times (w \times r) dm$   $Ho = \int r \times (w \times r) dm$  If we place xyz reference coordinate axes at point  $O$ , we can define  $Ho$ ,  $r$ , and  $w$  in terms of  $i$ ,  $j$ , and  $k$  components as follows:

$Ho = H_x i + H_y j + H_z k$   $r = x i + y j + z k$   $w = w_x i + w_y j + w_z k$  Substituting into the above integral expression for  $Ho$ , we have:

$H_x i + H_y j + H_z k = \int (x i + y j + z k) \times [(w_x i + w_y j + w_z k) \times (x i + y j + z k)] dm$  Computing the cross products and combining terms gives:

$H_x i + H_y j + H_z k = [\int x^2 dm - \int y^2 dm - \int z^2 dm] i + [-\int x y dm + \int x z dm + \int y z dm] j + [-\int x z dm - \int y z dm + \int x^2 dm] k$  Recognizing that the above integrals are moments of inertia and products of inertia, we can write the above as the following scalar equations:

$H_x = I_{xx} w_x - I_{xy} w_y - I_{xz} w_z$   $H_y = -I_{yx} w_x + I_{yy} w_y - I_{yz} w_z$   $H_z = -I_{zx} w_x - I_{zy} w_y + I_{zz} w_z$  If we choose a coordinate system such that at least two of the three orthogonal planes defined by the coordinate system are axes of symmetry for the body, then all the products of inertia become zero, and our equations reduce to:

$H_x = I_{xx} w_x$   $H_y = I_{yy} w_y$   $H_z = I_{zz} w_z$  If the axes are chosen as described above, they are called principal axes of inertia. We now have the angular momentum  $Ho$  in a useful form since the angular velocity can be measured and the moments of inertia ( $I$ ), which depend only upon the mass and physical dimensions of the body, can be looked up in a table or calculated by hand.

Our analysis of the gyroscope will be greatly simplified if we choose a coordinate system such that at least two of the three orthogonal planes defined by the coordinate system are axes of symmetry for the gyroscope. If the coordinate system is chosen to meet this criteria, then all the products of inertia will become zero, and we only have to include moments of inertia in our calculations. To accomplish this, we will use a rotating coordinate system with origin at the pivot point of the gyro. The rotating coordinate system will follow the gyro's nutation and precession but not its spin. We will call the angular velocity of the rotating reference  $W = \text{nutation} + \text{precession} = q' + f'$  and label the rotating axes as the xyz axes. We will also have a fixed reference coordinate system which will also have its origin at the pivot point of the gyro and we will call this the ABC axes. The angular velocity of the gyro with respect to the fixed ABC axes will be  $w = \text{nutation} + \text{precession} + \text{spin} = q' + f' + \gamma'$  (refer to Fig. 1 and Fig. 2). The angles  $q$ ,  $f$ , and  $\gamma$  are called Euler angles after the Swiss mathematician Leonhard Euler.

Since the xyz axes are rotating with respect to the fixed ABC axes, it is necessary to evaluate  $H'o$  taking into account that the unit vectors  $i$ ,  $j$ , and  $k$  are not constants since they are changing direction. We then have:

$(H'o)_{ABC} = H'x i + H'y j + H'z k + H_x(di/dt) + H_y(dj/dt) + H_z(dk/dt)$  where  $(H'o)_{ABC}$  is the time derivative of the angular momentum with respect to the fixed ABC axes. The time derivatives of the unit vectors can be expressed as:

$di/dt = W \times j$   $dj/dt = W \times k$   $dk/dt = W \times i$  The Sum of the Moments equation can then be written as:

$SMo = H'x i + H'y j + H'z k + W \times Ho$   $SMx i + SMy j + SMz k = H'x i + H'y j + H'z k + W \times Ho$  The tables one finds for moments of inertia for bodies of various geometrical shapes are for the principal axes of inertia and are typically listed as  $I_{xx}$ ,  $I_{yy}$ , and  $I_{zz}$ . Since the center of gravity of the flywheel of our gyro lies at a distance  $R$  from the origin  $O$  of our coordinate axes, the  $x$  and  $y$  axes are not principal axes of inertia, but they are parallel to the principal axes of inertia of the flywheel. We can therefore use the Parallel Axis Theorem to relate the  $x$  and  $y$  components of the moments of inertia to the  $I_{xx}$  and  $I_{yy}$  moments of inertia as shown below. The  $I_z$  component does not present a problem since the  $z$ -axis passes thru the flywheel's center of gravity so it is a principal axis of inertia:

$I_x = I_{xx} + mR^2$   $I_y = I_{yy} + mR^2$   $I_z = I_{zz}$  Keeping in mind the relationships between  $I_x$ ,  $I_y$ ,  $I_z$  and  $I_{xx}, I_{yy}, I_{zz}$ , we can now express the angular momentum of the gyro as:

$H_x = I_x w_x$   $H_y = I_y w_y$   $H_z = I_z w_z$  Substituting the above into the Sum of the Moments equation and taking the indicated time derivatives yields:

$SMx i + SMy j + SMz k =$

$(I_x w'x + I_y w'y + I_z w'z) + [(W_x i + W_y j + W_z k) \times (I_x w_x i + I_y w_y j + I_z w_z k)]$  Computing the cross products and combining terms, we get the following scalar equations for the Sum of the Moments:

$SM_x = I_x \dot{\omega}_x - I_y \dot{\omega}_z \dot{\phi} + I_z \dot{\omega}_y \dot{\psi}$   $SM_y = I_y \dot{\omega}_y - I_z \dot{\omega}_x \dot{\phi} + I_x \dot{\omega}_z \dot{\psi}$   $SM_z = I_z \dot{\omega}_z - I_x \dot{\omega}_y \dot{\phi} + I_y \dot{\omega}_x \dot{\psi}$  Referring to Fig. 2, we can express the xyz components of the angular velocity  $W$  of the rotating axes and the xyz components of the angular velocity  $w$  of the gyroscope as follows:

$$W = \dot{\phi} \mathbf{i} + \dot{\phi}' \sin \phi \mathbf{j} + (\dot{\phi}' \cos \phi) \mathbf{k}$$

$w = \dot{\phi} \mathbf{i} + \dot{\phi}' \mathbf{j} + \dot{\psi}' \mathbf{k}$   $w = \dot{\phi} \mathbf{i} + (\dot{\phi}' \sin \phi) \mathbf{j} + (\dot{\phi}' \cos \phi + \dot{\psi}') \mathbf{k}$  Substituting the components of  $W$  and  $w$  into the above scalar Sum of the Moments equations and computing the indicated time derivatives yields:

$SM_x = I_x \ddot{\phi} - I_y (\dot{\phi}')^2 \cos \phi \sin \phi + I_z \dot{\phi}' \sin \phi (\dot{\phi}' \cos \phi + \dot{\psi}')$   $SM_y = I_y (\dot{\phi}' \dot{\phi} \cos \phi + \dot{\psi}' \sin \phi) - I_z \dot{\phi}' (\dot{\phi}' \cos \phi + \dot{\psi}') + I_x \dot{\phi}' \dot{\phi} \cos \phi$   $SM_z = I_z (-\dot{\phi}' \dot{\phi} \sin \phi + \dot{\psi}' \cos \phi + \dot{\psi}'') - I_x \dot{\phi}' \dot{\phi} \sin \phi + I_y \dot{\phi}' \dot{\phi} \sin \phi$  In general, it would be very hard to arrive at a solution that satisfies these equations, however, in the specific case where the precession  $\dot{\phi}'$  is constant, the spin  $\dot{\psi}'$  is constant, and the nutation angle  $\phi = 90^\circ$  is a constant 90 degrees as shown in Fig. 3 below, the solution becomes quite easy:

In this case, we have:

$$\dot{\phi}' = 0 \quad \dot{\psi}'' = 0 \quad \dot{\psi}' = 0 \quad \cos(90^\circ) = 0 \quad \sin(90^\circ) = 1 \quad \text{and the Sum of the Moments equations reduce to:}$$

$SM_x = I_z \dot{\phi}' \dot{\psi}'$   $SM_y = 0$   $SM_z = 0$  so the only moment in this case is the moment about the x-axis. There are no negative signs in this equation and we consistently used the right-hand-rule in expressing all vector quantities, therefore, all of the vectors - the sum of the moments about the x-axis ( $SM_x$ ), the precession of the gyro about the y-axis ( $\dot{\phi}'$ ), and the spin of the flywheel about the z-axis ( $\dot{\psi}'$ ) all act along their respective positive axes as indicated in Fig. 3. Our analysis of the the gyroscope lying at  $90^\circ$  has boiled down to the following important result:

$SM_x = I_z \dot{\phi}' \dot{\psi}'$  If the only moment about the x-axis is the moment resulting from the weight of the flywheel (we are assuming the weight of the shaft is negligible), and if the flywheel is at a distance  $R$  from the pivot point (origin  $O$ ), and recalling that  $I_z = I_{zz}$ , we have:

$mgR = I_{zz} \dot{\phi}' \dot{\psi}'$  where  $m$  is the mass of the flywheel and  $g$  is the acceleration due to gravity. This equation tells us that if the flywheel is lying at  $90^\circ$  at a distance  $R$  from the pivot point and the flywheel is spinning at a constant angular velocity  $\dot{\psi}'$ , then the gyro will not topple over as might be expected, but instead, it will precess about the positive y-axis at a constant angular velocity of  $\dot{\phi}'$ .

For a solid circular disc,  $I_{zz} = 1/2 mr^2$  where  $r$  is the radius of the disc. If we instead concentrate most of the mass around the outer edge, then for a thin circular ring,  $I_{zz} = mr^2$ :

solid circular disk:  $mgR = 1/2 mr^2 \dot{\phi}' \dot{\psi}'$  thin circular ring:  $mgR = mr^2 \dot{\phi}' \dot{\psi}'$  To counter the moment  $mgR$ , a gyro that uses a solid circular disk as the flywheel will precess twice as fast as a gyro that uses a thin circular ring (assuming both flywheels have the same mass  $m$  and radius  $r$ ).

References:

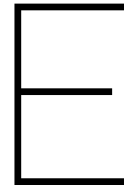
Engineering Mechanics - Statics and Dynamics, Third Edition, by R. C. Hibbeler (ISBN 0-02-354140-7)

Engineering Mechanics - Dynamics by Anthony Bedford and Wallace Fowler (ISBN 0-201-58197-3)

Many thanks to Robert M. Beal (email: [psisquared@Earthlink.net](mailto:psisquared@Earthlink.net)) for providing this document.

Website. Copyright © 2017 Glenn Turner. All rights reserved. site info Do not copy without prior permission. Click here for gyroscope products





# Hydrostatics

## E.1. Hydrostatics

Based on the assumption that the effect of a swiveling crane on the heeling angle of a vessel can be described using a quasi-static approach, a background is given on the static stability of a vessel. This chapter is mainly based on chapter 2 in Journee et al. [11] which is a summary made for education purposes based on broadly accepted science. This information is used to do static calculations on the swiveling crane compensated with the ballast train. Since as Sellars and Martin [36] states: "Heel control systems are often necessary on certain ship types while loading and unloading, this adaption helps to justify the extra costs.

### E.1.1. Definitions

Below the key definitions are given to describe stability when swiveling properly.

**Heel and Trim** Heel is defined as the angle of a vessel around CoG in the  $xy$ -plane, see E.1, commonly used in applications where inertia and time is neglected. A similar angle in the  $xz$ -plane is called trim for static applications. Trim will not be in the scope of this thesis, therefore no further attention will be spent on trim.

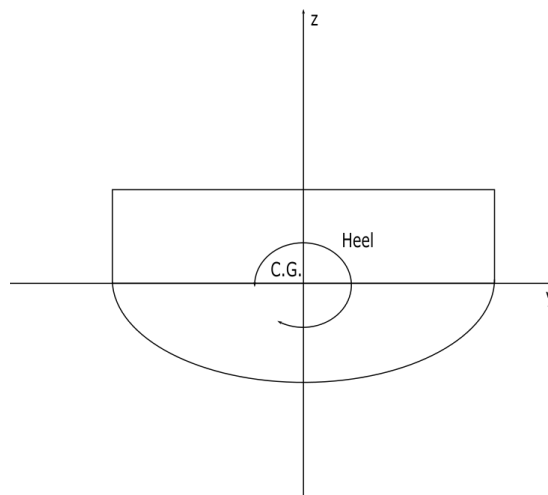


Figure E.1: Heeling angle explained

**Center of buoyancy** The center of buoyancy is defined as the location where the force is acting on. At the center of buoyancy the first moment of water volume is equal to zero.

**Center of gravity** The center of gravity can be described as the point where the whole mass is acting on. As with the center of buoyancy, the first moment of mass around this point equals zero. Three equilibria exist according to Journee et al. [11]

1. **Horizontal equilibrium** Sum of horizontal forces is zero
2. **Vertical equilibrium** Sum of vertical forces is zero
3. **Rotational equilibrium** Sum of moments about C.G. equals zero.

For this report, the rotational equilibrium is most important, assuming that the crane and load are small compared to vessel mass, and thus will alter GM significantly.

### E.1.2. Horizontal equilibrium

From a static perspective, there is no interest in evaluating the horizontal equilibrium of a floating structure, with the exception of the case in which restoring forces such as mooring systems or DP systems are present.

### E.1.3. Vertical equilibrium

The vertical equilibrium is best disclosed by presenting Archimedes law:

$$\rho g \nabla = gm \quad (\text{E.1})$$

What it depicts is that the submerged volume multiplied with the density of the fluid the object is submerged in, should equal the mass of the (partly) submerged object. As a result, when a floating structure of ship moves in the downward vertical direction, a resulting force will occur.

### E.1.4. Rotational equilibrium

When a moment is acting on an arbitrarily shaped floating body as shown in E.2 and there is a restoring moment, this indicates that the C.G. is not in the same vertical line as is the center of buoyancy. The distance between the two is called lever arm, and is denoted by  $y$ . If there is no external moment  $M_h$  working on the body, the two should be inline, since  $y$  must equal zero. We can write this equilibrium as:

$$M_h = \rho_{water} g \nabla y = gmy \quad (\text{E.2})$$

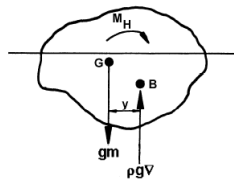


Figure E.2: Definition of heeling moment, source: Journee et al. [11]

### E.1.5. Restoring moment & Stability curve

As a result of applying a heeling moment  $M_h$  a ship will heel with an angle  $\phi$ . Due to this angle, the CoG,  $G$  and center of buoyancy  $B$  will not be positioned in a vertical line, resulting in a righting stability moment. We will name the CoG  $Z$ , the new center of buoyancy  $B_\phi$  after the heeling has occurred as depicted in E.3. Since we are dealing with statics, the heeling moment  $M_h$  should be equal to the restoring moment  $M_r$  which is defined as  $\rho g \nabla \overrightarrow{GZ}$  in which

$$\overrightarrow{GZ} = \overrightarrow{GN_\phi} \cdot \sin(\phi) \quad (\text{E.3})$$

$N_\phi$  is known as the meta center of the vessel. It is defined as the point of intersection between a vertical line through  $B$  and a line perpendicular to the deck and through  $B_\phi$ . This will eventually lead to the following expression for  $M_r$ :

$$M_r = \rho g \nabla \cdot \overrightarrow{GN_\phi} \cdot \sin(\phi) \quad (\text{E.4})$$

It can be seen from the above expression that the value of the stability lever arm  $\overrightarrow{GZ}$  determines the magnitude of the restoring moment for a vessel. For that reason, the static stability curve of a vessel is usually expressed in terms of  $\phi$  and  $\overrightarrow{GZ}$

In E.4 an example curve is shown. Since most ships are symmetric, so is the graph in many cases. An important parameter of ship stability is the angle of maximum  $GZ$ , which is also showed in the figure above.

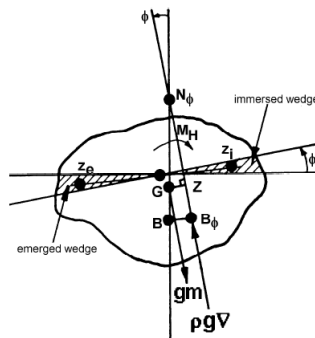


Figure E.3: Rotational equilibrium, source: Journee et al. [11]

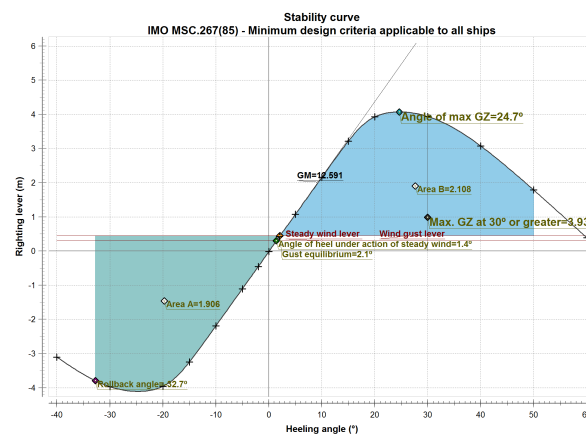


Figure E.4: A typical GZ-curve

**E.1.6. Crane action**

An application of the ballast train system can be to compensate for a swiveling crane. One can think of relatively fast movements with light loads due to limitations in the mass of the control system. In E.5 a schematic drawing of vessel equipped with a crane is shown. The crane can rotate around the z-axes. This is called swiveling. There are mainly two effects that the crane has on the heeling angle:

1. The crane is lifting a load
2. The crane swivels

Both these actions can result in a moment around the x-axis. In turn this will cause the vessel to heel. However, the ballast train system can reduce this angle by introducing a counteracting moment by moving to the opposite site of the vessel. In this report, both the moment induced by the crane and load and the ballast train system will be considered eccentric loading.

**E.1.7. Eccentric loading**

When a load is added to a vessel, in general 2 things happen: the draft will increase, and with that the characteristics, and when the eccentric load is placed outside the CoG the vessel will heel. The first effect cannot be compensated by the ballast train, however it does influence the roll behavior of the vessel, therefore a short introduction to both processes will be given below.

**Increasing draft** The increasing draft from the added weight  $p$  can be directly determined from Archimedes law. For vessels with a constant water plane area along the z-axis, or when the load added is sufficiently small compared to the ships mass, the change in draft can be expressed as:

$$\Delta T = \frac{p}{\rho A_{WL}} \tag{E.5}$$

This result can be derived easily from E.1. The derivation of this result will be left for the reader.

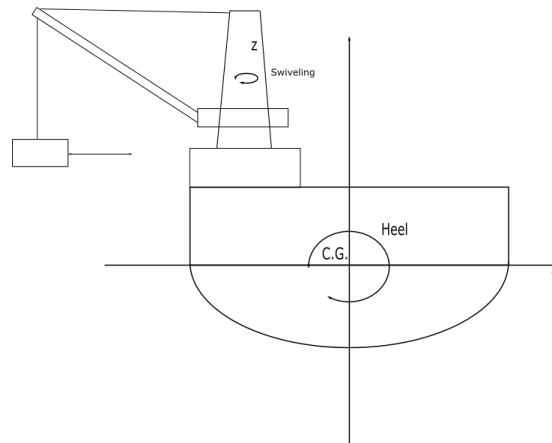


Figure E.5: Swiveling motion

**Resulting angle of roll** In Journee et al. [11] a description is given on how a ship can react to a heeling moment.

The heeling moment around the CoG produced by shifting a mass  $p$  by a horizontal distance  $c$  outside the CoG is given by:

$$M_h = gpc \cdot \cos(\phi) \quad (\text{E.6})$$

In which  $\phi$  is the angle of heel. As is shown in E.6, the heeling moment  $M_h$  is a function of  $\phi$ . We know since there must be an equilibrium, the heeling moment must equal the restoring moment:

$$M_h = M_r \quad (\text{E.7})$$

$$gpc \cdot \cos(\phi) = \rho g \nabla \cdot \overrightarrow{GN_\phi} \cdot \sin(\phi) \quad (\text{E.8})$$

Rewriting this equation eventually gives the following expression for  $\phi$ :

$$\phi = \arccos \left\{ \frac{\rho \nabla \overrightarrow{GN_\phi} \cdot \sin(\phi)}{p \cdot c} \right\} \quad (\text{E.9})$$

Which is a recursive expression that cannot be solved instantaneously, however with the use a calculation method such as Newton-Rhapson or Regula-Falsi the solution can be found iteratively. For small angles of roll a simplified expression can be derived:

$$\phi = \arctan \left\{ \frac{p \cdot c}{\rho \nabla \overrightarrow{GM}} \right\} \quad (\text{E.10})$$

In which

$$\overrightarrow{GM} = \overrightarrow{GN_\phi} \quad (\text{E.11})$$

for small angles of roll

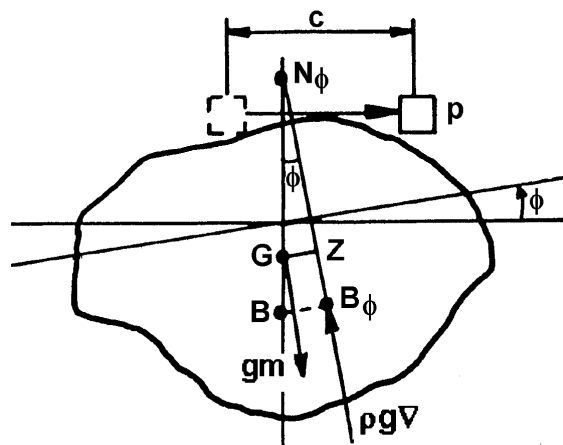


Figure E.6: The shifting of a load on deck, source: Journée et al. [11]